

Quantum Diffusion and scaling of  
localized interacting electrons

Dissertation  
zur Erlangung des Doktorgrades  
des Fachbereichs Physik  
der Universität Hamburg

vorgelegt von  
Ole Halfpap  
aus Pinneberg

Hamburg  
2000



# Abstract

A new numerical method is introduced that enables a reliable study of disorder-induced localization of interacting particles. It is based on a quantum mechanical time evolution calculation combined with a finite size scaling analysis. The time evolution of up to four particles in one dimension is studied and localization lengths are defined via the long-time saturation values of the mean radius, the inverse participation ratio and the center of mass extension. A systematic study of finite size effects using the finite size scaling method is performed in order to extract the localization lengths in the limit of an infinite system size. For a single particle, the well-known scaling of the localization length  $\lambda_1$  with disorder strength  $W$  is observed,  $\lambda_1 \propto W^{-2}$ . For two particles, an interaction-induced delocalization is found, confirming previous results obtained by numerically calculating matrix elements of the two-particle Green's function: in the limit of small disorder, the localization length increases with decreasing disorder as  $\lambda_2 \propto W^{-4}$  and can be much larger than  $\lambda_1$ . For three and four particles, delocalization is even stronger. Based on analytical arguments, an upper bound for the  $n$ -particle localization length  $\lambda_n$  is derived and shown to be in agreement with the numerical data,  $\lambda_n \propto \lambda_1^{2^{n-1}}$ . Although the localization length increases superexponentially with particle number and can become arbitrarily large for small disorder, it does not diverge for finite  $\lambda_1$  and  $n$ . Hence, no *extended* states exist in one dimension, at least for spinless fermions.

## Zusammenfassung

Ein neue numerische Methode zur Untersuchung der Lokalisierungseigenschaften wechselwirkender Teilchen wird eingeführt. Dabei wird die quantenmechanische Zeitentwicklung von Wellenpaketen mit bis zu vier Teilchen berechnet. Die Sättigungswerte des mittleren Radius und der Ausdehnung in Schwerpunktsrichtung für große Zeiten definieren die Lokalisierungslängen. Deren Abhängigkeit von der Systemgröße wird mit einem Skalierungsverfahren untersucht, das die Bestimmung der Lokalisierungslänge  $\lambda_1$  im Grenzfall eines unendlich ausgedehnten Systems erlaubt. Für ein einzelnes Teilchen wird die bekannte Skalierung der Lokalisierungslänge mit der Unordnung  $W$  gefunden,  $\lambda_1 \propto W^{-2}$ . Für zwei Teilchen wird eine Vergrößerung der Lokalisierungslänge beim Einschalten der Wechselwirkung beobachtet. Dies bestätigt frühere Ergebnisse, die durch Berechnung von Matrixelementen der Zweiteilchen Greensfunktion gewonnen wurden: Die Lokalisierungslänge skaliert für kleine Unordnung mit  $\lambda_2 \propto W^{-4}$  und kann damit wesentlich größer werden als  $\lambda_1$ . Eine wesentlich stärkere Delokalisierung ergibt sich für drei und vier Teilchen. Basierend auf analytischen Überlegungen wird eine obere Grenze der Lokalisierungslänge für  $n$  Teilchen hergeleitet und ihre Übereinstimmung mit den numerischen Daten wird gezeigt,  $\lambda_n \propto \lambda_1^{2^{n-1}}$ . Obwohl die Lokalisierungslänge stärker als exponentiell mit der Teilchenzahl anwächst und im Grenzfall kleiner Unordnung beliebig groß werden kann, divergiert sie nicht. Dementsprechend existieren keine *ausgedehnten* Zustände in einer Dimension, zumindest nicht für die hier behandelten spinlosen Fermionen.

# Contents

<b>1</b>	<b>Introduction</b>	<b>1</b>
<b>2</b>	<b>Anderson Localization</b>	<b>2</b>
2.1	Electronic wave functions . . . . .	2
2.2	Physics of localized states . . . . .	2
<b>3</b>	<b>Localization of interacting particles</b>	<b>5</b>
3.1	Localization of two interacting particles . . . . .	6
3.2	Spectral statistics of interacting particles . . . . .	15
3.3	Other approaches . . . . .	23
3.4	Summary of chapter 3 . . . . .	31
<b>4</b>	<b>Time evolution of wave packets</b>	<b>32</b>
4.1	Equation of motion method . . . . .	33
4.2	Finite size scaling . . . . .	37
4.3	Extracting $n$ -particle localization lengths . . . . .	41
<b>5</b>	<b>Two interacting particles</b>	<b>42</b>
5.1	Initial conditions . . . . .	44
5.2	Time evolution . . . . .	45
5.3	The two-particle localization length . . . . .	49
<b>6</b>	<b>More than two particles</b>	<b>56</b>
6.1	Three-particle wave packets . . . . .	57
6.2	Upper bound for the $n$ -particle localization length . . . . .	61
6.3	Four-particle wave packets . . . . .	66
6.4	Numerical effort . . . . .	73
<b>7</b>	<b>Finite densities: time-dependent Hartree-Fock</b>	<b>75</b>
7.1	Method . . . . .	75
7.2	Results . . . . .	77
<b>8</b>	<b>Summary</b>	<b>81</b>
<b>A</b>	<b>Data tables</b>	<b>96</b>

# 1 Introduction

*We used to think that if we know one, we knew two, because one and one are two. We are finding that we must learn a great deal more about 'and'.*

Sir Arthur Eddington  
from *The Harvest of a Quiet Eye* by A. Mackay

While a lot is known about disorder-induced localization of independent, non-interacting particles, we are just beginning to grasp the meaning of 'and', that is of correlations between the electrons due to their mutual interaction. And it is known by now that upon considering localization lengths of interacting particles, one and one is definitely not two but can be considerably more.

The influence of electron-electron interaction on disorder-induced localization has attracted considerable attention after the recent experimental discovery of a metal-insulator transition in two dimensions [1, 2, 3, 4] as it cannot be explained within the conventional scaling theory of localization [5].

One of the possible starting points to incorporate the influence of correlations among the electrons is to study localization properties for two interacting particles in a one-dimensional random system [6]. Recently, numerical results based on the two-particle Green functions showed unambiguously that the interaction increased the localization length of two-particle wave functions [7, 8, 9].

In this thesis, a new method to study localization effects of interacting particles is introduced. It is based on a quantum mechanical time evolution calculation for the wave packets combined with a finite size scaling analysis of the saturation values in the localized regime. With this method, localization lengths of two-, three-, and four-particle wave packets have been calculated which can provide a firm base for approximations necessary for larger particle numbers. *The localization length increases superexponentially with increasing particle number, one and one is more than two. But the localization length remains finite for any finite disorder strength and particle number.*

This thesis is organized as follows. In section 2, basic concepts and main experimental results of disorder-induced localization are introduced. Section 3 gives an overview of theoretical approaches to treat disorder and interaction *non-perturbatively* on an equal footing, focusing mainly on recent numerical work for small particle numbers. The new method is laid out in section 4, with the quantum mechanical time evolution method described in 4.1 and the finite size scaling in 4.2. Results for two interacting particles are presented in section 5, showing the reliability of the method and laying the foundation for the results for larger particle numbers in section 6. The physical origin of the enhancement of the localization length is discussed in section 7 after the presentation of approximate results for finite densities obtained using the time dependent Hartree-Fock equations. A summary is given in section 8.

## 2 Anderson Localization

### 2.1 Electronic wave functions

Electron eigenstates in free space are given by plane waves [10],

$$\psi_{\vec{k}}(\vec{r}) = \exp(i\vec{k}\vec{r}). \quad (1)$$

In the periodic potential of an ideal crystal, Bloch's theorem holds [11]: based on the translational symmetry of the Hamiltonian, the plane wave is modulated by a function that has the periodicity of the lattice,

$$\psi_{\vec{k}}(\vec{r}) = u(\vec{r}) \exp(i\vec{k}\vec{r}), \quad (2)$$

with  $u(\vec{r}) = u(\vec{r} + \vec{R})$  where  $\vec{R}$  is an arbitrary lattice vector. In real crystals, impurities, vacancies or dislocations break the translational invariance and hence the validity of Bloch's theorem. But only in 1958 it was shown by Anderson, that this kind of disorder can completely change the electron eigenstates and hence the physics of disordered systems [12]. In contrast to extended eigenstates in free space or in a periodic potential, electrons can become localized in some part of the system, reflected in a finite return probability even for arbitrarily long times. This happens if disorder is large or the density of states at that energy is small. The corresponding eigenstates are characterized by the localization length  $\lambda$ , the exponential decay length of their envelope,

$$\psi(\vec{r}) = f(\vec{r}) \exp(-|\vec{r} - \vec{r}_0|/\lambda), \quad (3)$$

with a randomly varying function  $f(\vec{r})$ . Localized and extended states exist in different energy regions, separated by the mobility edge [13].

In the following, the main theoretical results concerning this disorder-induced Anderson localization and some physical phenomena directly related to it will be briefly discussed.

### 2.2 Physics of localized states

The consequences of electron localization are most pronounced in the transport properties of a disordered system. Localized electrons cannot contribute to transport at temperature  $T=0$ , if the sample is larger than the localization length of the electronic states. Upon varying the Fermi level, the system can therefore undergo a quantum phase-transition from a metal with extended states to an insulator with localized states. At finite temperatures, transport in the insulating regime occurs via phonon mediated hopping between different localized states. Localization effects can then be identified by the dependence of the resistance on temperature and dimensionality. Anderson had predicted that disorder is most effective in systems with a small number of nearest neighbors leading to a small connectivity, figure 3 in [12]. Thus it was obvious that localization effects would be most pronounced in low dimensions where the number of nearest neighbors is reduced.

In one-dimensional systems, it was much easier to analyze the localization of electrons theoretically than to perform experiments. It was first argued by Mott and Twose in 1961 [14] that in a one-dimensional system all electron states are localized. This was proven more rigorously in 1973 [15]. But a direct comparison to experiments was out of reach until Thouless

extended the exact results to quasi one-dimensional geometries in 1977 [16]. One of the best experiments on quasi one-dimensional systems was performed by Gershenson and coworkers in 1997 [17, 18]. They measured the resistance of a couple of parallel quantum wires as a function of temperature. The data could be fitted very well with an exponential increase of the resistance with decreasing temperature,  $R(T) = \exp(T_0/T)$ , as predicted by the theory for phonon assisted hopping between strongly overlapping localized states, in contrast to Mott's theory on variable range hopping discussed below. The key observation was the doubling of the localization length in a strong magnetic field, resulting in a decrease of  $T_0$  by a factor of 2. This had been predicted theoretically in 1983 [19, 20] and is not valid for dimensions  $d \geq 2$ .

The experimental investigation of two-dimensional electron systems started already in the seventies, when experimental evidence for the localized states proposed by Anderson was still lacking. Mott predicted the following temperature dependence of the resistivity for variable range hopping of the electrons,

$$\rho \propto e^{(T_0/T)^{\frac{1}{d+1}}}. \quad (4)$$

In the early experiments [21, 22, 23], reviewed in [24], the Mott-law was found for small carrier densities,  $n_s \approx 2 \cdot 10^{11} \text{cm}^{-2}$ . For larger densities,  $n_s > n_c \approx 2 \cdot 10^{11} \text{cm}^{-2}$ , a temperature independent conductivity was found, indicating a metallic state with a finite zero temperature conductivity. Since a transition from localized to extended states under variation of the Fermi energy was expected theoretically, the metallic state was not surprising at that time.

In 1979, the scaling theory of localization predicted the absence of diffusion for non-interacting electrons in one and two dimensions [25]. According to this theory, no extended states were supposed to exist in two dimensions for arbitrarily small disorder and no true metallic behavior should have been observable. This result and the general idea of the one parameter scaling theory were supported by field theoretical methods [26, 27] and numerical scaling techniques [28, 29, 30, 31].

What was wrong with the early experiments? Why was a temperature independent conductivity observed? The localization length was much larger in two dimensions than in one dimension. That made an experimental proof of the localization of all states very difficult. Inelastic scattering occurred before the electrons diffused up to their localization domain and phase coherence was lost. In this regime, localization length larger than phase coherence length, the disorder led only to a small correction to the classical conductivity, with a logarithmic dependence on temperature in contrast to the strong localization regime with exponential temperature dependencies [32]. These weak-localization predictions were observed experimentally by many authors [33, 34], reviewed in [35]. Recently, upon analyzing in detail the crossover from strong to weak localization in GaAs/AlGaAs heterostructures even the localization length was extracted from the experimental data and excellent agreement with the theory was reported [36].

The overwhelming success of weak-localization theory led to the conclusion that indeed no true metallic state could exist in 2D. This belief started to turn around again when Kravchenko and coworkers reported new experimental evidence for a transition in very high mobility silicon MOSFETs [1, 37]. The mobility in their samples reached up to  $7.1 \times 10^4 \text{cm}^2 \text{V}^{-1} \text{s}^{-1}$ . For temperatures below 1-2 K they observed a sharp drop of the resistivity with decreasing temperature. The effect was stronger than the weak-localization

correction which had been found at slightly higher temperatures. Decreasing the temperature further down to 20 mK, they found no indications for electron localization.

The described behavior occurred in samples with electron densities above  $10^{11}\text{cm}^{-2}$ . In low-density samples with an even higher influence of the Coulomb interaction, an insulating behavior was observed, possibly related to the formation of a pinned electron solid. For the lowest mobility of about  $0.5 \times 10^4 \text{cm}^2 \text{V}^{-1} \text{s}^{-1}$ , no sharp drop in the resistivity was observed, the experimental data was consistent with that of conventional silicon MOSFETs [34].

Similar observations have afterwards been reported for SiGe superlattices [38, 39, 40], dilute GaAs-AlGaAs hole gases [4], p-type GaAs [41, 42, 43], and n-type GaAs [44]. The importance of Coulomb correlations was demonstrated in [45]. The combination of density scaling with electric field scaling [2] allowed to extract the dynamical exponent  $z=0.8$  and the correlation length exponent  $\nu=1.5$ . The suppression of the metallic state by a magnetic field [46, 47, 48] and by local magnetic moments [49, 50] was possibly related to the electron spin [51, 52]. That the system was in a real quantum state was demonstrated in [53]. An observed reflection symmetry indicated that the transport processes on both sides of the transition were related [54]. A continuous transition from the new  $B=0$  transition to the known quantum Hall transition at finite magnetic field was demonstrated in [55]. The influence of spin-orbit interaction was argued to be relevant in [56, 57, 58]. The existence of a true metallic phase at  $T=0$  was again questioned in [59] where quantum correction due to disorder and interaction were found. Insulating *and* metallic logarithmic temperature corrections were reported in [60]. For further experiments on this topic, see [3, 61, 62, 63, 64, 65, 66, 67, 68].

Theoretically, a number of different models were used so far to explain at least some of the experimental results. They were based on superconductor to insulator transitions [69, 70, 71, 72], temperature-dependent impurity scattering [73], phenomenological assumptions about the  $\beta$ -function in the presence of interaction [74], percolation transition of a new liquid phase [75, 76, 77], generalized variable range hopping [78], non-Fermi liquid behavior [79], renormalization group theory of disorder and interaction [80, 81], based on Finkelsteins theory [82], spin-orbit interaction [83, 84, 85], and the influence of electron-electron interaction [86, 87, 88, 89, 90, 91, 92, 93, 94, 95, 96, 97, 98, 99, 100]. Nevertheless, a detailed understanding of the experiments is still missing.

In three dimensions, the scaling theory of localization [25] predicted the existence of a metal-insulator transition. This transition was an example for a quantum phase-transition, characterized by a fundamental change of the ground state as a function of pressure, impurity concentration, or some other tuning parameter. Experiments were mainly performed on doped semiconductors, see [101] and references therein. At low donor concentration, electrons were localized in hydrogen like orbitals at the donor atoms, e. g. at P in Si. With increasing concentration, the orbitals started to overlap and an impurity band was formed in which metallic conduction could take place above a critical concentration. Comparison with theory is made using the critical exponent  $\mu$  which described the scaling of the conductivity  $\sigma$  as a function of the tuning parameter  $x$ ,

$$\sigma = |x - x_c|^\mu \quad . \quad (5)$$

The critical exponent was considered to be universal, i. e. it should not depend on the specific properties of the sample, but rather on the symmetries of the Hamiltonian. For

compensated semiconductors values of  $\mu \approx 1$  were reported [102, 103, 104] in contrast to  $\mu \approx 0.5$  for uncompensated semiconductors [105, 106, 107, 108]. Since without compensation there were almost as many electrons as hopping centers, one expected a large influence of electron correlations. Theoretically predicted exponents range from  $\mu = 1$  [25] to  $\mu = 1.57$  [109], based on theories which do not include interaction. Including it, a lower bound of  $\mu = 2/3$  was derived [110]. This contradiction between theory and experiment may be solved in the near future since in recent experiments on uncompensated samples larger values of the critical exponents were found. Taking into account both sides of the transition,  $\mu = 1.0$  was reported in Si:P [111] and  $\mu = 1.6$  in Si:B [112, 113]. Using a smaller critical region,  $\mu = 1.2$  was found in Ge:Ga [114]. But a detailed description of the influence of interaction effects on the metal-insulator transition with predictions of the critical exponents is still missing.

To summarize, the first stone was laid in 1958 and in the following two decades the theory was completed without including interaction effects, culminating in the success of the scaling theory and numerical calculations. In the 1980s, the relevance of electron-electron interaction became obvious and the latter was included perturbatively into the theory. In the metallic regime additional terms in the weak localization correction to the conductivity were found [32], while the Coulomb gap changed Mott's hopping law in the insulating regime [115]. Recently, it became evident that many of the above described experimental features cannot be explained by considering disorder or interaction as a perturbation. Instead, both have to be treated on equal footing. Problems directly related to this very active area of research are the complete understanding of the integer and fractional quantum Hall effect with the missing prove of the localization of Laughlin's quasi-particles [116], the experimentally observed persistent currents in small metallic rings which are larger than theoretically predicted by two orders of magnitude [117, 118], the unexplained yet observed metal-insulator transition in two dimensions, and the question of dephasing due to electron-electron interaction in disordered systems [119].

Since analytical calculations going beyond perturbation theory are very complicated for interacting electrons in disordered systems, main results were found relying on numerical calculations for a small number of particles. I will summarize the most important ones in the next section, concentrating on the aspect of localization.

### 3 Localization of interacting particles

The minimum number of particles needed to study interaction effects is two. This rather obvious statement tells a lot about the early approaches to study the influence of interaction on disorder-induced localization. In comparison to a disordered system with finite electron density, a two-electron system is "simple" enough for an exact study and can still provide useful information, necessary to construct the full theory.

In this section, results obtained following the above strategy will be discussed, concentrating in the first part on localization properties. So far, exact calculations have been performed only for two interacting particles. In the second part, different aspects of the problem, mainly related to spectral statistics, will be discussed. These include generalizations to higher particle numbers. In the third part, other approaches to the problem of two

and more interacting particles will be mentioned, before summarizing the main results.

### 3.1 Localization of two interacting particles

#### 3.1.1 The early approaches

The first to study localization of two interacting electrons was Dorokhov in 1990 [120]. He considered two particles with a harmonic attraction. In the absence of a the random potential, the center of mass motion is the sum of two plane waves, whose wave vector depends on the total energy and the energy of the relative motion,

$$\psi(R, r) = \sum_n v_n(r)[A_n e^{ik_n R} + B_n e^{-ik_n R}]. \quad (6)$$

The main assumption for the disordered case was that only the pre-factors of the plane wave become position dependent,  $A_n \rightarrow A_n(R)$ . The influence of the disorder on  $k_n$ , on the relative motion and the coupling of the relative and the center of mass motion was neglected. Dorokhov mapped this problem onto the one of a single particle in a quasi one-dimensional system with a finite number of transverse channels, being essentially the number of energetically available oscillator states. For a single open channel, the localization length was slightly larger than without interaction due to the smoothing of the random potential by the ground state wave function of the oscillator. For a larger number of open channels, the localization length increased strongly. The maximum value of the two-particle localization length  $\lambda_2$  was reported to be the square of the one-particle localization length  $\lambda_1$ ,  $\lambda_2 = k_F \lambda_1^2$ .

This effect was not appreciated until Shepelyansky found a similar result in 1994 [6]. He considered an Anderson tight binding Hamiltonian for two particles with an on-site interaction of strength  $U$ ,

$$(\epsilon_{n_1} + \epsilon_{n_2} + U\delta_{n_1, n_2})\psi_{n_1, n_2} + V(\psi_{n_1+1, n_2} + \psi_{n_1-1, n_2} + \psi_{n_1, n_2+1} + \psi_{n_1, n_2-1}) = E\psi_{n_1, n_2}, \quad (7)$$

with random potential energies  $\epsilon_{n_1}, \epsilon_{n_2}$  and a hopping amplitude  $V$ . Transforming the Hamiltonian to the basis of non-interacting two-particle eigenstates  $\chi_{m_1, m_2}$  with energies  $E_{m_1}$  and  $E_{m_2}$  yielded,

$$(E_{m_1} + E_{m_2})\chi_{m_1, m_2} + U \sum_{m_1', m_2'} Q_{m_1, m_2, m_1', m_2'} \chi_{m_1', m_2'} = E\chi_{m_1, m_2}, \quad (8)$$

with an interaction matrix

$$Q_{m_1, m_2, m_1', m_2'} = \langle \chi_{m_1, m_2} | U | \chi_{m_1', m_2'} \rangle = U \int \phi_{m_1}(x) \phi_{m_2}(x) \phi_{m_1'}(x) \phi_{m_2'}(x) dx. \quad (9)$$

The crucial point was the following estimate of the elements of the interaction matrix. Since the one-particle eigenstates  $\phi_{m_i}$  were exponentially localized on the scale of the one-particle localization length  $\lambda_1$ , the matrix elements were exponentially small whenever the wave functions were located away from each other. Only if all four wave functions were centered in a region of size  $\lambda_1$ , there was a non-negligible matrix element. It was of the order of  $\lambda_1^{-3/2}$  since the integral in (9) contained  $\lambda_1$  non-negligible random terms of the order of  $\lambda_1^{-2}$ , which

was given essentially by the normalization of the wave functions. Neglecting correlations among these elements and taking all other elements as zero, Shepelyansky showed that the problem was equivalent to a special type of band random matrix model, see page 16. Performing numerical calculations with this model, he found for the two-particle localization length,

$$\lambda_2 \simeq \frac{U^2}{32V^2} \lambda_1^2. \quad (10)$$

This implied that in the limit of small disorder and hence large  $\lambda_1$ , the interaction could lead to a drastic enhancement of the localization length due to the interaction,  $\lambda_2/\lambda_1 \propto \lambda_1 \gg 1$ . Moreover, the enhancement effect was predicted to be insensitive to the sign of the interaction which loses its influence during the estimation of the matrix elements.

This results was generalized by Imry [121, 122], employing the Thouless block scaling picture [16]. One divides the system into small blocks of size  $L$ . Then, the transport properties of the system are related only to the level separation within the blocks,  $\Delta$ , and the coupling to the next blocks,  $t$ . The dimensionless conductance is given by  $g = (t/\Delta)^2$ . If the coupling to the next block is smaller than the level spacing, no extended states can be build up. In contrast, if the coupling is larger than the level spacing, states in many blocks are coupled and extended states exist, leading to a higher conductance. On the other hand the scaling theory of localization [25] predicts for the conductance in one dimension  $g = \lambda/L$ . This follows from integrating the beta function,  $\beta(g) = d \ln g / d \ln L = -1$ , valid for  $\lambda \approx L$ . Imry's main idea was to consider blocks of size  $L = \lambda_1$ , yielding  $g_1 \sim 1$ . The inter-block coupling between two-particle states was estimated to be  $t \sim U \lambda_1^{-3/2}$  using Shepelyansky's estimate of the interaction matrix elements. The mean level spacing was simply the bandwidth divided by the number of levels,  $\Delta \sim B/\lambda_1^2 \sim V/\lambda_1^2$  since the bandwidth was proportional to the hopping term. This gave a conductance for two particles  $g_2 = c \lambda_1 (U/V)^2$  with a constant  $c < 1$ . If the single particle localization length was large enough the conductance  $g_2$  was larger than  $g_1 \sim 1$ . Due to the choice of the block size,  $g_2 = \lambda_2/L = \lambda_2/\lambda_1$ , yielding again Shepelyansky's result, equation (10).

In two dimensions, the delocalization was exponentially large since  $g = a \ln(\lambda/L)$  followed from integrating  $\beta(g) = -a/g$ . Calculating  $g_2$  with the block scaling argument,  $\lambda_2/\lambda_1$  depended now exponentially instead of linearly on  $g_2$ ,

$$\lambda_2/\lambda_1 \propto e^{g_2/a} \propto e^{(U\lambda_1)^2/(Va)^2}. \quad (11)$$

In three dimensions the critical disorder at which the metal-insulator transition occurs was predicted to shift to larger disorder values by switching on the interaction.

Both arguments, the one by Shepelyansky and the one by Imry, are based essentially on the same uncontrolled assumptions concerning the statistical properties of the interaction matrix in the basis of non-interacting eigenstates (9). The direct proof of the enhancement of the two-particle localization length in comparison to the one-particle one was subject of many numerical investigations following the initial work.

### 3.1.2 Transfer matrix method

First direct evidence for the interaction assisted transport was put forward by Frahm *et al* [123]. The transfer matrix method [29, 30, 31] was employed to study finite samples of size  $L=100$ . The configuration space of the two electrons was then a  $100\times 100$  square lattice and the transfer matrix was calculated along one of the main axes. Averaging was performed by studying a number of samples with different random potential realization. The two-particle localization length defined as the inverse of the smallest Lyapunov exponent was shown to depend on disorder as

$$\lambda_2 \propto W^{-3.3} \propto \lambda_1^{1.65}. \quad (12)$$

In addition, the transfer matrix was calculated along the diagonal of the configuration space, see also [6]. The necessarily fixed transverse size was obtained by restricting the relative coordinate to be smaller than a certain size, hence the name “bag model”. The observed delocalization was similar to the one reported for the finite samples, equation (12). The deviation from Shepelyansky’s prediction,  $\lambda_2 \propto \lambda_1^2$ , were traced back to the statistical properties of the interaction matrix, section 3.3.2. Instead of being Gaussian, the distribution of interaction matrix elements was characterized by a sharp peak at zero and very long tails. Depending on the averaging procedure used to extract a typical value in order to improve the block scaling picture described above, agreement with the result obtained with transfer matrix method, equation (12), was reported.

Unfortunately it was shown later that the transfer matrix method, widely used to calculate localization properties for non-interacting particles, suffered from problems in the interacting case. The main one was the failure to reproduce correctly the result without interaction,  $\lambda_2 = c\lambda_1$ , with a constant  $c \approx 0.5$ .

First, it was shown by Römer and Schreiber [124] that in the finite size transfer matrix calculation the result without interaction was enhanced compared to the one-particle localization length. The on-site interaction gave only a small additional enhancement. Upon studying systematically the system size dependence they found that both  $\lambda_2(U=0)$  and  $\lambda_2(U=1)$  decreased with increasing system size and that both approached the one-particle result in the limit of infinite system size. In a subsequent comment [125] results in favor of the delocalization effect were listed without discussing the question why the method failed. In the reply [126] the failure of the method was stressed again, leaving open the task to prove the existence of the delocalization effect by some other method.

Second, it was shown by Halfpap *et al* [127, 128] and Römer *et al* [129] that also for the bag model, the localization length in the absence of the interaction was enhanced in comparison to the single particle one. The influence of the on-site or medium range interaction was rather weak since the behavior of the localization length was dominated by a boundary effect. Although it could be interpreted as a kind of interaction, a detailed study of the disorder or interaction dependence of the localization length was not possible. A discretization of the Schrödinger equation in center of mass and relative coordinates suggested by Halfpap *et al* reduced the influence of the boundary *and* of the interaction [127, 128]. While the zero disorder limit, equation (6), could be performed in contrast to [123], again the one-particle localization length could not be reproduced for  $U=0$ . However, in this case it was not a failure of the method since similar results were obtained using a quantum diffusion method [130]. Especially, it was shown with both methods, that the localization length diverged

exponentially for small disorder in the limit of infinite system size [130]. Both, the problem with the  $U = 0$  limit and the divergence for small disorder, seemed to be related to the discretization procedure, but that is not completely understood yet.

Since the transfer matrix method is one of the best methods to calculate localization lengths for non-interacting particles, there is some need to understand why it does not work for interacting particles. Therefore, I will try to clarify the issue, starting from the overestimation of the localization length without interaction.

An infinite quasi one-dimensional sample with  $N$  channels is characterized by a set of  $N$  Lyapunov exponents,  $\gamma_1 > \dots > \gamma_i > \dots > \gamma_N$ , describing the exponential behavior of initial conditions. The inverse of the smallest Lyapunov exponent  $\gamma_N$  defines the localization length. Another sample with a different realization of the random potential gives exactly the same result since averaging over the random potential is performed due to the *infinite* size of the sample. For a *finite* size of the sample, different sets of disorder give different results,  $\gamma_i^m$ , distributed according to a distribution  $\{\gamma_i^m\}$  for each Lyapunov exponent. In all numerical calculations, essentially the mean value of  $\{\gamma_N^m\}$  is calculated due to the necessary orthogonalizations [127]. The numerical algorithm was proven to give an approximate value of the Lyapunov exponent in the infinite system [131]. Hence, one can assume that each distribution  $\{\gamma_i^m\}$  is centered around the limiting value of the infinite size sample,  $\gamma_i$ , with a width,  $\sigma_{\gamma_i}$ , which decreases with increasing sample length. The key parameter to understand the observed behavior is the ratio of the spacing between consecutive Lyapunov exponents,  $\Delta\gamma$ , and the width of their distributions,  $\sigma_{\gamma_i}$ . This ratio is large for reasonable system sizes since  $\Delta\gamma$  is large in a calculation for a non-interacting system, figure 1. The smallest

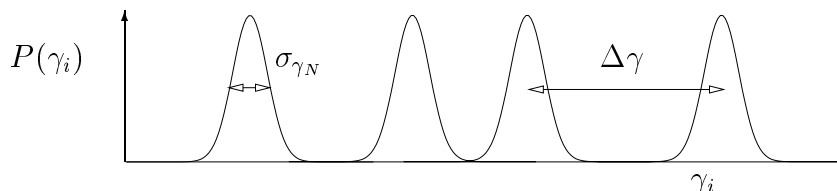


Figure 1: Qualitative distributions  $P(\gamma_i)$  for different Lyapunov exponents  $\gamma_i$  of a quasi one-dimensional non-interacting system.

calculated Lyapunov exponent,  $\gamma_{\min}^m \equiv \min(\gamma_1^m, \dots, \gamma_i^m, \dots, \gamma_N^m)$ , coincides almost always with  $\gamma_N^m$ . Averaging  $\gamma_{\min}^m$  over a number of samples is calculating the mean value of the distribution  $\{\gamma_N^m\}$  and hence approximates correctly the limiting value for an infinite sample. The calculation for a two-dimensional system in [124] gave the correct localization length up to  $\lambda_{2D} \approx 25$ , where finite size effects came into play.

For two particles, the situation is different. The transfer matrix calculation is performed in configuration space, each channel has the *same* disorder potential. The only difference between them is the energy. In this situation, the spacing between the lowest consecutive Lyapunov exponents is small, figure 2. This is reflected by the large fluctuations as a function of the interaction strength shown in figure 1 in [123]. Therefore, the average of  $\gamma_{\min}^m$  is *not* sampling only the distribution corresponding to the smallest Lyapunov exponent of the infinite system,  $\{\gamma_N^m\}$ . Whenever another exponent  $\gamma_{i \neq N}^m$  is smaller than  $\gamma_N^m$ , the arithmetic mean value  $\overline{\gamma_{\min}^m}$  underestimates the Lyapunov exponent for the infinite system

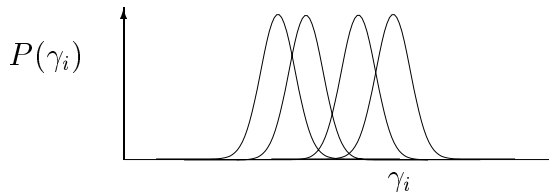


Figure 2: Qualitative distributions  $P(\gamma_i)$  for different Lyapunov exponents  $\gamma_i$  of the finite size transfer matrix calculation for two particles.

$\gamma_N$ , overestimating the localization length. Increasing the system size decreases the widths of the distributions and correspondingly reduces the number of cases with  $\gamma_{\min}^m \neq \gamma_N^m$ . In the limit of an infinite sample,  $\gamma_{\min}^m = \gamma_N^m = \gamma_N$  giving the correct localization length in agreement with the extrapolation in [124].

In the presence of an interaction between the two particles, the argument of the preceding paragraph has to be modified only slightly: along the direction of the transfer matrix calculation there are paths which are not influenced and those which are influenced by the interaction. The latter lie along the diagonal of the configuration space and are suppressed by a factor of  $\sqrt{2}$  since the distance from one end of the sample to the other is longer along the diagonal than along the coordinate axis. Hence, in addition to the situation described above, there is another distribution corresponding to Lyapunov exponents influenced by the interaction. The mean value of this distribution is supposed to be smaller than  $\gamma_N$ , for small enough disorder, compare with the discussion on page 12. This is the delocalization due to the interaction. The existence of this distribution with even smaller values of  $\gamma_i^m$  reduces  $\overline{\gamma_{\min}}$  compared to  $\overline{\gamma_{\min}}(U=0)$ , resulting in the small enhancement of  $\lambda_2(U=1)$  compared to  $\lambda_2(U=0)$  [124]. However, upon increasing the system size, the calculated localization length is reduced as described above and shown in [124]. Only for system sizes that allow for a separation of the distributions corresponding to the channels with and without influence of the interaction, an estimate of the two-particle localization length in the presence of interaction is possible. In the limit of infinite system size, the largest localization length will be calculated and this should be the two-particle one. Unfortunately, the systems sizes required for a numerical proof are too large. Estimates based on a careful investigation on the distribution of Lyapunov exponents suggested sizes definitely larger than  $N=2500$ , more probable are sizes around  $N=100000$  [132].

### 3.1.3 Green function method

Another possibility to study the localization properties of interacting particles was needed. For non-interacting electrons also the Green function method was very successful. The one-particle Green function,  $G_1$ , contained information about all the eigenstates of the Hamiltonian and a localization length could be defined via the exponential decay of the matrix elements [28, 29].

$$G_1(E, n, m) = \sum_{\alpha} \frac{\phi_{\alpha}(n)\phi_{\alpha}(m)}{E - E_{\alpha}}, \quad (13)$$

$$\frac{1}{\lambda_1} = - \lim_{|n-m| \rightarrow \infty} \frac{1}{|n-m|} \ln |\langle n | G_1 | m \rangle|. \quad (14)$$

The generalization of this method to the two-particle Green function  $G$  was a natural approach. Von Oppen *et al* [133] defined a two-particle localization length using matrix elements between double occupied sites,

$$\frac{1}{\lambda_2} = - \lim_{|n-m| \rightarrow \infty} \frac{1}{|n-m|} \ln |\langle n, n | G | m, m \rangle|. \quad (15)$$

Projecting the Dyson equation  $G = G_0 + G_0 \hat{U} G$ , where  $G_0$  denotes the two-particle Green function in the absence of the interaction and  $\hat{U} = U \hat{P} = U \sum_n |n\rangle \langle n|$ , onto double occupied sites and solving for  $\tilde{G} = \hat{P} G \hat{P}$  yielded,

$$\tilde{G} = \frac{\tilde{G}_0}{U} \frac{1}{1/U - \tilde{G}_0}, \quad (16)$$

$$\langle n, n | \tilde{G}_0 | m, m \rangle = \sum_{\alpha, \beta} \frac{\phi_\alpha(n) \phi_\beta(n) \phi_\alpha(m) \phi_\beta(m)}{E - E_\alpha - E_\beta}. \quad (17)$$

Arguing that the first part of equation (16) decays on the scale  $\lambda_1$ , only the second part was investigated, interpreting it as the Green function of some "Hamiltonian"  $\tilde{G}_0$  at "energy"  $1/U$ . Solving first the non-interacting Anderson model to calculate  $\tilde{G}_0$ , neglecting exponentially small matrix elements in order to obtain a band matrix, and employing then efficient recursive Green function methods [134] to calculate  $\tilde{G}$ , the following scaling behavior was observed,

$$\frac{\lambda_2}{\lambda_1} = f\left(\frac{U\lambda_1}{V}\right) = \frac{1}{2} + C \frac{|U|\lambda_1}{\pi V}, \quad (18)$$

where  $C$  was a constant and  $V(=1)$  the hopping matrix element. The  $U=0$  limit was conjectured from the data. The approximation to neglect the first factor of equation (16) could not be justified in this limit. Though the problem of this limit still existed, at least the extrapolation worked and the error seemed to be only an artifact of the method. However, equation (18) contradicted the findings by Shepelyansky and Imry in being linear instead of quadratic in the interaction strength. The extrapolation to  $U=0$  could not be done within their approaches.

In a subsequent work, the above results were generalized to an approximate treatment of finite densities [135]. Assuming the existence of a Fermi surface and considering the scattering of only two particles above it without creation of additional particle-hole pairs, the same method could be employed. The only difference was that for the calculation of  $\tilde{G}_0$  only states above the Fermi energy were used. For small excitation energies close to the Fermi energy the enhancement effect disappeared since only a small fraction of all states was available to build up the two-particle wave function. For larger excitation energies, the delocalization effect was recovered, the relevant energy scale is the bandwidth.

Later, Song and Kim studied the localization length defined in equation (15), by calculating the two-particle Green's function without any approximation [8]. Without interaction,

$$\lambda_2(U=0, W) \approx 70W^{-2.1 \pm 0.1}, \quad (19)$$

slightly larger than the predicted  $\lambda_1/2$  but with the correct disorder dependence in contrast to the transfer matrix method results. This discrepancy was conjectured to be related to energy averaging since only the two-particle energy was well defined,

$$\langle 1, 1 | G_2(0) | M, M \rangle \sim \int dE \langle 1 | G_1(E) | M \rangle \langle 1 | G_1(-E) | M \rangle. \quad (20)$$

For  $U \neq 0$ , Song and Kim used the idea of finite size scaling, section 4.2, and obtained the localization length in the limit of an infinite system size,

$$\lambda_2^\infty(U=1, W) \sim W^{-2.9 \pm 0.2}. \quad (21)$$

All data could be scaled reasonably well by assuming a scaling form

$$\lambda_2(U, W) = W^{-2.1} g(|U|W^{-\Delta}) \quad \text{with} \quad \Delta = 4.0 \pm 0.5. \quad (22)$$

This first numerically exact method by Song and Kim gave strong evidence for the existence of interaction-induced delocalization. For the first time a direct comparison of the data with and without interaction was possible. But the effect was much weaker than predicted before.

Generalizing this method, Song and von Oppen used the two-particle Green function to define a set of different localization lengths, depending on the direction in configuration space, along which the decay of the Green function was studied [136]. Since the projection of the Dyson equation did not work in this situation, a decimation scheme was used to get iteratively rid of all irrelevant matrix elements of the Green function. Three main results were obtained. First, decay lengths measured along the center of mass direction  $\lambda_{2,a}$  in configuration space were strongly enhanced by the interaction. No dependence on the fixed relative coordinate  $a$  even for  $a > \lambda_1$  was found. Second, for fixed center of mass coordinate the decay along the relative coordinate was hardly influenced by the interaction. Third, the one-particle decay length  $\lambda_f$  parallel to one axes in configuration space was larger by almost a factor of 2 than  $\lambda_{2,a}$  at  $U = 0$ , but increased only weakly with the interaction. Hence, a critical  $U_c$  existed beyond which  $\lambda_f < \lambda_{2,a}$ . Only for  $U > U_c$ , the shape of the wave function was highly anisotropic [137, 138, 139, 140] and the transfer matrix calculation for finite size systems could reveal an enhancement in the limit of large system sizes.

Another type of decimation method for evaluating the matrix elements of the two-particle Green function was proposed by Leadbeater *et al* [9]. Good agreement of  $\lambda_2(U=0)$ , defined via equation (15), with the expected  $\lambda_1/2$  was reported. The two-particle localization length was only slightly larger than  $\lambda_1/2$ . A direct evaluation of the integral in equation (20) proved the conjecture by Song and Kim [8]. For small  $|U|$ ,  $\lambda_2$  increased linearly with  $|U|$ . For large  $|U|$ ,  $\lambda_2$  decreased again when the interaction started to split the band into lower and upper Hubbard band. A duality between  $U$  and  $\sqrt{24}/U$  found from level statistics in [141], section 3.2.5, was in accordance with the data only for  $W = 5$ . The position of the strongest enhancement was disorder dependent. Upon changing the energy, the sign of the interaction became relevant and the data was consistent with  $\lambda_2(U, E) = \lambda_2(-U, -E)$  as pointed out by Halfpap *et al* [128]. For a negative energy, i. e. closer to the ground state, an attractive interaction  $U = -1$  was more favorable for delocalization. After having applied a finite size scaling procedure, section 4.2,  $\lambda_2^\infty(U, W) \propto W^{-\alpha(U)}$  was reported with  $2.2 \leq \alpha(U) \leq 3.1$ . Since

after the finite size scaling the localization length for  $U = 0$  was slightly larger than before, all comparisons have been made with  $\lambda_2^\infty(0, W)$ . Based on a random matrix model, which was more appropriate than the one derived by Shepelyansky, the following fit function was proposed in [142] which was better than equation (10) for smaller values of the localization length,

$$\lambda_2^\infty(U, W) \propto \lambda_2^\infty(0, W)^{\beta(U)} \left( 1 + \frac{c}{\lambda_2^\infty(0, W)} \right). \quad (23)$$

Taking into account the second term ( $C \neq 0$ ) improved the fits. Values of  $\beta(U)$  between 1 and 1.5 were found [9]. Rewriting the fit proposed by von Oppen *et al* [133], page 11, as

$$\lambda_2^\infty(U, W) - \lambda_2^\infty(0, W) \propto \lambda_2^\infty(0, W)^\beta, \quad (24)$$

$\beta \approx 2$  was found for  $\lambda_2^\infty(0) < 10$ . For larger localization lengths,  $\beta \approx 1.5$  was more appropriate. The scaling form proposed in [8], equation (22), did not work for all interaction strengths but a reasonable scaling of all data could be obtained using

$$\lambda_2^\infty(U, W) - \lambda_2^\infty(0, W) = g[f(U)\lambda_2^\infty(0, W)]. \quad (25)$$

The slope of  $g$  exhibited a crossover from 2 for small localization lengths to 1.5 for larger ones. The functional dependence of  $f(U)$  could be described with a crossover from  $\sqrt{U}$  to  $U$  for increasing  $U$ , leading to a crossover from a  $U$  to a  $U^2$  dependence for the two-particle localization length in the regime in which the slope of  $g$  equals 2. Such a crossover was predicted in [143], discussed on page 18, but for larger  $U$  and independent on the disorder. The best functional form for  $f(U)$  was a logarithmic one.

The same decimation method was also used to study the delocalization effect for an interacting electron-hole pair [144], which might be important for an experimental realization [145]. The only difference was that the two particles move in different random potentials. The results were very similar to the two interacting particle problem, the only difference was that scaling with equation (25) yielded a single slope of  $g$  of 1.6 for *all* data points.

Another method for calculating the two-particle Green function was put forward by Frahm [7], using the relation between the Green functions with and without interaction,  $G_0$  and  $G$ , equation (16). Essentially one just had to calculate the non-interacting two-particle Green function  $G_0$  and multiply it with the inverse of  $1 - G_0 U$ . The numerical calculation of the inverse of a matrix scaled with the third power of the matrix size and required  $N^3$  operations. It was not the limiting factor since calculation of  $G_0$  according to equation (16) required  $N^4$  operations. Employing an elegant method to reduce this number of operations to  $N^3$ , larger system sizes could be reached. The limit of infinite system size was reached by an extrapolation of the data according to

$$\frac{1}{\lambda_2(N)} \approx \frac{1}{\lambda_2(\infty)} + \frac{C}{N}. \quad (26)$$

Neglecting as in [133] the exponentially small elements of  $G_0$  in equation (16) and performing the matrix inverse by a recursive Green function technique [134, 146] the localization length was also calculated for quasi-infinite samples and shown to be similar to the extrapolated

values. Without interaction, again a slight enhancement of  $\lambda_2$  compared to  $\lambda_1/2$  was found as in [8, 9]. A number of different fit functions was tried for  $U \neq 0$ . The data was in qualitative agreement with the results by von Oppen *et al* [133],  $\lambda_2/\lambda_1 \approx 0.5 + 0.054|U|\lambda_1$ . Using the exponent of  $\lambda_1$  as an additional fit parameter, also  $\lambda_2/\lambda_1 - 0.5 \propto \lambda_1^\alpha$  with  $\alpha \approx 0.9$  did work,  $\alpha \approx 1.0$  was found for an offset of 0.55. The slight deviations from linearity could also be described by  $\lambda_2/\lambda_1 - 0.5 \propto \lambda_1/\ln(C\lambda_1)$  [147], see page 25. However, the best fit was obtained using  $\lambda_2 = a\lambda_1 + c(U)\lambda_1^2$ . A linear  $U$ -dependence as in [133] was found only for very small interaction strengths. The correction  $c(U) \propto |U|\sqrt{1 + (U/4)^2}$  proposed in [148], page 18, was also observed only for very small interaction strengths. Generalizing the arguments of [148],  $c(U) \approx A|U|/(|U| + 1)$  was derived analytically and shown to give excellent agreement with the numerical data.

Recently, the Green function method was used to study localization of two particles in a two-dimensional system. Ortuño and Cuevas [90] combined the approach of [7, 8, 133] with the finite size scaling procedure [29]. Calculating the localization length for systems of length  $L = 42$  and width  $M = 1 \dots 6$ , they reported a transition from localized to extended states. The critical disorder was  $W_c = 9.3 \pm 0.2$  and the critical exponent  $\nu = 2.4 \pm 0.5$  for  $U = 1$ . Römer *et al* used the decimation method [9, 144] to calculate the localization length for samples of length  $L = 52$  and widths  $M = 2 \dots 8$  [99]. They observed a transition to extended states for values of  $U \geq 0.4$  with a critical disorder  $W_c \propto U^{0.36 \pm 0.03}$  and a critical exponent decreasing with increasing interaction strength from 3.4 ( $U = 0.4$ ) to 2.3 ( $U = 2.0$ ). For  $U = 1$ , the exponent was slightly larger than reported in [90], while the critical disorder is a bit lower. This was attributed to a different definition of the two-particle localization length.

Both the transfer matrix method and the Green function method were proven to be very useful for calculating the localization properties of non-interacting electrons. But as discussed above, the transfer matrix method cannot be reliably applied to study localization of interacting particles, while this is still possible with the Green function method. So far, only localization lengths of two interacting particles have been calculated. A restriction of the configuration space to the subspace of double occupied sites led to a reduction of the numerical effort. This restriction cannot be generalized to higher particle numbers. While a generalization is in principle possible with the decimation method, one loses a main advantage of the method, namely that the influence of a Hubbard type interaction is important only at the last decimation step, close to the end of the numerical calculation. Hence, results for different interaction strengths are easily obtainable. It is also not a priori clear, which matrix elements to calculate from the  $n$ -particle Green function in order to get information about the localization properties.

In the main part of this thesis, I will introduce a completely different method to study localization of interacting particles. First, it is important to have a method which does not rely on Green function in order to check the results described above. Second, our method can be generalized straightforwardly to larger particle numbers.

In order to allow for a better classification, I will first review some different approaches not directly related to localization. This allows to discuss different aspects of the problem of few interacting particles in a random potential and their relation to localization properties.

## 3.2 Spectral statistics of interacting particles

### 3.2.1 Eigenstates

Direct information about the influence of interaction can be gained from the eigenstates of the two-particle problem.

Weinmann *et al* used the Lanczos algorithm to diagonalize the two-particle Hamiltonian for small rings [137]. A magnetic flux piercing the ring was used as a tool to find states with a correlated motion of the two electrons. Without interaction, the energy of the states should be  $h/e$  periodic with the magnetic flux. With interaction,  $h/2e$  periodic states were observed, indicating that two electrons move coherently through the ring. The corresponding wave functions showed a strong asymmetry, being further extended in center of mass than in relative direction. Although the existence of correlated two electron motion was directly demonstrated, the results did not allow more than a qualitative estimate of the two-particle localization length.

Araújo *et al* considered the Cooper problem and found by exact diagonalization that near the ground state an attractive interaction led to delocalization for small disorder while it enhanced localization for large disorder [149]. The filled Fermi sea was modeled by calculating first the non-interacting eigenstates. In diagonal representation of the eigenstates, a large energy was added to the energy of states below  $E_F$  before the Hamiltonian was transformed back to position representation. The resulting full matrix was used to construct the two-particle matrix.

Evangelou *et al* discussed different types of two-particle states [150]: most of the states were not influenced by the on site interaction (electrons far apart) while some states were delocalized by the interaction (electrons close to each other). States with two tightly bound electrons could be stronger localized due to the interaction.

### 3.2.2 Level curvatures

Edwards and Thouless had argued that the conductance of a disordered diffusive system of non-interacting electrons could be related to the dependence of energy levels on a change in the boundary conditions, the level curvature [151, 152]. The larger the level curvature, the larger was the conductance. This relation was verified numerically [153]. Although the relation between the conductance and the level curvature was not proven for interacting particles, it was a reasonable approach to analyze the level curvature for two particles.

This was done analytically by Akkermans and Pichard. The typical curvature was increased by the interaction in the localized regime ( $L \leq \lambda$ ), while it was decreased in the metallic regime ( $L \geq \lambda$ ) [154].

These results were supported by numerical calculations by Wobst and Weinmann [155]. The increase of the curvature in the localized regime was found to be most pronounced near the band center. Data for different disorder values and system sizes were scaled onto a common curve. The relevant scaling parameter was the typical curvature without interaction,  $g(0)$ , not size and disorder independently,

$$\frac{g(U)}{g(0)} = \left( \frac{g(0)}{g_{\text{crit}}} \right)^{m(U)}. \quad (27)$$

The slope of the scaling curve  $m(U)$  showed qualitatively the existence of the duality between small and large interaction strengths [141], page 21.

### 3.2.3 Random matrix theory

Information on the localization properties of interacting particles can also be gained from random matrix theory. The main idea is not to study a particular and often complicated Hamiltonian but rather the properties of a quite general one belonging to the same symmetry class. Originally, only three different classes of random matrices were considered, corresponding to systems with orthogonal, unitary or symplectic symmetry. This was very useful in the framework of nuclear physics where statistical properties of energy spectra could be understood on the basis of random matrix theory. For example the distribution of spacings between consecutive energy levels in a uranium nucleus agreed well with the predictions of random matrix theory. In the beginning of the 1980s, the importance of random matrix theory for understanding the properties of disordered solids was realized. Based on work by Efetov [19], it was shown that the physics of diffusive electron transport could be described by random matrix theory [156]. For example, the nearest neighbor level spacing statistic in a diffusive conductor was in accordance with the predictions of random matrix theory. It followed the famous Wigner surmise,

$$P_W(s) = \frac{\pi s}{2} e^{-\pi^2 s^2/4}, \quad (28)$$

with the spacing between consecutive levels  $s$ . Actually, equation (28) was derived for  $(2 \times 2)$ -matrices but is a very accurate approximation for the general case of  $(N \times N)$ -matrices. Its main feature is the level repulsion for small spacings, i. e.  $P_W(s=0) = 0$ . In contrast, for a system with localized states, the spacing statistics is Poisson,

$$P_P(s) = e^{-s}, \quad (29)$$

revealing a high probability to find consecutive levels with small spacings,  $P_P(s=0) = 0$ . Since the transition from Wigner to Poisson statistics that takes place upon increasing the disorder in order to drive the metal-insulator transition cannot be analyzed within the original random matrix theory, suitable generalizations were proposed. For example, a Poisson statistic was observed for band random matrices, characterized by having only a limited number of  $2b + 1$  non-zero diagonals. For  $b \approx N$ , these matrices were nearly filled and display a Wigner Dyson statistic, the eigenstates were extended. For  $b^2 \leq N$ , the matrices were more sparse and the energy levels followed the Poisson statistic, the eigenstates were localized. In the context of the two interacting particle problem yet another type of random matrix was important as can already be seen from the work of Shepelyansky [6]. He mapped the Hamiltonian in the basis of non-interacting two-particle states onto a band random matrix with an additional, strongly fluctuating diagonal part. The band random matrix arised from the matrix elements of the interaction in that basis, equation (9). The additional diagonal part was the sum of the two one-particle energies and indicated the existence of a preferential basis. The matrix was different in the basis of the non-interacting two-particle eigenstates, while generally the statistical properties of random matrices were independent on the chosen basis. Although this approach neglected completely the correlations among the matrix

elements, it was the starting point for further investigations.

Frahm and Müller-Groeling [157] and independently Fyodorov and Mirlin [158] derived analytical results for the band random matrix with a preferential basis invoked by Shepelyansky based on earlier work for band random matrices [159, 160, 161]. These results explained and generalized numerical work by Jacquod and Shepelyansky [162]. The local density of states,  $\rho_W$ , which characterized the spreading of the eigenstates over the states of the original, preferential basis was shown to have a Breit-Wigner form,

$$\rho_W(E - E_n) \equiv \sum_i |\psi_i(n)|^2 \delta(E - E_i) = \frac{\Gamma}{2\pi[(E - E_n)^2 + \Gamma^2/4]} \equiv \rho_{\text{BW}}, \quad (30)$$

where  $n$  labels the states of the preferential basis and  $\psi_i(n)$  and  $E_i$  are the eigenstates and corresponding energies. The spread width  $\Gamma$  gave roughly the number of states of the preferential basis that contribute to an eigenstate. With  $b$  the bandwidth,  $W_b$  the variance of the diagonal entries, and a variance of the off-diagonal elements scaling with  $b^{-1/2}$ , the following results were obtained for the spread width  $\Gamma$ , the localization length  $\xi$ , defined as exponential decay length of the envelope, and the inverse participation ratio  $\xi_{\text{IPR}}$  in the localized regime [123],

$$\Gamma = \frac{\pi}{3W_b} \left(1 - \frac{1}{3W_b^2}\right), \quad (31)$$

$$\xi = \frac{\pi^2 b^2}{18W_b^2} \left(1 - \frac{2}{3W_b^2}\right), \quad (32)$$

$$\xi_{\text{IPR}} = \frac{\pi^2 \xi}{12W_b^2}. \quad (33)$$

Especially the last result was interesting since  $\xi_{\text{IPR}} \neq \xi$ . This discrepancy was related to the spiky structure of the eigenstates [162]. For the two-particle problem, one had  $b = \lambda_1^2$ ,  $W_b \approx V\sqrt{\lambda_1}/U$  and  $\lambda_2 = \xi/\lambda_1$  [6, 123] leading in first order to equation (10). The ratio of the two-particle localization length to the one-particle localization length was,

$$\frac{\lambda_2}{\lambda_1} = \frac{\xi}{\lambda_1^2} = \frac{\xi}{b} = \frac{\pi}{3W_b} \frac{b}{W_b} \frac{\pi}{6} = \Gamma \rho A = A \frac{\Gamma}{\Delta_2}, \quad (34)$$

where  $A$  was a constant and  $\rho = b/W_b$  was the density of coupled states, given as total number of coupled states divided by the bandwidth. For a system of size  $L = \lambda_1$  this was identical to the inverse of the mean level spacing  $\Delta_2$ . This leads us back to the block scaling picture employed by Imry [121], page 7, since  $\Gamma = t^2/\Delta_2$  was estimated using Fermi's golden rule [143]. Studying  $\Gamma$  for systems of size  $L = \lambda_1$  can thus give information about localization on much larger length scales, provided the mapping to the random matrix model is correct.

### 3.2.4 Breit-Wigner width

This relation between the Breit-Wigner width  $\Gamma$ , introduced in equation (30), and the localization length was exploited by Jacquod *et al* [148] who calculated  $\Gamma$  for the clean system

analytically. With moderate disorder, i. e. large  $\lambda_1$ ,  $\Gamma$  was either zero, if the particles are far apart, or given by the value on the scale  $L = \lambda_1$ . The enhancement effect was then calculated according to equation (34). Taking into account the correct two-particle density of states  $\rho(E)$  [130], they reported  $\Gamma \propto U/\sqrt{1+U^2}$  for small  $U$  and  $E^2 \ll U^2$ , and  $\Gamma \propto U^2$  for  $E^2 \gg U^2$  and supported their results by numerical calculations of  $\Gamma$ .

To observe the  $U^2$  behavior of the localization length, one needed small  $U$  values, leading to small  $\Gamma$ . Since the enhancement effect was given by  $\Gamma\rho > 1$  this required larger values of  $\lambda_1$  than available in direct studies of the localization length so far.

In a subsequent work, the study of the Breit-Wigner width was generalized to quasi-particles [163, 164]. Upon constructing the two-particle Hamiltonian in the basis of non-interacting eigenstates, only states above the Fermi sea were used to calculate the interaction matrix,  $E_{m_1}, E_{m_2} \geq E_F$  in equation (8). As done by von Oppen *et al* [135], intermediate electron-hole excitations were neglected. For small excitation energies, a linear increase of  $\Gamma$  was found as expected from the density of available scattering states and the enhancement effect vanished. However, unexpectedly it was found that this behavior depends crucially on the disorder strength. For slightly higher disorder,  $\Gamma$  became independent of the energy in both two- and three-dimensional systems. The reason was shown to be a failure of the ergodic analytical estimate of  $\Gamma$  which was not understood. These results showed that the restriction due to the Pauli principle is less severe in higher dimensions. Possibly even parameter regions exist in which the enhancement effect survives for arbitrarily small excitation energy. In three dimensions, evidence for extended states,  $\Gamma\rho > 1$ , was put forward for disorder values *larger* than the critical disorder for single particles.

A slightly different approach was used by Weinmann and Pichard [143]. Studying the two-particle Hamiltonian in the basis of non-interacting eigenstates (8), they also found the Breit-Wigner form for the local density of states (30). For a detailed analysis, they did not calculate  $\rho_W$  but the number variance  $\Sigma_2(E)$ , for which the knowledge of the energies was sufficient. For energies  $E < \Gamma$  the levels were correlated and followed the Wigner Dyson predictions. On scales  $E > E_c(U) \approx \Gamma$  the levels became uncorrelated. This crossover was studied via  $\Sigma_2(E)$ , the variance of the number of levels in a given energy interval  $E$ . For small interaction strengths, a linear increase of the crossover energy  $E_c$  with  $U$  was found. This was related to Rabi-oscillations between just two consecutive levels for  $E_c < \Delta_2$ . For larger interaction,  $E_c$  scaled with  $U^2$ , the crossover occurred for  $E_c > \Delta_2$ . While this was seen in two dimensions, in one dimension the considered values of  $\lambda_1$  were too small. Before the crossover was observed, the upper Hubbard band started to split and  $E_c$  decreased, see page 21. The main results concerning  $E_c$  were confirmed using a random matrix model with a preferential basis, analyzed before in [165]. For stronger and stronger influence of the preferential basis the crossover from Wigner-Dyson to Poisson behavior occurred for lower and lower excitation energies. The dependence of this crossover on the strength of the preferential basis, the ratio of diagonal to off-diagonal elements, showed the same two regimes as the two-particle problem. Relating the results for  $E_c$  to the localization length, arguments for  $\lambda_2/\lambda_1 - 1/2 \propto U\sqrt{\lambda_1}$  in the regime of the Rabi-oscillations (small  $U$ ) were given.

The approach by Weinmann and Pichard was extended to  $n$  particles by Weinmann *et al* [166]. The main difference was that due to the two-body interaction, states directly coupled ( $\Gamma^{(d)}$ ) were roughly  $\Delta_2$  apart and states consecutive in energy ( $\Delta_3$ ) were coupled only via

higher order terms in a perturbation theory in the interaction strength ( $\Gamma^{(i)}$ ). In contrast to the two-particle case, the spread width  $\Gamma$  as calculated from the Breit Wigner form of the local density of states was *not* related to the energy  $E_c$  below which the spectrum shows Wigner-Dyson rigidity. While  $\Gamma^{(i)}$  defined the scale important for spectral statistics, the local density of states was dominated by the larger of the two terms.

This hierarchy of coupled states led to the existence of three different regimes, depending on the interaction strength. For  $U < U_{c1}$  again Rabi-oscillations between a few coupled states occurred. The effective interaction matrix elements scaled as  $U_n^{\text{eff}} \propto U^{n/2}$  and  $U_n^{\text{eff}} \propto U^{(n+1)/2}$  for  $n$  even and odd, respectively. This  $U_n^{\text{eff}}$  defined as before the scale below which the Wigner Dyson rigidity existed. At  $U_{c1}$ , the coupling between neighboring energy levels  $\Gamma_n^{(i)}$  was of the same order as the  $\Delta_n$  and the nearest neighbor level spacing distribution showed a sharp crossover from Poisson (29) to Wigner-Dyson (28) behavior. At the same interaction strength,  $\Gamma^{(d)}$  equaled  $\Delta_2$ . This indicated a breakdown of perturbation theory since higher order terms had the same order of magnitude than first order terms and the perturbation series did not converge. However, a complete mixing of all basis states, related to ergodicity, did not take place until at  $U_{c2}$ ,  $\Gamma_n^{(i)}$  was of the order of  $\Delta_2$ , the level spacing of directly coupled levels. In this regime,  $\Gamma_n^{(i)} \propto U^{n/(n-1)}$  was predicted, now setting the scale for both the local density of states and the spectral statistics. These results were confirmed qualitatively by numerical diagonalization of  $3 \times 3 \times 3$  systems with three particles. The nearest neighbor level spacing distribution exhibited a crossover from Poisson to Wigner-Dyson behavior as a function of the interaction strength related to  $U_{c1}$ . In order to define the energy scale at which deviations from Wigner-Dyson behavior occurred,  $\Sigma_2(E)$  was investigated. For  $U < U_{c1}$ ,  $E_c$  scaled with  $U^2$ , as predicted. For  $U > U_{c1}$ ,  $E_c$  scaled with  $U$ , indicating the breakdown of perturbation theory from which  $E_c \propto \Gamma_3^{(i)} \propto U^4$  was expected. So far, there is no explanation for this linear increase,  $E_c \propto U$ . Calculating  $\Gamma_3$  from the local density of states (30), at  $U_{c2}$  a crossover with increasing interaction strength from  $\Gamma_3 \propto U^2$  (as for two particles) to  $\Gamma_3 \propto U^{3/2}$  (ergodic mixing) was observed. For smaller interaction strengths,  $\Gamma_3$  was dominated only by  $\Gamma_3^{(d)}$  and did not show any change at  $U_{c1}$ .

The Breit Wigner width was also used to investigate the level statistics within the two-body random interaction model. In this model,  $n$  fermions are located on  $m$  orbitals with random one-particle energies  $\epsilon_m \in [0, m]$ . These states are coupled via randomly distributed two-body interaction matrix elements,  $U_{n_i, n_j} \in [-U, U]$ . Due to the absence of hopping, this model is conceptually simpler than the Anderson model. Nevertheless, it can provide insight into the influence of a realistic interaction.

Georgot and Shepelyansky showed that the local density of states of the two-body random interaction model had the Breit-Wigner form and investigated the dependence of the spread width  $\Gamma$  and of the inverse participation ratio  $\xi$  on the interaction strength [167]. Their numerical results were well described by the Fermi golden rule estimate  $\Gamma = U^2 \rho_c 2\pi/3$ , with the density of coupled states  $\rho_c$ . The inverse participation ratio was shown to follow  $\xi \approx \Gamma \rho_n \approx 2U^2 \rho_c \rho_n$ , valid for  $U_c \approx 1/\rho_c$ . At  $U_c$ , all states were well coupled and the nearest neighbor spacing distribution shows a transition from Poisson to Wigner-Dyson behavior [168], compare with the result for the Anderson Hamiltonian in [166]. In addition, the behavior of the quantities above was investigated close to the Fermi energy. Taking into account that at a low temperature  $T$  only few particles interacted and that the effective

density of states was reduced near  $E_F$ , a critical temperature and correspondingly a critical excitation energy at which the transition to the Wigner-Dyson regime takes place was found [168]. These critical quantities were related to the question of the quasi-particle lifetime in finite systems discussed in [169, 170, 171, 172, 173].

Studying analytically the Breit-Wigner width, Shepelyansky and Sushkov found that the three-particle localization length scales as  $\lambda_3 \propto \lambda_1^3$  [174]. Their argument was based on an estimate for the average coupling in second order perturbation theory between two different three-particle states assuming that they were all within a distance  $\lambda_1$ ,  $U \sim (U_{12}U_{23})/(\lambda_1^3\Delta_1)$ . The spread width was then roughly given by  $\Gamma_1 \sim U^2\rho_3$ , see page 17, with  $\rho_3$  the density of three-particle states inside the one-dimensional block of size  $\lambda_1$ . The three-particle localization length was only a few steps away. For one of the particles, the average transition rate had to be multiplied by the frequency of collisions involving this particle,  $\tilde{\Gamma}_1 \sim \Gamma_1\lambda_1/\lambda_2$ , using the ergodicity inside the block. A diffusion rate  $D \sim \tilde{\Gamma}_1\lambda_1^2$  followed since the average transition size was  $\lambda_1$ . From the diffusion rate they estimated a localization time at which diffusion stopped since the energy resolution became better than the mean level spacing. This yielded the above result for the three-particle localization length. All the steps in the argument have to be considered carefully since for example it was shown that the wave packet did *not* grow diffusively, but rather logarithmically in time [139, 140], see pages 26 and 46.

### 3.2.5 Nearest neighbor spacing distribution $P(s)$

In contrast to the number variance  $\Sigma_2(E)$  or the Breit Wigner width  $\Gamma$ , which contain information about long-range spectral correlations, the nearest neighbor spacing distribution  $P(s)$  provides information about short-range fluctuations. As described in section 3.2.3, a transition from Poisson (29) to Wigner-Dyson behavior (28) takes place if neighboring states are strongly coupled by the interaction. Only in the *insulating* regime this interaction-induced coupling of non-interacting eigenstates leads to a delocalization in real space. In the metallic regime, the relation between eigenstates and localization lengths is much less clear. For non-interacting particles, the transition from Poisson to Wigner-Dyson occurs with decreasing disorder strength and the metal-insulator transition can be identified investigating the size dependence of  $P(s)$  for different disorder values. In the insulating regime,  $P(s)$  moves closer and closer to a Poisson distribution with increasing system size, in the metallic regime it moves closer and closer to the Wigner-Dyson distribution. At the critical point, a different, size-independent distribution was observed [175]. In order to measure the distance to the Poisson or the Wigner-Dyson distribution, a scaling variable  $\eta$  was defined that changes smoothly from 0 (Wigner-Dyson) to 1 (Poisson),

$$\eta = \frac{\int_0^{s_0} (P(s) - P_W(s)) ds}{\int_0^{s_0} (P_P(s) - P_W(s)) ds}, \quad (35)$$

with  $s_0 = 0.4729 \dots$ , the first intersection point of  $P_P(s)$  and  $P_W(s)$ . Sometimes a different measure was used,

$$\gamma = \frac{\text{var}[P(s)] - \text{var}[P_W(s)]}{\text{var}[P_P(s)] - \text{var}[P_W(s)]}. \quad (36)$$

Waintal *et al* used this method to study the level statistics for two interacting particles [141]. For systems of size  $L = \lambda_1$ ,  $\eta(U)$  decreased for increasing  $U$  from 1 to a minimal value of 0.386 at  $U \approx 2$  and increased for larger  $U$  again to the Poisson value. Chaotic mixing of the levels as described by the Wigner distribution was not reached for two particles with an on-site interaction in one dimension. The increase of  $\eta$  for large  $U$  was related to the existence of a different preferential basis for  $U \rightarrow \infty$ . For small interaction strengths, the non-interacting eigenstates formed a preferential basis, see page 16. In the opposite limit, the preferential basis found in [142] consisted of molecular states in the upper Hubbard band [176] and hard core boson states in lower Hubbard band. Investigating the interaction matrix (9) in both limits, a duality transformation  $U \rightarrow \sqrt{24}t^2/U$  was found analytically and confirmed numerically by studying the Breit-Wigner width. This explained the symmetry observed in  $\eta(U)$ . At the “critical” interaction strength where maximum mixing of the states occurred,  $\eta(W)$  showed a similar behavior as  $\eta(U)$ , decreasing with increasing disorder down to a minimal value reached for  $\lambda_1(W) \approx L$ . For  $L > \lambda_1(W)$ ,  $\eta$  increased back to 1. In the regime of maximum mixing,  $P(s)$  was close to the semi-Poisson,  $P(s) = 4s \exp(-2s)$ , also found at the mobility edge of the three-dimensional Anderson Hamiltonian [175]. The wave functions exhibited a multifractal behavior.

Qualitatively the same behavior was found by Halfpap *et al* for  $\gamma(U)$  [176]. In addition, the density of states was discussed. For small interaction strengths, it was similar to the one of a single particle in two dimensions while for larger interactions the upper Hubbard band with the molecular states discussed in [141, 142, 150] appeared. The density of states was important for the detailed evaluation of  $\Gamma$  in [148], page 18. For three particles, Halfpap *et al* found a density of states similar to the one of the three-dimensional one-particle problem [130]. This finding holds in general for  $n$  particles since for small disorder and interaction strength only the hopping terms are relevant and they equal those of the  $n$ -dimensional one-particle problem, page 37. Using the number variance  $\Sigma_2(E)$ , a smooth crossover to a Wigner distribution with increasing interaction strength at fixed size  $L \approx \lambda_1$  was demonstrated for  $n=3$  [130].

For two particles in two dimension, Cuevas studied  $\gamma(W)$  for long and short range interactions and system sizes  $L \times L$  with  $6 \leq L \leq 20$  [91]. In both cases a critical behavior was observed and analyzed based on the finite size scaling method, discussed in section 4.2. For long range interactions the critical disorder and the critical exponent were  $W_c = 10.2 \pm 0.2$  and  $\nu = 1.2 \pm 0.2$ , respectively. The critical disorder increased monotonously with increasing interaction strength. In contrast, a maximal value of  $W_c$  around  $U = 2$  was observed for a nearest neighbor interaction. For larger  $U$ , the critical disorder decreased again due to the splitting of the upper Hubbard band. At the critical point,  $P(s) \propto s$  for  $s \rightarrow 0$  and  $P(s) \propto \exp(-s)$  for  $s \rightarrow \infty$ . In addition, the inverse participation number for a small number of states was calculated [97]. Curves for different sizes crossed as a function of the disorder strength similar to the results for  $\gamma$ . However, there was no common crossing point due to finite size effects and a finite size scaling analysis could not be performed.

Shepelyansky investigated the level statistics of two Coulomb-interacting electrons via  $\eta$ , but as a function of excitation energy  $\epsilon$ , the energy above the two-particle ground state. By truncating the one-electron eigenbasis at high excitation energies, system sizes up to  $24 \times 24$  could be handled [92, 177]. For small enough disorder, a common crossing point of the curves  $\eta(\epsilon)$  for different system sizes was found, indicating the presence of a transition as a

function of excitation energy. At the critical excitation energy, the nearest neighbor spacing distribution resembled the critical  $P(s)$  of the three-dimensional Anderson model.

Instead of a rather sharp transition with a common crossing point, Talamantes *et al* found only a smooth crossover upon studying  $\gamma$  (36) [96]. Evidence for delocalization of the wave functions was found only at smaller disorder values. This indicated that in spite of the presence of level mixing for finite system sizes, its persistence in the limit of infinite system sizes and the relation to delocalization in real space was not obvious.

Jacquod studied level statistics via  $\eta$  (35) for up to 6 interacting quasi-particles in three dimensions after projecting out low energy Slater determinants [178]. For a disorder larger than the critical disorder for a single particle, a critical behavior was observed as a function of the interaction strength. At the critical point, a size independent distribution was found that depended on the number of particles. The higher the particle number, the closer the distribution was to the Poisson distribution, indicating the possibility of a vanishing level repulsion in the thermodynamic limit. The author supposed that this would only happen if the disorder was in the critical regime of the one-particle Anderson model. Starting from a localized situation, the level repulsion was expected to survive.

In a series of papers, Berkovits and coworkers investigated the level statistics of small two-dimensional systems (up to  $4 \times 4$ ) and  $N \leq 6$ . When the one-particle spectrum showed Wigner-Dyson rigidity (metallic system,  $\lambda > L$ ), the non-interacting many-body levels exhibited a Poisson behavior except for the level spacing between the ground and the first excited state, which showed still a Wigner-Dyson behavior since only a single one-particle state was changed. In the presence of interaction, the Wigner-Dyson statistics was recovered for the excited levels [179]. The Wigner-Dyson statistics was observed only for intermediate excitation energies and interaction strengths and a finite size scaling was proposed based on the excitation energy [180, 181]. For an insulating system at larger disorder leading to a one-particle spectrum with Poissonian statistics, a crossover in a quantity similar to  $\eta$  but with different limits in the integral in equation (35) was found. An explanation involving tightly bound exciton states was proposed since the crossover was similar to the single-particle one [182]. In contrast to the metallic situation described above, the crossover occurred rather uniformly with increasing excitation energy or interaction strength. Detailed calculations of the localization lengths of electron-electron pairs, electron-hole pairs and single electrons in the strongly insulating regime led to the conclusion that only the electron-hole pairs had an enhanced localization length due to the interaction, both single electrons and electron-electron pairs had a suppressed localization length [183, 184]. This difference was related to the different density of states. While being roughly constant for the electron-hole pairs, it was considerably smaller due to the presence of the Coulomb gap for single electrons and electron-electron pairs.

Studying ground state local currents of  $4 \times 4$  lattices with 8 electrons, Berkovits and Avishai observed a transition from a diffusive behavior with randomly oriented local currents to a plastic flow of aligned local currents with increasing interaction strength [185].

This result was corroborated by Benenti *et al* who studied the first few excited states of 4 electrons on a  $6 \times 6$  lattice by exact diagonalization. For intermediate interaction strength the ground state was neither characterized by a Fermi glass, the Anderson localized state existing for small interaction strength, nor by a Wigner crystal for large interaction strength [86, 94, 186]. Instead, it was characterized by an ordered flow of local currents in the ground

state. For small disorder, the average current was enhanced by an order of magnitude due to the interaction. Studying the distribution of the current amplitudes and the decay of the typical currents as a function of the interaction strength, a phase diagram as a function of disorder and interaction strength was proposed. Further investigations revealed that the level spacing distribution in the intermediate phase was close to the Wigner distribution for excitations energies of the order of the Fermi energy, indicating a breakdown of the description in terms of weakly interacting quasi-particles. The transition from the Fermi glass to the new phase was characterized by an alignment of local currents while the transition to the Wigner crystal is dominated by a decreasing amplitude of the local currents [187].

Recently, Berkovits *et al* argued that the findings described above cannot be interpreted as a signature of the metal-insulator transition since they were not directly related to zero temperature transport properties. Based on exact diagonalizations for 4 electrons on a  $6 \times 6$  lattice and investigating local tunneling amplitudes and conductances, they concluded that the interaction enhances the insulating features [188].

### 3.3 Other approaches

#### 3.3.1 Non-linear $\sigma$ -model

Frahm *et al* improved the mapping of the two-particle problem onto a random matrix problem by taking into account even the exponentially small matrix elements, neglecting only the correlations among them. Then, they derived a non-linear  $\sigma$ -model, [19, 27], that was suitable to describe the motion of the two electrons on scales larger than  $\lambda_1$ . The motion could not be resolved on smaller length scales. Comparing it to Efetov non-linear  $\sigma$ -model for a disordered metal, they obtained the following results [189]. The local density of states has a Breit-Wigner form whose width  $\Gamma$ , related to the inverse lifetime, depended on the distance between the two electrons. States with large electron separation had a very long lifetime. The size of the two-electron pairs, i. e. the relative distance between the electrons, was shown to grow logarithmically in time and the center of mass extension grew sub-diffusively,  $R^2 \propto t / \ln t$ , until diffusion stopped at  $\lambda_2 \propto \lambda_1^2$ . In a subsequent work [190], this approach was elaborated further and the original work by Dorokhov [120] was generalized to  $n$  particles. The localization length of  $n$  tightly bound particles was  $\lambda_n \propto \lambda_1^n$ , assuming that the disorder did not couple center of mass and relative degrees of freedom.

#### 3.3.2 Interaction matrix

The original reasoning by Shepelyansky [6] and Imry [121] as well as the application of results from band random matrices with preferential basis [157, 158] and the non-linear  $\sigma$ -model [189, 190] depend crucially on assumptions about the interaction matrix in the basis of non-interacting two-particle eigenstates, equation (9). Statistics of the matrix elements were obtained via calculating the non-interacting eigenstates and direct evaluation of equation (9), starting with the work by Frahm *et al* [123], described on page 8.

Von Oppen *et al* found a Lorentzian distribution for the matrix elements [133]. An appropriate random matrix model gave qualitatively the same results as the one proposed by Shepelyansky [6]. Xiong and Evangelou derived similar results for the two- and three-particle interaction matrix, the latter was only more sparse than the former [191].

The most detailed analysis was performed by Römer *et al* [192]. As also observed in [123, 133, 191], all diagonal elements were positive and depended on the sign of the interaction. The distribution of off-diagonal elements was symmetric around zero but strongly non-Gaussian, in contrast to the assumption by most authors which had mapped the two-particle problem onto random matrix models. The rather long tails of the distribution led to deviations of the root mean square value of the distribution  $u_{\text{rms}} = \sqrt{\langle u \rangle}$  from the typical value  $u_{\text{typ}} = \exp[\langle \log(|U|) \rangle]$ . The mean value was dominated by a few large matrix elements leading to oscillations between two states. Delocalization was more appropriately described by the typical value. In dependence on  $\lambda_1$ , they found  $u_{\text{typ}} \sim \lambda_1^{-1.95}$  and  $u_{\text{rms}} \sim \lambda_1^{-1.5}$ . Using the estimate for  $u_{\text{typ}}$  to repeat the block scaling argument from page 7,  $\lambda_2 \propto \lambda_1^{1.1}$  and hence a vanishingly small effect was observed [192].

This analysis shows how careful every simplified estimate has to be considered. In view of the direct numerical evidence for the delocalization by the interaction it is obvious that the correlations among the matrix elements cannot be neglected. In a way, neglecting the correlations is counterbalanced by a wrong estimate of the typical matrix elements.

Ponomarev and Silvestrov studied analytically the interaction matrix elements, arguing that for small disorder the central region of the eigenstates was better described by plane waves than by random functions. This led to a suppression of the interaction matrix elements compared to the rough estimates by Shepelyansky and Imry [6, 121]. With these refined estimates a more appropriate random matrix model was derived for which numerical calculations were performed. The enhancement effect was described by

$$\frac{\lambda_2}{\lambda_1} \sim \lambda_1^{\gamma(U)} \left(1 + \frac{c}{\lambda_1}\right). \quad (37)$$

Their second important result was the prove of the existence of another preferential basis for large interaction strengths, which was used to obtain the duality between small and large interaction strengths in [141].

Fixing the initial state  $\phi_{m_1}(x)\phi_{m_2}(x)$ , Waintal and Pichard calculated the coupling elements to all final states  $\phi_{m_1'}(x)\phi_{m_2'}(x)$ , equation (9). They investigated fluctuations of these coupling terms using a multifractal analysis [193], as for one-particle wave functions in a two-dimensional system. On length scales smaller than the one-particle localization length, multifractal behavior of the coupling elements was observed. This is related to the non-Gaussian statistics of all coupling elements found in [123, 192]. Due to the strong fluctuations, the effective density of coupled states,  $\rho_{\text{eff}} \propto \lambda_1^\alpha$ ,  $\alpha \approx 1.75$ , was smaller than the naïve estimate  $\alpha = 2$ . From the block scaling arguments, an enhancement effect  $\lambda_2 \propto \lambda_1^{1.5}$  followed.

Römer *et al* showed that the simplified mapping onto a random matrix model via the interaction matrix led to wrong results for toy models. In a two-dimensional as well as in a one-dimensional Anderson model, an additional perturbing potential was introduced [194]. While this was shown to decrease the localization length, using the same arguments as Shepelyansky [6], an enhancement was predicted from a random matrix model.

These studies show that mappings onto random matrix models [6, 121, 123, 158, 189, 190] as well as simplified models like the two-body random interaction model (page 19) [167, 168] have to be considered carefully. The same holds when evaluating the two-particle localization length using Fermi's golden rule via the Breit-Wigner width  $\Gamma$  [143, 148, 162, 163, 166].

These approaches yielded useful information on the influence of the interaction but for a direct extraction of the localization length one should go beyond the simple estimates.

### 3.3.3 Kicked rotator

The kicked rotator is a standard model for chaotic systems, describing a normal pendulum on which the gravitational force acts periodically for short moments. The quantum mechanical version is described by an evolution operator for a single period,

$$\hat{S} = e^{-i[H_0(n)+V(\theta,t)]}, \quad (38)$$

and can be mapped onto the one-dimensional one-particle Anderson Hamiltonian with a pseudo-random sequence of on-site energies [195, 196]. A generalization to two and three dimensions is possible [197]. Higher dimensions can be modeled effectively in a one-dimensional system using a special form of the perturbation  $V$  [198, 199].

Borgonovi and Shepelyansky studied two interacting kicked rotators and found an enhancement of the localization length due to the interaction [200]. For an effective dimension  $d_{\text{eff}} = 2.5$  they found a delocalization transition below the one-particle delocalization border [201]. The distance between the two particles was shown to grow logarithmically with time as predicted in [189]. This was estimated to give a logarithmic reduction of the final localization length,  $\lambda_2 \propto \lambda_1^2 / \ln \lambda_1$ . With an additional noise term destroying the interference effects that would otherwise have led to localization, the diffusion rate was strongly enhanced due to the interaction [147]. The reason was that the average size of jumps between subsequent decoherent processes increased from  $\lambda_1$  to  $\lambda_2$ . A growing pair size due to the noise should influence the results only for long times, but this could not be proven numerically.

### 3.3.4 Diffusion

The results for the kicked rotator are based on the time evolution of some initial condition. A similar analysis was also performed for the two-particle Hamiltonian, starting with the work by Shepelyansky who showed that the localization radius of a two-particle wave packet was larger with interaction than without it [6].

From the knowledge of all eigenstates, Evangelou *et al* calculated for a single sample the time evolution of the mean radius, equation (65). For intermediate interaction strengths larger values were reached than for small and large interaction strengths in agreement with the duality derived in [141].

Further investigations were performed by Brinkmann *et al* who studied the time evolution of electron-hole pairs using the semiconductor Bloch equations [145, 202]. While for  $U = 0$ , the saturation value of the inverse participation number was reached quickly, this saturation value increased for finite interaction strengths and the growth of the inverse participation number proceeded more slowly. The growth was argued to be a diffusive process. The sign of the interaction was shown to be important for energies away from the middle of the band, see also Halfpap *et al* [128]. For energies closer to the ground state, an attractive interaction was more favorable for delocalization than a repulsive interaction. The main new idea was that the two particles could have different masses and exist in different random potentials. The model might be relevant for optical observations using ultrashort time of flight experiments. However, the results were qualitatively similar to the two electron problem, see also [144].

De Toro Arias *et al* investigated in detail the short time dynamics of two electrons, concentrating on the center of mass extension,  $R(t)$ , and the size of the pair, the relative distance between the two particles  $r(t)$ . In configuration space, the wave packets have cigar like shapes for long times similar to the shape of some eigenstates observed in [137]. Concerning the dynamics, the interaction reduced the spreading along the center of mass direction for short times during the ballistic motion. This seemed to be related to the reduction of the level curvature in the metallic regime due to the interaction [154]. On intermediate time scales a slow sub-diffusive growth of the center of mass extension was observed. In contrast to the prediction of a diffusive growth from the non linear  $\sigma$ -model [189],  $R(t)$  was not proportional to  $t^{1/2}$  but rather to  $\log(t)$ . At the same time, a logarithmic growth of the size of the wave packet was in agreement with the prediction in [189] and with findings from the kicked rotator [200]. For long times,  $R(t)$  saturated. A detailed study of the saturation values was not performed, the largest enhancement effect observed was  $R(U = 1)/R(U = 0) \approx 3.5$ . If the initial condition corresponded to two nearby but at  $t = 0$  not interacting particles, the duality between small and large interaction could be seen by looking at  $R(t)$  at fixed times. In the ballistic regime,  $R(t)$  was suppressed by an interaction and returns back to the original value for large interaction strengths. In the sub-diffusive regime,  $R(t)$  was enhanced for intermediate interaction strengths. If the initial condition corresponded to two interacting particles, one probed with increasing interaction strength only the molecular states discussed in [141, 142] and the spreading of the wave packet was suppressed.

### 3.3.5 Harper model

The Harper equation describes an electron in a one-dimensional quasi-periodic potential and is related to electron motion in a two-dimensional square lattice with a strong magnetic field,

$$2\lambda \cos(\hbar n + \beta)\phi_n + \phi_{n+1} + \phi_{n-1} = E\phi_n. \quad (39)$$

The one-dimensional model can display both localized and metallic behavior. For  $\lambda < 1$ , the eigenstates are extended, for  $\lambda > 1$  they are exponentially localized and  $\lambda = 1$  corresponds to a critical situation with power law localized states.

Shepelyansky studied the time evolution of two interacting electrons in this quasi-periodic potential [203]. The interaction effects were quite different from the case of two particles in a random potential. For  $\lambda = 1$ , he found a diffusive behavior for  $U = 0$ . This diffusion was slowed down by the interaction, the diffusion constant was reduced. It turned out that one part of the states contributing to the initial state became *localized* due to the interaction while the other part remained unchanged. The return probability was always enhanced by the interaction and remained finite for all values of  $\lambda$ , even in the metallic case. The different influence of the interaction in comparison to the random potential was attributed to the interaction-induced destruction of tiny resonance conditions which in the non-interacting system allowed to tunnel between quasi-resonant sites leading to metallic behavior.

Barelli *et al* studied two interacting particles in the Harper model by direct diagonalization [204]. Even for  $U \neq 0$ , a big part of the spectrum resembled closely the Hofstadter butterfly, the spectrum for a single electron described by the Harper equation. The second part was a shifted butterfly and was shown to be related to situations in which the two particles were

close to each other. These states became localized due to the interaction. A more elaborated version of this work together with a semi-classical analysis was given in [205].

Evangelou and Katsanos [206] studied the properties of the eigenstates for two electrons described by the Harper equation, too. They observed molecular states as in the random potential and found essentially the same localization properties as discussed by Barelli *et al.* The diffusion was slowed down by the interaction while for a localized system, the saturation value of the mean radius could be enhanced for intermediate interaction.

Eilmes *et al* employed the transfer matrix method to analyze the localization properties of two interacting particles in the Harper model [207]. While most of the results were similar to those discussed above [204, 205, 206], for a long range interaction a shift of the metal-insulator transition from  $\lambda = 1$  to  $\lambda \approx 0.92$  was found, i. e. the region of localized states increased due to the presence of the interaction.

### 3.3.6 Few impurities

Aharony *et al* studied a model in which the electrons interacted only at a number of impurities,  $I$ . In that case the exact solution could be derived by finding the roots of a  $I \times I$  determinant [208, 209]. While apparently much easier than a direct diagonalization of an  $I^2 \times I^2$  matrix in case of a random system, the construction of the determinant required the two-particle Green function without interaction and thus involved at least an  $I^3$  operation, see page 13. Studying a single impurity, parameter regions with zero, one, and two bound states were observed. Screening of the impurity due to the interaction with a bound state led to characteristic resonances for the transmission of the second electron. Preliminary results for two impurities were also reported.

### 3.3.7 Approximations for finite densities

A number of attempts were made to investigate the localization properties at finite electron densities. Apart from the few-particle calculations already discussed [86, 94, 179, 180, 181, 182, 183, 184, 185, 186, 187], page 23, all of them relied in some way or another on approximations that were introduced to cut the exponentially growing Hilbert space of the problem.

One of the simplest of these is the Hartree-Fock approximation, based on the assumption that the many-body wave function can be approximated by a Slater determinant built from single particle orbitals. This leads to a set of self-consistent equations that can be solved numerically. In each step, the problem is solved in the one-particle Hilbert space instead of the full  $n$ -particle Hilbert space. While the obtained ground states energy gives an upper bound to the exact ground state energy due to the variational principle by Ritz, the meaning of the one-particle orbitals is much less evident.

An extensive study of the interplay between disorder and interaction in three dimensions was performed by Tusch and Logan [210]. They studied localization properties at half filling via the participation ratio of the single particle orbitals. An intermediate interaction enlarged the metallic phase to stronger disorder values. For larger interaction strengths, local moments became important, the density of states decreased at the Fermi level, and the single particle orbitals became localized.

Using similar methods, the occurrence of local moments in the metallic regime had been shown previously by Milovanović *et al* [211].

Epperlein *et al* found a localizing influence of the interaction close to the Fermi energy in their Hartree-Fock study [212]. This was attributed to the reduced density of states due to the Coulomb gap. Only away from  $E_F$ , the interaction led to a delocalization, measured via the participation ratio of the single particle orbitals. This results was compared to exact diagonalizations, showing that the density of states and the localization properties close to the Fermi level were well described by the results from the Hartree-Fock approximation [213]. The level statistics showed a transition to a metallic state only for hopping terms larger than in the non-interacting case, attributed to the presence of the Coulomb gap.

Talamantes *et al* studied the level statistics of two-dimensional many electron systems [214]. Generalizing the classical Coulomb glass without hopping to the quantum Coulomb glass with hopping, the latter was treated as a small perturbation. Studying 72 electrons on 144 sites, first the 5000 lowest energy states of the classical systems were found. In this reduced Hilbert space, the quantum Coulomb glass matrix was set up and diagonalized. A clear tendency for a crossover from Poisson to Wigner behavior in the nearest neighbor spacing statistics was observed, which was stronger for a Coulomb than for Hubbard interaction and related to delocalization in real space. Similar results were obtained for three-dimensional systems [215], showing that the effect of electron correlations in favor of delocalization was more important than the reduction of the density of states due to the Coulomb gap in contrast to [212, 213].

A more reasonable restriction of the Hilbert space was employed by Vojta *et al*. Instead of taking the states with the lowest classical energy, they took a certain number of low energy Slater determinants constructed from the single particle orbitals of a Hartree-Fock calculation [216]. Known in quantum chemistry as configuration interaction, this method provided a more accurate restriction to low energy states than the one employed by Talamantes *et al* [214, 215] and was valid not only for small hopping terms. In this restricted basis the Hamiltonian was exactly diagonalized [89]. The DC-conductivity was shown to be enhanced due to the interaction only in the strongly localized regime (small hopping or large disorder). For larger hopping, the conductivity was larger, but now the interaction had an opposite effect and reduced the conductivity. Similar results were obtained for one- [217] and three-dimensional systems [218], and using the sensitivity to a change of the boundary conditions [219]. Investigating the return probability it was shown that the enhancement of localization at  $E_F$  was weaker than predicted by the Hartree-Fock results [212, 213]. Away from the Fermi energy, a strong delocalization was found in agreement with earlier results [220].

Shepelyansky and Song generalized the results for two particles in two dimensions [92] to higher particle numbers by restricting the Hilbert space to low energy Slater determinants constructed from the non-interacting eigenstates. As in [92], page 21, they found a transition from Poisson to Wigner behavior in the nearest neighbor spacing distribution. It occurred at a finite excitation energy and did not depend on system size and number of particles, as long as the filling factor was constant [87, 221].

Benenti *et al* used the configuration interaction approach to study the opening of the Coulomb gap in two dimensions [222]. The distribution of spacings between the ground state and the first excited state showed a crossover from Poisson to Wigner-Dyson behavior as a function of the interaction strength. Using  $\gamma$  as defined in equation (36), a size independent

distribution was observed for a critical interaction strength which was smaller than the values found for the phase boundaries of the intermediate phase in [94], page 23, and therefore not related to this transition. These findings were associated with the crossover in the hopping resistivity from Mott behavior, equation (4), to Efros-Shklovskii behavior in the presence of the interaction-induced Coulomb gap. In addition, it was shown that the inverse compressibility, the discrete second derivative of the ground state energy with respect to the particle number, exhibited a smooth crossover from a  $L^{-2}$  to a  $L^{-1}$  decay in the size dependence. For this reason, the theoretical analysis of addition spectra of quantum dots based on the constant interaction model and random matrix theory failed to explain the experiments. The behavior of the single (or many) particle excited levels was not related in a simple way to the addition spectrum.

Waintal *et al* used an even more approximate method to study localization effects in two-dimensional samples [88]. After calculating all non-interacting eigenstates, they first neglected the low energy ones which were assumed to be related to electrons localized on single sites characterized by exceptionally large potential fluctuations. Then a restricted number of low energy Slater determinants was constructed from this set and only in this subspace the Hamiltonian was diagonalized. Three, four, and five particles were studied using systems with sizes  $L = 24, 28, 31$ , respectively, yielding roughly the same density. The inverse participation number of the ground state was shown to increase with interaction strength, a signature of interaction-induced delocalization. A localization length was defined via the length scale over which a slight change in the random potential affected the ground state charge density. Only short distances were considered in order to avoid boundary problems. This localization length increased with interaction strength, the increase was most pronounced for the system with the largest particle number. A finite size scaling analysis, section 4.2, revealed in the limit of an infinite system a transition to a metallic phase at a critical interaction strength of order one. For quasi one-dimensional samples, no critical behavior was found [86].

### 3.3.8 Luttinger liquid

In strictly one dimension, the Luttinger liquid model allows for an exact treatment of the interaction. After linearizing the dispersion relation and considering states with negative energies to be filled, the model can be solved analytically in terms of a Bogolubov transformation. The Hamiltonian can be written in a bosonic form in terms of the collective charge and spin density excitations [223]. While in principal being an ideal starting point for investigating the influence of interaction on localization, it turns out to be very difficult to include disorder degrees of freedom since they lead to a non-linear Hamiltonian.

Attempts were made to include the effect of disorder using perturbation theory [224, 225] and in a renormalization group study [226, 227]. A repulsive interaction strengthened localization, while an attractive interaction tended to weaken it, eventually leading to a metallic state characterized by dominating superconducting fluctuations for sufficiently strong attractive interactions.

This result is in apparent contradiction to the work for two particles where the interaction-induced delocalization was found for attractive as well as for repulsive interaction. But for energies closer to the ground state the attractive interaction was more favorable for

delocalization [128, 202], indicating that this contradiction is very probably only related to the energy chosen mostly to be in the middle of the band for the two-particle calculations.

### 3.3.9 Density matrix renormalization group

The results for the Luttinger model discussed above were checked numerically using the density matrix renormalization group method pioneered by White [228]. This method allows to calculate the ground state of a one-dimensional system with a finite electron density. One starts with a small building block of the total system which is diagonalized. Upon coupling this block with an additional site, only a certain number of low energy states are considered thus reducing the Hilbert space. Iterating this procedure, the ground state energy and wave function can be calculated. Schmitteckert *et al* applied the method to interacting fermions in a one-dimensional random potential [229, 230, 231]. Localization properties were calculated by investigating the change of the ground state energy upon changing the boundary conditions, the ground state phase sensitivity, page 15. As predicted, a delocalized region was found for strong attractive interactions, while a repulsive interaction decreased the localization length. Only for large disorder and intermediate repulsive interaction, a small increase of the ground state phase sensitivity was observed. In contrast, single samples could exhibit drastic variations with interaction strength. Whenever there was a reorganization of the ground state due to the interaction, for example while going from a situation where the electrons were localized in the deep potential fluctuations to a situation where the ground state was a periodic array of charges, the phase sensitivity increased dramatically up to four orders of magnitude [232, 233]. Similar results were also obtained on a Hartree-Fock level [234]. Recently, a localization length was defined using the dependence of the ground state sensitivity on system size. A small enhancement was found for intermediate repulsive interaction [235].

Close to the reorganizations of the ground state, the latter can be described as a superposition of two localized states which are insensitive to a change in boundary conditions. If a state is constructed from two independent localized states, its own localization length is most probably larger than those of the contributing states. This is the basis for the delocalization of two-particle wave functions and also explains qualitatively the large effect of the ground state reorganizations for finite densities.

### 3.3.10 Quantum Monte Carlo method

Denteneer *et al* calculated the temperature dependent conductivity in the two-dimensional disordered Hubbard model via the current-current correlation function with a Monte Carlo technique [98]. At half filling, insulating behavior was found. At quarter filling, metallic behavior was observed below a critical disorder strength. Preliminary results indicated a metallic scaling with lattice size, too. Near the critical disorder, the spin susceptibility diverged on both sides of the transition, indicating the importance of spin degrees of freedom and possibly of local moments.

This result was in contrast to work by Yi *et al* who studied the Anderson Hubbard Hamiltonian in two dimensions by means of a quantum real space renormalization group method. An insulating ground state was reported at *and* away from half filling [236].

### 3.4 Summary of chapter 3

In the early approaches, the problem of two interacting particles was mapped onto different, already familiar models using some approximations. Dorokhov exploited the similarity of two tightly bound particles in one dimension to a single particle in a quasi one-dimensional system. Shepelyansky derived a single particle random matrix model based on the analysis of the interaction matrix in the preferential basis of non-interacting two-particle eigenstates. The same analysis was the base of the revival of the Thouless block scaling picture by Imry. All approaches led to an interaction induced delocalization of two-particle wave packets.

But both mappings had their shortcomings. Upon studying numerically the bag model in center of mass and relative coordinates, Halfpap *et al* demonstrated that the coupling of the relative and the center of mass motion cannot be neglected in contrast to the key assumption by Dorokhov. Starting from toy models in which additionally added potential elements had been shown to *decrease* the localization length, Römer *et al* derived Shepelyansky's random matrix model from which an *increase* of the localization length followed.

Careful investigations of the interaction matrix elements indicated that correlations cannot be neglected. This questions the simplified translation of results from random matrix theory and a non-linear  $\sigma$ -model to two-particle localization lengths. The same problem exists for the results obtained for the Breit-Wigner width since its only proven relation to the few particle localization length was derived from random matrix theory. All analytic approaches to the problem suffer from the impossibility to include correlation effects. This can only be done with numerical calculations.

Numerical calculations were performed with the transfer matrix and the Green function method. Though initial results of the transfer matrix method supported the interaction induced delocalization, it was later shown that the method could not provide reliable results with nowadays computing technology. For finite samples, an unambiguous prove of the effect required too large systems. In the same way, the bag model suffered from the failure to produce correctly the non-interacting localization length due to a boundary effect. While direct diagonalizations revealed the asymmetry of certain two-particle eigenstates, the numerical breakthrough was the application of the finite sample Green function method. This allowed to prove unambiguously that interaction led to delocalization of two-particle wave functions and to study the functional dependence on disorder and interaction. It also led to the observation of a transition for two particles in two dimensions.

In addition to these direct numerical approaches to study the localization length of two interacting particles, a lot of effort was spent on calculating the spectral properties, including generalizations to larger particle numbers. But in contrast to the one-particle case where a transition from Poisson to Wigner in the nearest neighbor spacing statistics indicated directly the insulator to metal transition, the situation was much more complicated with interacting particles. A direct mapping of the level statistics to the localization properties turned out to be impossible. And the relevance of results for very small systems for the explanation of the experimentally observed metal-insulator transition is subject to an ongoing debate.

In spite of the invested effort over the last years, the field of research on the interplay between interaction and disorder is far from being closed soon. In order to tackle the main issue, the metal-insulator transition in two dimensions, the two-particle calculations, especially about the localization properties, have to be extended to larger particle numbers

and the ground state calculations for small two-dimensional systems have to be extended to larger system sizes. This thesis bridges the gap between these two approaches. By presenting exact results for the localization properties of up to four particles, it provides a firm base for the approximations which are necessary in order to extend the finite density calculations to larger system sizes.

In the following, a new numerical method to study few-particle localization lengths and results for up to four particles will be presented. So far, this has been performed only in the strongly insulating regime, by direct diagonalization of very small systems and by calculating the ground state phase sensitivity with the density matrix renormalization group method. Our method allows to study much larger localization lengths. It takes all states of the spectrum into account and yields an upper bound for the conductivity.

## 4 Time evolution of wave packets

The time evolution of wave packets provides one of the most direct numerical tools to study the electronic properties of disordered solids. Already in 1977 it was employed by Weaire and Williams to calculate the inverse participation number averaged over all states within an energy window [237].

Kramer and Weaire extended the method in order to calculate the conductivity of a disordered system [238]. The existence of a metal-insulator transition was probed in two and three dimensions [239]. Due to the available computing power only relatively small samples could be treated leading to large finite size effects. At that time, the time evolution was not the right tool to judge the existence of extended states, as pointed out by De Raedt [240]. This became possible with the development of recursive methods like the transfer matrix method or the Green function method which allowed the study of much larger samples, at least in one direction. Thereafter, the time evolution was used to study the critical behavior at the Anderson transition [241, 242] or the influence of a time dependent potential on the motion of the electrons [243]. In both cases, an anomalous diffusion or a diffusive behavior could be analyzed very well. Recently, the time evolution of wave packets was investigated by direct calculation for one-dimensional Hamiltonians with long range random hopping [244, 245]. Time evolution on percolation clusters was studied by Dräger and Halfpap [246].

In the following, it will be shown that the equation of motion method can be used to study the localization properties of few-particle wave packets very accurately. In combination with finite size scaling, it is competitive to the calculation of matrix elements of the Green function and thus provides a second, independent tool. More important, it can easily be generalized to higher particle numbers as will be shown.

How can a method be competitive for the interacting case that was not at all competitive in the absence of interaction? The reason is simple. The efficiency of the Green function and the transfer matrix method for calculating localization lengths in quasi one-dimensional samples was based on a recursive calculation. There was no need to store the full Hamiltonian! Computer time and memory requirements were reduced drastically in comparison to the time evolution method which requires the storage of the full Hamiltonian. In contrast, as discussed in section 3.1.3, all *exact* methods for the calculation of the two-particle localization length needed the full Hamiltonian. Therefore, time evolution methods are much more competitive

for interacting particles than in the non-interacting situation. All recursive methods are based on suitable approximations [7, 133], which however work much better for the Green function than for the transfer matrix method, compare the discussion about the bag model on page 8. While concentrating on matrix elements between double occupied sites [133] or employing elegant ways for the calculation of the matrix elements [7] might give an advantage to the Green function methods for two particles, the time evolution method can more easily be extended to higher particle numbers.

First, based on the instructive example of the one-dimensional Anderson tight binding Hamiltonian for a single particle, the method is presented in the form used throughout this thesis. Generalization to higher dimensions or larger particle numbers are given explicitly. Then the finite size scaling is introduced before the quantities suitable to extract the  $n$ -particle localization length are defined.

## 4.1 Equation of motion method

Consider the Anderson tight binding Hamiltonian for a single particle in a one-dimensional random potential: it contains a term representing the kinetic energy and another representing the random potential,

$$\hat{H} = \hat{H}_{\text{kin}} + \hat{H}_{\text{pot}} = V \sum_{\langle j \neq j' \rangle} c_j^\dagger c_{j'} + \sum_j \varepsilon_j c_j^\dagger c_j. \quad (40)$$

The first sum is restricted to nearest neighbors on the lattice. The off-diagonal hopping matrix elements  $V = -1$  define the energy scale. The random potential is represented by the diagonal elements  $\varepsilon_j$ , which are independently distributed at random according to a box function, whose width  $W$  measures the disorder strength,  $\varepsilon_j \in [-W/2, W/2]$ . The lengths are measured in units of the lattice constant  $a = 1$ .

The time evolution,  $|\psi(t)\rangle$ , of an initial condition,  $|\psi(t=0)\rangle$ , is given by the unitary transformation [10],

$$|\psi(t)\rangle = e^{-i\hat{H}t/\hbar} |\psi(t=0)\rangle. \quad (41)$$

In contrast to methods developed earlier [239], we implement a procedure devised by Suzuki [247, 248, 249, 250]. First, the time  $t$  of the iteration is split into small time steps  $\tau = t/N$ ,

$$|\psi(t)\rangle = \left( \prod_N \exp \left[ -\frac{i}{\hbar} \hat{H} \tau \right] \right) |\psi(t=0)\rangle. \quad (42)$$

This is exact since the Hamiltonian is time independent and commutes with itself. In the next step, the Hamiltonian matrix  $H$  is split into three additive parts,  $H = H_1 + H_2 + H_3$ , as shown below for a one-dimensional chain with five sites,

$$\begin{pmatrix} \varepsilon_1 & V & 0 & 0 & 0 \\ V & \varepsilon_2 & V & 0 & 0 \\ 0 & V & \varepsilon_3 & V & 0 \\ 0 & 0 & V & \varepsilon_4 & V \\ 0 & 0 & 0 & V & \varepsilon_5 \end{pmatrix} = \begin{pmatrix} \varepsilon_1 & 0 & 0 & 0 & 0 \\ 0 & \varepsilon_2 & 0 & 0 & 0 \\ 0 & 0 & \varepsilon_3 & 0 & 0 \\ 0 & 0 & 0 & \varepsilon_4 & 0 \\ 0 & 0 & 0 & 0 & \varepsilon_5 \end{pmatrix} + \begin{pmatrix} 0 & V & 0 & 0 & 0 \\ V & 0 & 0 & 0 & 0 \\ 0 & 0 & 0 & V & 0 \\ 0 & 0 & V & 0 & 0 \\ 0 & 0 & 0 & 0 & 0 \end{pmatrix} + \begin{pmatrix} 0 & 0 & 0 & 0 & 0 \\ 0 & 0 & V & 0 & 0 \\ 0 & V & 0 & 0 & 0 \\ 0 & 0 & 0 & 0 & V \\ 0 & 0 & 0 & V & 0 \end{pmatrix}. \quad (43)$$

The general decomposition can be written as

$$\begin{aligned}
H_1 &= \sum_j \varepsilon_j c_j^\dagger c_j \\
H_2 &= - \sum_{j \in \mathbb{N}_{\text{odd}}} c_{j+1}^\dagger c_j + c_j^\dagger c_{j+1} \\
H_3 &= - \sum_{j \in \mathbb{N}_{\text{even}}} c_{j+1}^\dagger c_j + c_j^\dagger c_{j+1}.
\end{aligned} \tag{44}$$

Each of the three parts can be easily diagonalized and the exponential of each can be calculated analytically, yielding for example,

$$e^{-iH_2\tau/\hbar} = \begin{pmatrix} \cos(\tau V/\hbar) & -i \sin(\tau V/\hbar) & 0 & 0 & 0 \\ -i \sin(\tau V/\hbar) & \cos(\tau V/\hbar) & 0 & 0 & 0 \\ 0 & 0 & \cos(\tau V/\hbar) & -i \sin(\tau V/\hbar) & 0 \\ 0 & 0 & -i \sin(\tau V/\hbar) & \cos(\tau V/\hbar) & 0 \\ 0 & 0 & 0 & 0 & 0 \end{pmatrix}. \tag{45}$$

The exponential of this sum is now approximated by a product of exponentials of the parts. A first order accurate approximation in  $\tau$  is the Trotter-Suzuki formula, familiar from the theory of path integrals. Higher order approximation have been derived by Suzuki [247, 248, 249, 250], yielding more complicated products. In the present case a fourth order decomposition is implemented which has been used before in the context of dephasing by time dependent random potentials [243],

$$e^{\tilde{\tau}(H_1+H_2+H_3)} = S(\tilde{\tau}p)S(\tilde{\tau}[1-2p])S(\tilde{\tau}p) + O(\tilde{\tau}^4), \quad \text{with} \quad \tilde{\tau} = -\frac{i\tau}{\hbar}, \tag{46}$$

$$S(x) = e^{H_1 x/2} e^{H_2 x/2} e^{H_3 x} e^{H_2 x/2} e^{H_1 x/2}, \quad \text{and} \quad p = (2 - \sqrt[3]{2})^{-1}. \tag{47}$$

Instead of a product of three exponentials for the first order approximation, a product of 15 exponentials is necessary for the fourth order one. This number can be reduced to 13 by combining neighboring terms which contain the same part of the Hamiltonian. In general, the higher the order of the approximation, the more terms are required. There are two main advantages of this method. First, the approximation is unitary, i. e. norm and energy of the wave packet are conserved. Second, the deviations from the exact solution are known to scale as  $\|\psi(t) - \psi^{(4)}(t)\| \leq c^{(4)} t \tau^4$ , allowing  $\tau$  to be chosen such that the discretization error can be neglected up to the largest times considered.

The time evolution of a single particle wave function in a one-dimensional random potential is shown in the left plot of figure 3, presenting  $\overline{\log |\psi(j)|^2}$  for different times. To get typical amplitudes, logarithmic averaging over 100 disorder realizations has been performed. The wave packet spreads with time over the lattice and reaches a stationary state for long times. This indicates the complete localization of all states in the spectrum. The exponential localization is clearly visible,  $\lambda(W=7) \approx 2.5$ , taking into account that the absolute square instead of the modulus is plotted. The localization length depends on the strength of the disorder, right plot in figure 3. In order to extract the localization length of the wave

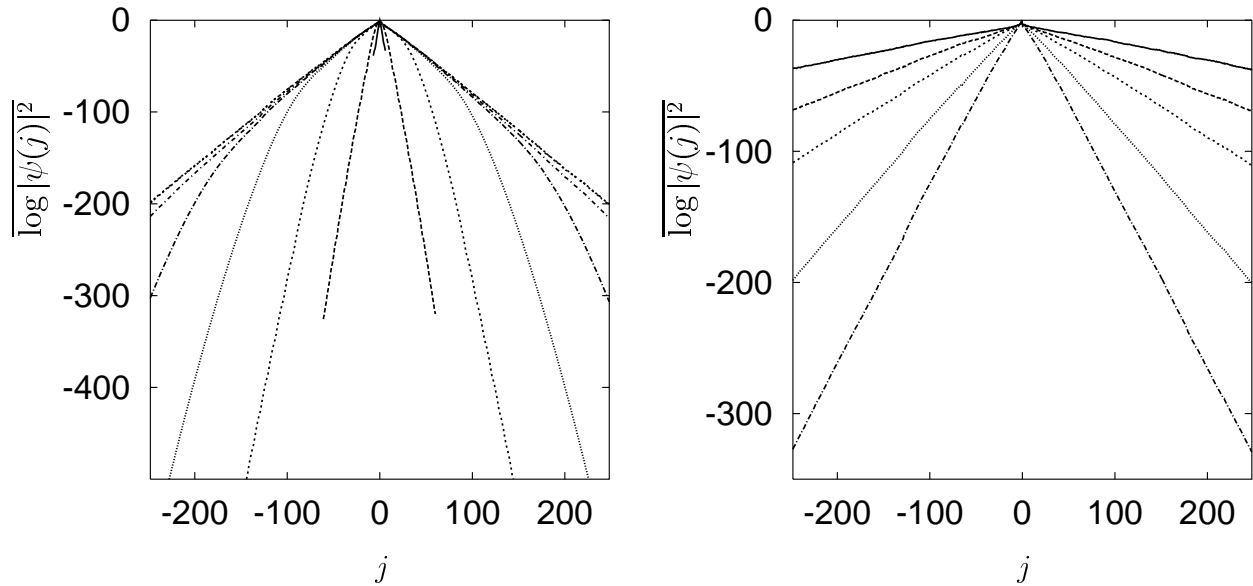


Figure 3: Left: time evolution of a typical wave packet in a one-dimensional random potential. Initially,  $\psi(j) = \langle j | \psi(t=0) \rangle = \delta_{j,0}$ . Snapshots taken at  $t = 0.1, 1, 10, 30, 60, 100, 1000,$  and  $10000$ , inner to outer curves. Right: stationary states for different disorder values,  $W = 3, 4, 5, 7,$  and  $9$  (top to bottom), localization lengths are  $15.7, 7.9, 4.7, 2.5,$  and  $1.5$ .

packet directly from the data, useful quantities are the mean radius,  $\text{MR}(t)$ , and the inverse participation ratio,  $\text{IPR}(t)$ ,

$$\text{MR}(t) = \sqrt{\langle \psi(t) | j^2 | \psi(t) \rangle - (\langle \psi(t) | j | \psi(t) \rangle)^2}, \quad (48)$$

$$\text{IPR}^{-1}(t) = \sum_j |\langle j | \psi(t) \rangle|^4. \quad (49)$$

The time evolution of both quantities is shown in figure 4 for different disorder values. Here and in the following, these quantities are already averaged over different disorder realizations. Two regimes are visible. For short times, the mean radius increases ballistically,  $\text{MR}(t) \propto t$ . For long times, it saturates. The saturation values define localization lengths  $\lambda_{\text{MR}}$  and  $\lambda_{\text{IPR}}$ .

The generalization to higher dimensions or more particles is straightforward. In fact, both are directly related. To account for the interaction, a third part is added to the Anderson tight binding Hamiltonian, equation (40). Different types of interaction have been studied,

$$\hat{H}_{\text{int}} = U \sum_{\langle j \neq j' \rangle} c_j^\dagger c_j c_{j'}^\dagger c_{j'} \quad , \quad (\text{nearest neighbor}), \quad (50)$$

$$\hat{H}_{\text{int}} = U \sum_j c_j^\dagger c_j^\dagger c_j c_j \quad , \quad (\text{on-site}), \quad (51)$$

$$\hat{H}_{\text{int}} = U \sum_{j,j'} \frac{c_j^\dagger c_j c_{j'}^\dagger c_{j'}}{|j - j'|} \quad (\text{Coulomb}). \quad (52)$$

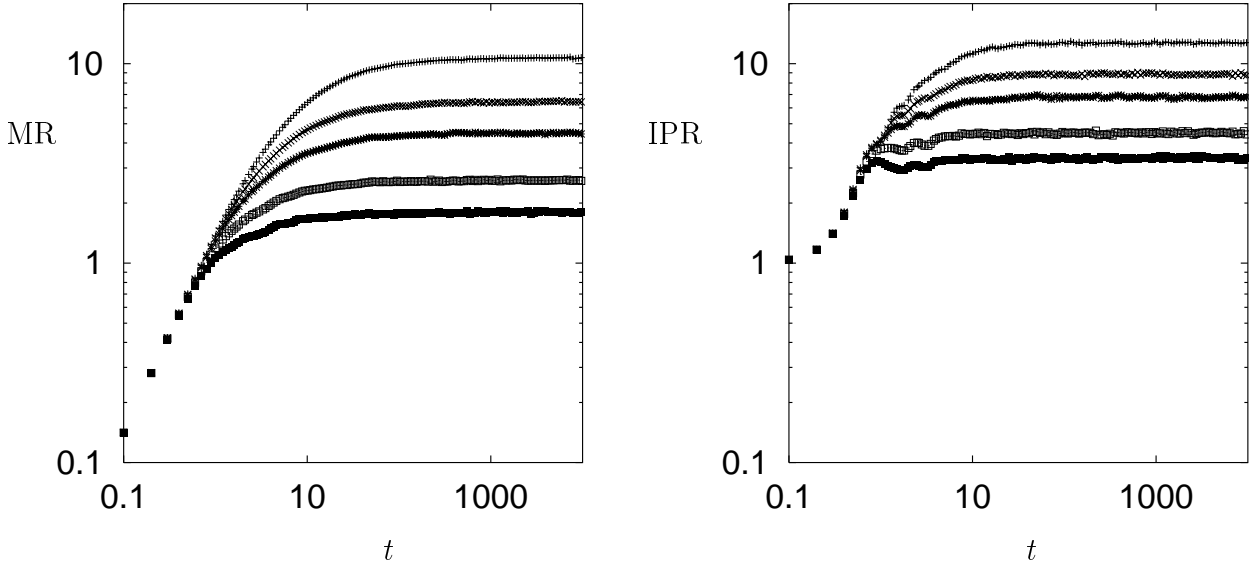


Figure 4: Time dependence of mean radius (left) and inverse participation ratio (right) for different disorder values,  $W = 3, 4, 5, 7,$  and  $9$ , top to bottom curves.

The  $n$ -particle Hamiltonian in one dimension is equivalent to an  $n$ -dimensional one-particle Hamiltonian upon going to configuration space. The mapping is straightforward for distinguishable particles. The indistinguishability of quantum mechanical particles constrains the possible wave functions in configuration space to those with a certain spatial symmetry, discussed below. For two distinguishable particles, the  $L^2$  basis states in configuration space are given by  $c_{j,k}^\dagger |0\rangle = a_j^\dagger b_k^\dagger |0\rangle$ , where  $c_{j,k}^\dagger$  creates a two-particle state in configuration space. This is equivalent to creating one particle on site  $j \in [1, L]$  ( $a_j^\dagger$ ) and the other on site  $k \in [1, L]$  ( $b_k^\dagger$ ) in real space. Written in the configuration space operators, the Hamiltonian reads,

$$\hat{H} = \sum_{j,k} [\varepsilon_j + \varepsilon_k + U(j, k)] c_{j,k}^\dagger c_{j,k} + \sum_{\langle j,k \neq j'k' \rangle} c_{j,k}^\dagger c_{j',k'}, \quad (53)$$

where the second sum is restricted to nearest neighbors on the two-dimensional lattice. The resulting matrix is extremely sparse, as the one of the two-dimensional Anderson Hamiltonian. The only difference is the non-trivial form of the diagonal elements, which include the sum over the single particle potential values and the interaction energy  $U(j, k)$ . The latter is given by  $U\delta_{j,k\pm 1}$  (nearest neighbor),  $U\delta_{j,k}$  (on-site), or  $U/|j - k|$  for Coulomb interaction.

The generalization to  $n$  particles is straightforward. The off-diagonal hopping elements are those of the  $n$ -dimensional Anderson Hamiltonian. The diagonal elements are a sum over the  $n$  one-particle potential values and the  $n(n - 1)/2$  two-body interaction energies,

$$\langle j_1 \dots j_n | \hat{H} | j_1 \dots j_n \rangle = \sum_{i=1}^n \varepsilon_{j_i} + \sum_{\substack{i,k=1 \\ i < k}}^n U(j_i, j_k). \quad (54)$$

The Hamiltonian is then decomposed as before. The first matrix is again the diagonal part,

equation (54). The off-diagonal part is split into  $2n$  matrices of the form,

$$\hat{H}_{2i-1} = \sum_{\substack{j_1, \dots, j_i, \dots, j_n \\ j_i \in \mathbb{N}_{\text{odd}}}} c_{j_1, \dots, j_i+1, \dots, j_n}^\dagger c_{j_1, \dots, j_i, \dots, j_n} + c_{j_1, \dots, j_i, \dots, j_n}^\dagger c_{j_1, \dots, j_i+1, \dots, j_n}, \quad (55)$$

$$\hat{H}_{2i} = \sum_{\substack{j_1, \dots, j_i, \dots, j_n \\ j_i \in \mathbb{N}_{\text{even}}}} c_{j_1, \dots, j_i+1, \dots, j_n}^\dagger c_{j_1, \dots, j_i, \dots, j_n} + c_{j_1, \dots, j_i, \dots, j_n}^\dagger c_{j_1, \dots, j_i+1, \dots, j_n}, \quad (56)$$

compare with equation (44). The  $n$ -particle problem has not only a larger Hilbert or configuration space, in addition it requires a decomposition into more parts for calculating the time evolution.

Working in configuration space, one must not forget that quantum mechanical particles are indistinguishable. This requires a wave packet in configuration space that is symmetric (or antisymmetric) under exchange of any two coordinates. Only initial wave packets fulfilling this condition are allowed. Due to the symmetry of the Hamiltonian, this property is maintained during the time evolution. For numerical purposes, it is useful and necessary for larger particle numbers to restrict the calculation to one of the symmetric parts in configuration space. This reduces the actual system size by a factor of  $n!$  and allows to enlarge the maximally reachable one-dimensional system size  $L$  by a factor of  $\sqrt[n]{n!}$ . Since the numerically achievable system size decreases drastically with increasing particle number, the implementation of the symmetry is very important for an accurate investigation of finite size errors. The latter is crucial for obtaining reliable results especially for more than two particles. Approaches to solve this problem will be described in the following.

## 4.2 Finite size scaling

There are several ways to deal with finite size effects. The simplest is to neglect them and to use the largest possible system size. In order to justify this approach, the size dependence of the results has to be studied. Then one can try to extrapolate the results for finite system to that of the infinite system, see for example the work by Frahm [7], discussed on page 13, equation (26). This has to be done separately for each point in the disorder interaction parameter space. In contrast, the finite size scaling analysis, widely used for studying localization lengths in the absence of interaction, takes the whole data set to extract the localization length of the infinite system. The main assumption is that the reduced localization length,  $\Lambda(W, L) \equiv \lambda(W, L)/L$ , is a function of a single variable. This scaling variable is the ratio of the localization length in the infinite system,  $\lambda^\infty$ , depending only on the disorder strength, and the system size  $L$ ,

$$\Lambda(W, L) = f\left(\frac{\lambda^\infty(W)}{L}\right). \quad (57)$$

There are two limiting regimes for the function  $f$ . If no finite size effects exist, i. e. very large ratio of system size to localization length, the localization lengths  $\lambda(W, L)$  for different system sizes are equal. Consequently,  $\Lambda(W, L) = \lambda^\infty(W)/L$  and  $f(x) = x$ . If instead the localization length  $\lambda^\infty(W)$  is larger than the system size, the measured length  $\lambda(W, L)$  will be proportional to the system size and  $\Lambda(W, L) = f(x) \approx \text{const}$ . Between these two limiting

regimes, the functional form of  $\Lambda_W(L)$  is the same for all disorder values  $W$ , leading to a set of similar curves in the  $\Lambda_W, L$  coordinate system, left part of figure 5. By an appropriate rescaling of the argument,  $L$ , with the scaling parameter  $\lambda^\infty(W)$ , all curves fall on top of each other and form a single scaling curve  $f$ , right part of figure 5. The rescaling is done best on a logarithmic scale where it amounts to shift the curves for different disorder values by  $\ln \lambda^\infty(W)$ . It is performed numerically by a least square fit involving the complete data set [29]. A free parameter remains since the whole curve can be shifted arbitrarily. This parameter is fixed by extrapolating the results for the largest disorder to infinite system sizes or assuming that finite size effects are negligible in this case.

For a single particle, the complete data set and the resulting scaling curve is shown in figures 5 and 6 for the mean radius and the inverse participation ratio, respectively. The

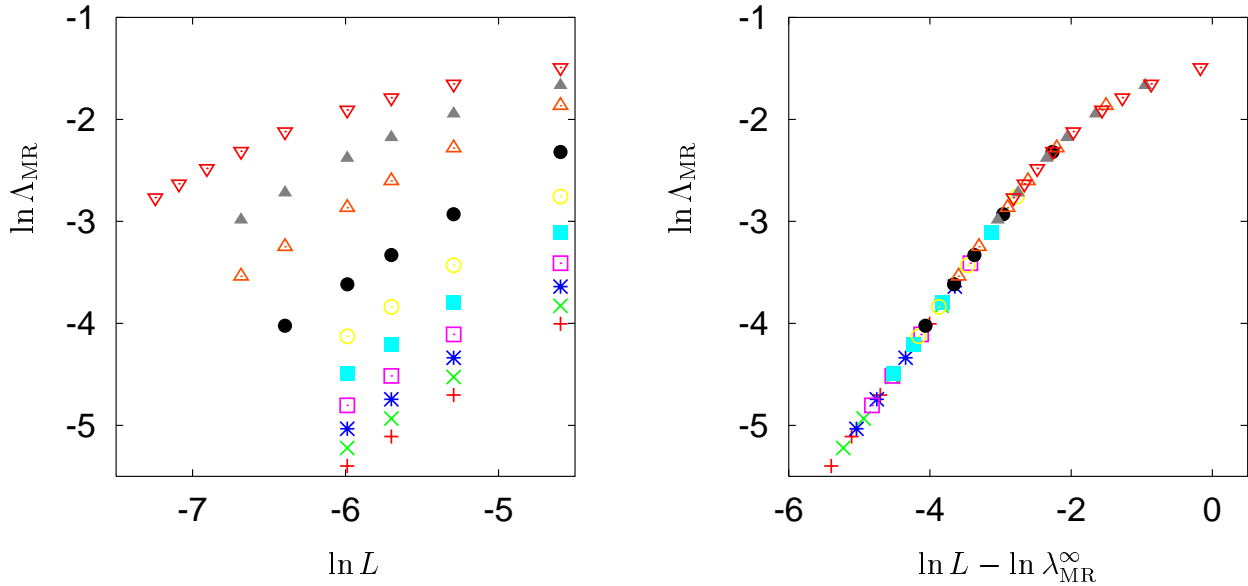


Figure 5: Left: data set for the mean radius, disorder values  $W = 1, 1.5, 2, 3, 4, 5, 6, 7, 8,$  and  $9$  (top to bottom), system sizes  $L = 100, 200, 300, 400, 600, 800, 1000, 1200, 1400$  (right to left). Right: corresponding scaling curve.

quality of the scaling curves, right plot in figure 5 and left plot in figure 6, reveals the validity of the finite size scaling assumption. Since rather large system sizes can be reached, the main part of the scaling curves is in the regime  $f(x) = x$ . The main result is the right part of figure 6, showing the resulting localization lengths for the infinite system. While the result for the mean radius is in agreement with the known  $W^{-2}$  dependence of the single particle localization length for small disorder, strong deviations exist for the inverse participation ratio. This can be understood by expanding the initial condition in terms of eigenstates  $\phi_i$ ,

$$|\psi(t=0)\rangle = \sum_i c_i |\phi_i\rangle \implies |\psi(t)\rangle = \sum_i c_i e^{-iE_i t/\hbar} |\phi_i\rangle. \quad (58)$$

Inserting this into the definition of the mean radius, equation (48), one obtains in the stationary, time averaged limit in which oscillating terms of the form  $\exp[i(E_i - E_j)t/\hbar]$  are

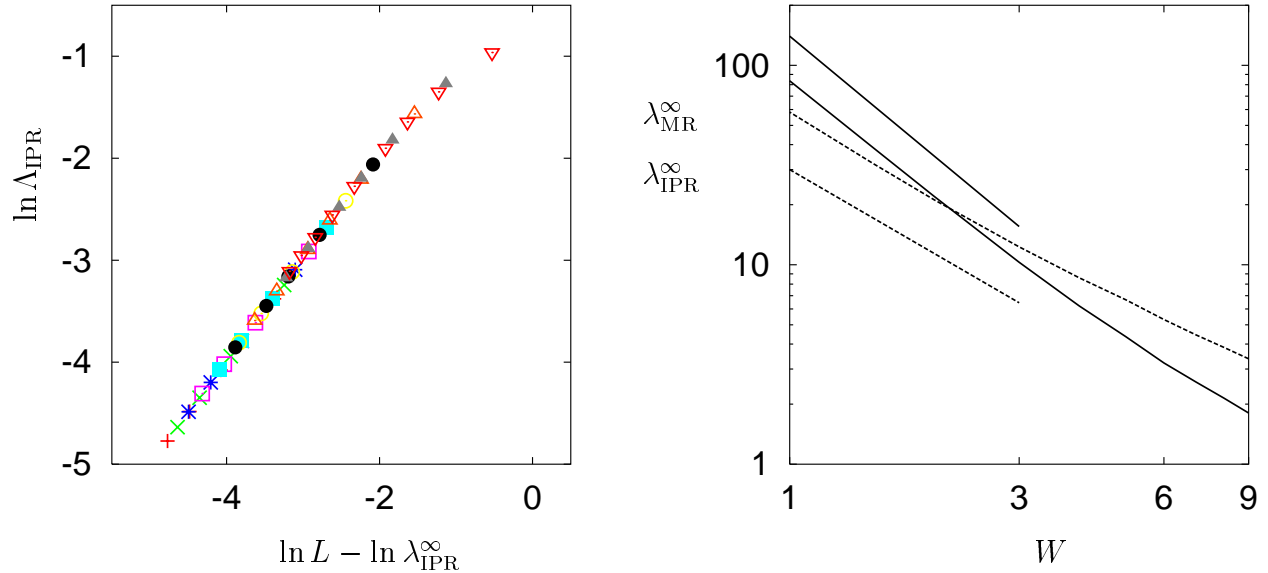


Figure 6: Left: scaling function for the inverse participation ratio, parameters as in figure 5. Right: disorder dependence of the localization lengths  $\lambda_{\text{MR}}^{\infty}$  (solid line) and  $\lambda_{\text{IPR}}^{\infty}$  (dashed line). Short lines indicate slopes of  $W^{-2}$  (solid) and  $W^{-1.4}$  (dashed).

negligible,

$$\lambda_{\text{MR}}^2 = \sum_i |c_i|^2 (\langle \phi_i | j^2 | \phi_i \rangle - \langle \phi_i | j | \phi_i \rangle^2) + \sum_i |c_i|^2 \langle \phi_i | j | \phi_i \rangle^2 - \sum_{i,i'} |c_i c_{i'}|^2 \langle \phi_i | j | \phi_i \rangle \langle \phi_{i'} | j | \phi_{i'} \rangle. \quad (59)$$

The first sum is an average over the mean radii of individual eigenstates weighted with the expansion coefficients. The last sum gives the expectation value of the position operator and is zero upon averaging since  $j \in [-L/2, L/2]$  and  $\langle j | \psi(t=0) \rangle = \delta_{j,0}$ . The second sum can be estimated to be of the order of an averaged localization length squared. To perform this estimate, one assumes that all values  $\langle \phi_i | j | \phi_i \rangle \in [-L/2, L/2]$  can occur and that the expansion coefficients decay exponentially with distance from the origin,

$$\lambda_{\text{MR}}(t \rightarrow \infty) \approx \left[ \sum_i |c_i|^2 \text{MR}_{\phi_i}^2 + O(\bar{\lambda}^2) \right]^{1/2}. \quad (60)$$

For the inverse participation ratio, the situation is more complicated since the product of four exponentials introduces further terms,

$$\text{IPR}^{-1}(t \rightarrow \infty) = \sum_j \left( \sum_i |c_i \phi_i|^4 + \sum_{i \neq i'} |c_i \phi_i|^2 |c_{i'} \phi_{i'}|^2 \right). \quad (61)$$

An upper estimate for  $\text{IPR}^{-1}$  is obtained by neglecting the second term which cannot be expressed in terms of the inverse participation ratio of individual eigenstates,

$$\lambda_{\text{IPR}} = \text{IPR}(t \rightarrow \infty) \leq \frac{1}{\sum_i |c_i|^4 / \text{IPR}_{\phi_i}}. \quad (62)$$

Even if the mean energy of the initial condition is chosen in the middle of the band, equation (58) reveals that all eigenstates of the system contribute. Depending on the energy, they have different localization lengths. Those in the middle of the band will have a larger one than those close to the band edges. It is even more important that the strongly localized states close to the band edges scale differently with disorder strength [251]. The averaging performed during the calculation of the mean radius favors states with large localization lengths and deviations from the usual  $W^{-2}$  scaling are negligible. In contrast, the inverse participation ratio is dominated by states in the band tails with very small localization lengths. This is the reason for the different behavior of the two quantities as a function of the disorder strength. Based upon a detailed analysis, a logarithmic correction,  $\lambda_{\text{IPR}} = \lambda/(a \ln \lambda + b)$  was proposed [252]. Valid in the regime  $\lambda \gg 1$ , it fits the low disorder data of figure 6.

If one could restrict the states contributing to the initial wave packet to a certain energy range, their localization lengths would be similar and inverse participation ratio and mean radius of the wave packet should give similar results. This restriction can be done by applying the operator  $[\hat{1} - (E\hat{1} - \hat{H})^2/E_{\text{max}}^2]^m$  to the initial wave packet. The energies taken into account are then situated in the interval  $E \pm E_{\text{max}}\sqrt{1 - 2^{-1/m}}$  [28, 237]. The analysis described above was repeated with a small energy window ( $m = 10000$ ) around the middle of the band,  $E = 0$ . The results are displayed in figure 7. Now, both quantities behave indeed very similar, a

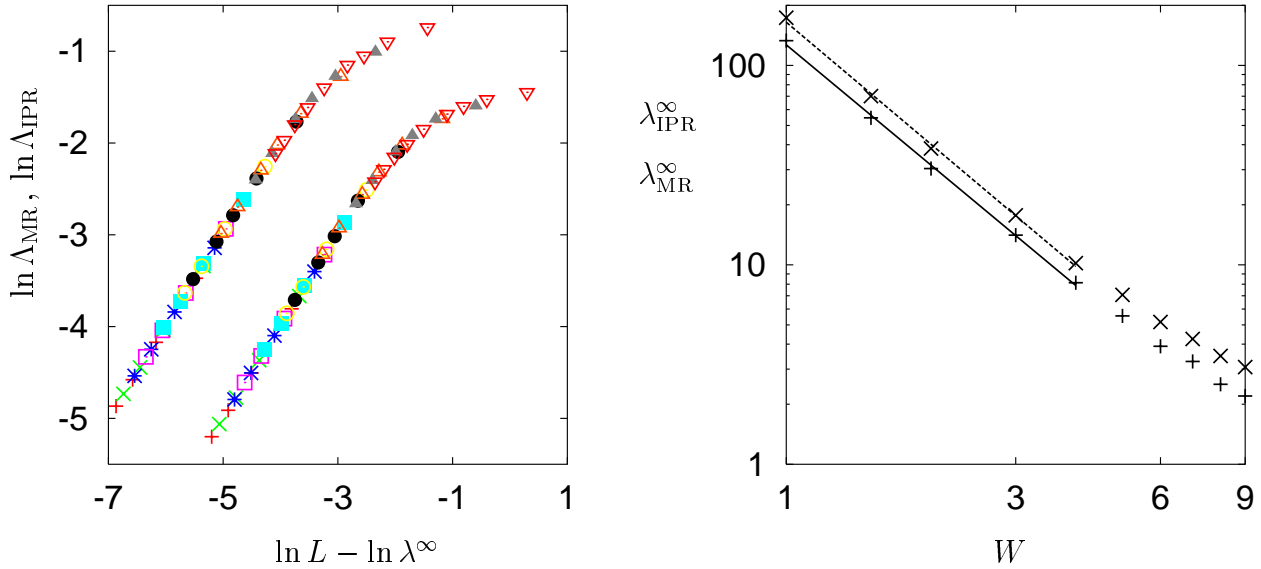


Figure 7: Left: scaling function for the inverse participation ratio (left curve, shifted by -2) and the mean radius obtained using a small energy window around  $E = 0$ , parameters as in figure 5. Right: disorder dependence of the localization lengths  $\lambda_{\text{MR}}^\infty$  (+) and  $\lambda_{\text{IPR}}^\infty$  (x). Solid and dashed lines are power law fits for  $W \in [1, 4]$ , equations (63) and (64).

power law fit  $\lambda^\infty(W) = aW^b$  gives for  $W \leq 4$ ,

$$\lambda_{\text{MR}}^\infty = (126 \pm 4)W^{-2.00 \pm 0.04}, \quad (63)$$

$$\lambda_{\text{IPR}}^{\infty} = (164 \pm 6)W^{-2.03 \pm 0.05}. \quad (64)$$

Estimating the goodness  $Q$  of the fits with the  $\chi^2$  test [253] gives  $Q = 0.392$  and  $Q = 0.387$  for the mean radius and the inverse participation ratio, respectively. Note that both quantities increase upon selecting an energy window in the middle of the band since eigenstates with smaller localization lengths cannot contribute anymore to the averaging in equations (60) and (62). While the disorder dependence is in agreement with the theory, the absolute value is larger than expected. This difference is related to the application of the operator  $[\hat{1} - (E\hat{1} - \hat{H})^2/E_{\text{max}}^2]^m$ , which increases (decreases) the expansion coefficients if the energy of the eigenstate is inside (outside) the energy interval [138]. The initial wave packet is spread onto the lattice before the time evolution starts. Larger initial values of the mean radius result in larger saturation values.

There is one main difference between the finite size scaling described above and the original approach used for quasi one-dimensional samples, see [29] for a detailed description. Originally, the length scale  $L$  was the *transverse* size of the system. Along the transfer direction, the systems were essentially infinite,  $M \gg L$ . While thus very large localization lengths  $M \gg \lambda(W, L) \gg L$  could be reliably studied, the anisotropic increase of the system size with the scaling variable has been criticized. In our case, the system size is fixed in all directions in configuration space,  $L = M$ . While leading to an isotropic increase of the system with the scaling variable, every resulting localization length larger than the system size has to be considered with great care. This should be kept in mind for the remaining part of this thesis. It also has to be considered upon analyzing the results for two particles in two dimensions. Finite size effects that could be interpreted as a metallic branch of the scaling curve can easily be produced numerically if the localization length is much larger than the system size.

### 4.3 Extracting $n$ -particle localization lengths

Quantities quite similar to the mean radius and the inverse participation ratio of one-particle wave packets can be used to extract an  $n$ -particle localization length from the time evolution of  $n$ -particle wave packets. Equations (48) and (49) can easily be generalized to the  $n$ -dimensional configuration space,

$$\text{MR}(t) = \frac{1}{\sqrt{n}} \sqrt{\langle \psi(t) | \sum_{i=1}^n j_i^2 | \psi(t) \rangle - \sum_{i=1}^n (\langle \psi(t) | j_i | \psi(t) \rangle)^2}, \quad (65)$$

$$\text{IPR}^{-1/n}(t) = \sum_{j_1, \dots, j_n} |\langle j_1, \dots, j_n | \psi(t) \rangle|^4. \quad (66)$$

In the absence of interaction, all directions in configuration space are equivalent and the above quantities are well suited for studying localization of  $n$ -particle wave packets. However, it will be shown that in the presence of interaction, the extension of the wave packet in configuration space depends strongly on the direction considered. Since the interaction is most important when the particles are close to each other, the mean extension in center of mass direction turns out to be a very useful quantity,

$$\text{CM}(t) = \frac{1}{\sqrt{n}} \sqrt{\langle \psi(t) | (\sum_{i=1}^n j_i)^2 | \psi(t) \rangle - \left( \langle \psi(t) | \sum_{i=1}^n j_i | \psi(t) \rangle \right)^2}. \quad (67)$$

The pre-factor is chosen in such a way that the result can directly be compared to the one-particle localization length. Strictly speaking, the center of mass is defined as  $\text{CM} = (\sum_{i=1}^n j_i)/n$  leading to a  $1/n$  pre-factor in equation (67). This reduction of the localization length related to the higher total mass is neglected in order to allow for a better comparison of the data for different particle numbers. For two particles, the mean distance between them has been calculated, too,

$$\text{RD}(t) = \frac{1}{\sqrt{2}} \sqrt{\langle \psi(t) | (j_1 - j_2)^2 | \psi(t) \rangle - (\langle \psi(t) | j_1 - j_2 | \psi(t) \rangle)^2}. \quad (68)$$

These quantities not only probe the spatial anisotropy of the wave packet. The center of mass extension for example is related to the conductivity of the  $n$ -particle system. This can be seen upon coupling the full Hamiltonian to an external field,

$$\hat{H}_{\text{ext}} = -\frac{e}{c} \int j(r) A(r, t) dr \quad , \quad (69)$$

and applying time dependent perturbation theory. The term linear in the field defines the conductivity and a straightforward calculation yields

$$\sigma(\omega) \propto \omega \sum_i |\langle \phi_0 | R | \phi_i \rangle|^2 \delta(\varepsilon_i - \varepsilon_0 - \hbar\omega). \quad (70)$$

Here,  $|\phi_0\rangle$  and  $|\phi_i\rangle$  are the ground and excited  $n$ -electron states with energies  $\varepsilon_0$  and  $\varepsilon_i$ , respectively, and  $R = \sum_i x_i/n$  is the center of mass coordinate. For  $\omega \rightarrow 0$  only excited states very close to the ground state contribute. An upper bound is

$$\sigma(\omega) \leq \omega \text{const} \langle \phi_0 | R^2 | \phi_0 \rangle. \quad (71)$$

As long as the expectation value remains finite, the conductivity vanishes for  $\omega \rightarrow 0$ . The calculated localization length  $\lambda_{\text{CM}}$ , equation (60), includes the ground state expectation value and thus gives an upper bound for the conductivity. *As long as  $\lambda_{\text{CM}}$  remains finite, the conductivity will vanish in the zero frequency limit.*

The arguments about the relation of the quantities measured during the time evolution to the individual eigenstates remain valid for  $n$  particles, too. Hence, a diverging  $\lambda_{\text{CM}}$  indicates that at least one eigenstate in the system has an infinite localization length while a diverging  $\lambda_{\text{IPR}}$  requires an infinite localization length of all contributing eigenstates. This follows from the different averages, equations (60) and (62), respectively.

## 5 Two interacting particles

In the preceding section, the time evolution method was introduced. The important quantities like the mean radius and the center of mass extension of  $n$ -particle wave packets were defined. And it was shown that single particle localization lengths can be reliably studied with this method.

The results for two interacting particles that will be presented in this section reveal that the time evolution method in combination with a finite size scaling analysis is also suited well for the study of the localization properties of *interacting* particles. First, it will

be demonstrated that in the absence of interaction the results agree with the predictions. Hence in contrast to the transfer matrix method, any enhancement effect is related to the interaction. Second, the observed enhancement of the localization length in the presence of the interaction is shown to be in agreement with results obtained via the Green function method.

The time evolution for two interacting particles can easily be calculated using the methods described in section 4.1. A typical spreading of the wave packet in configuration space with time is shown in figure 8. Initially, the influence of the interaction can hardly be

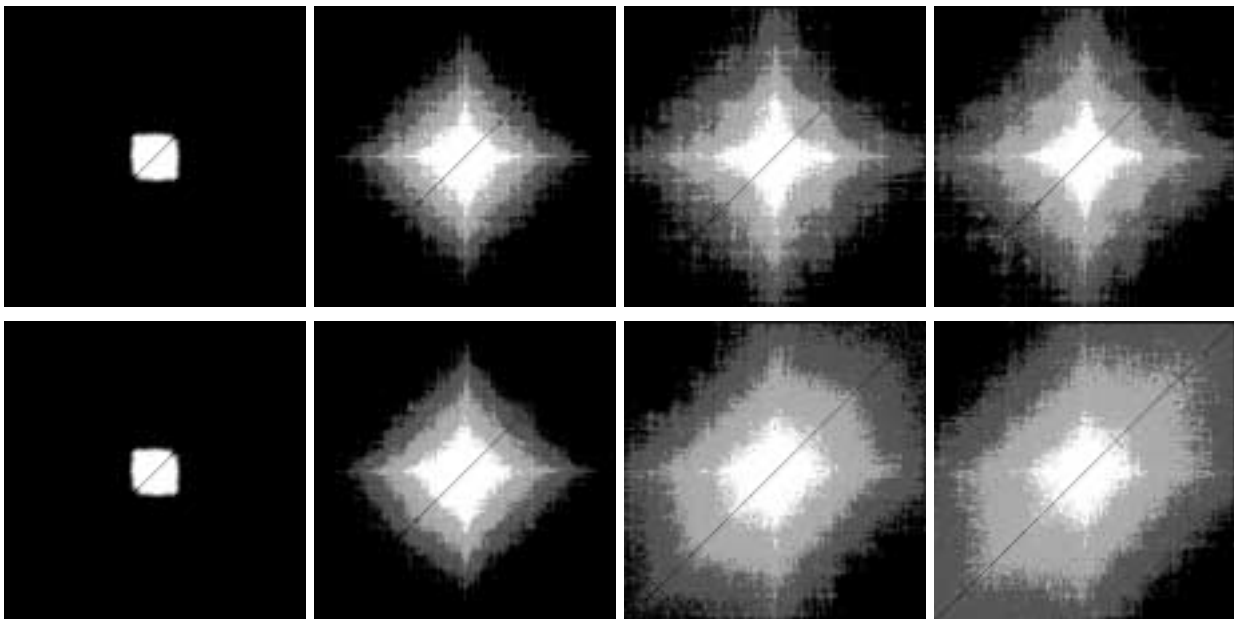


Figure 8: Time evolution of a two-particle wave packet without interaction (top) and for a nearest neighbor interaction of strength  $U=1$  (bottom) for times  $t=10, 100, 1000$ , and  $10000$  (left to right). The plots show the typical amplitude  $|\psi_{j_1, j_2}(t)|^2$ , averaged over 30 disorder realizations. Grey scale coding from white ( $f(x)=1$ ) to black ( $f(x)=0$ ) is performed using a step function  $f(x)=[\Theta(x-0.1) + \Theta(x-0.01) + \Theta(x-0.001)]/3$ .

seen,  $t \leq 100$ , first two columns of figure 8. Only after the one-particle localization domain has been explored, the interaction leads to a further growth of the wave packet. The fact that this growth persists only along the center of mass direction in configuration space reveals a correlated motion of the two particles due to the interaction as underlying physical mechanism. For a time much larger than the one-particle localization time, this growth stops, revealing as for a single particle the localization of all states in the spectrum.

In the following, after a few necessary technical remarks, the time evolution and the different localization lengths defined above, are discussed. They reveal the reliability of the new method for the calculation of localization lengths for interacting particles.

## 5.1 Initial conditions

The choice of suitable initial conditions is very important for the investigation of the interacting particle problem. If the initial wave packet corresponds to two particles far away from each other, no effect is expected. Only if the two particles are close to each other, a major contribution to the wave packet comes from two-particle eigenstates with an interaction induced larger localization length. In addition, the delocalization mechanism should be most efficient for large enough single particle localization lengths, that is for energies in the middle of the band. This can only be achieved if the total energy is in the middle of the band, too. However, restricting the energy distribution of the states that build up the initial wave packet, the relative distance between the electrons grows. This disadvantage is larger than the advantage due to the energy selection. For this reason, it is reasonable to consider initial states without energy selection. Nevertheless, the mean energy should be in the middle of the band. Then, due to the van Hove singularity in the density of states at  $E=0$ , figure 9, most of the contributing eigenstates will indeed have energies in the middle

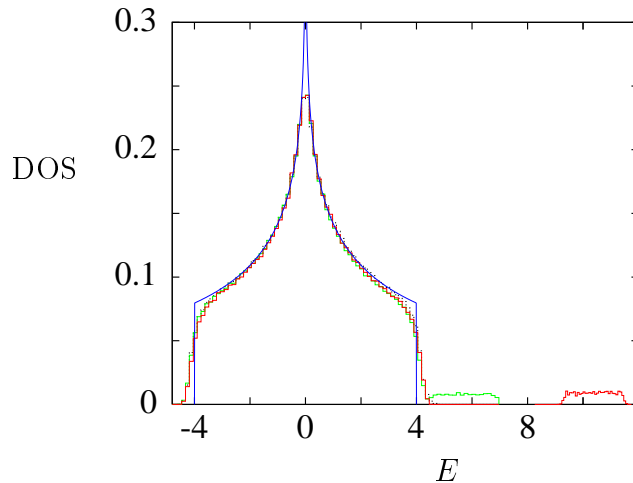


Figure 9: Density of states of two-particle wave functions. Interaction energies  $U = 1, 5, 10$  (yellow, green, and red line) are compared to the density of states for a two dimensional tight binding lattice (blue line).

of the band, even if there is no direct energy selection.

How can the mean energy be fixed? For strongly localized initial states where each particle occupies a single lattice site, the energy of the wave packet is only given by the potential energies at these sites plus maybe a contribution from the interaction energy. A mean energy in the middle of the band can be obtained by choosing the potential energies at the initial sites adequately, e. g.  $\varepsilon_0 = \varepsilon_2 = 0$ .

The remaining question is the initial distance between the two particles. As long as it is shorter than the one-particle localization length, the long time dynamics is independent of the initial condition. Only the short time dynamics is influenced. For a symmetric spatial wave function, i. e. particles with opposite spins, initial conditions with two particles on the same site and on neighboring sites were analyzed [140]. For two particles on the same site, the ratio between the center of mass and the relative extension showed that the interaction

suppressed the motion in center of mass direction for short times. This suppression was related to the fact that sites along the center of mass direction in configuration space had on average an energy difference of  $U$  and were thus harder to reach. A similar behavior was observed for two particles initially being on neighboring sites.

This reduction of the ballistic motion is less pronounced if the disorder is chosen such that it compensates the interaction locally in order to achieve a mean energy in the middle of the band. In simple words, the short range interaction defines a wall in configuration space. This wall does not hinder the relative spreading, but the one along the center of mass direction. This effect is weaker when the local compensation introduces holes into the wall. Note that the center of mass and the relative extension defined in [140] always start from zero at  $t=0$ , even if the two particles are located far from each other. They differ slightly from equations (67) and (68) which measure really the center of mass extension and the distance between the two particles and hence can have different starting values. In this case, a more adequate measure than the ratio of center of mass and relative coordinate is given by a direct comparison of results with and without interaction, e. g. the time evolution of  $\text{CM}(U=1)/\text{CM}(U=0)$  or  $\text{CM}(U=1) - \text{CM}(U=0)$  using the same disorder realizations for both calculations.

## 5.2 Time evolution

One advantage of the quantum diffusion method for studying localization properties is that the time evolution yields important information about the physical mechanism leading to the interaction-induced delocalization.

In figure 10, the time evolution of the center of mass extension is shown with and without interaction for different disorder values. Note the logarithmic scale on the time axis which

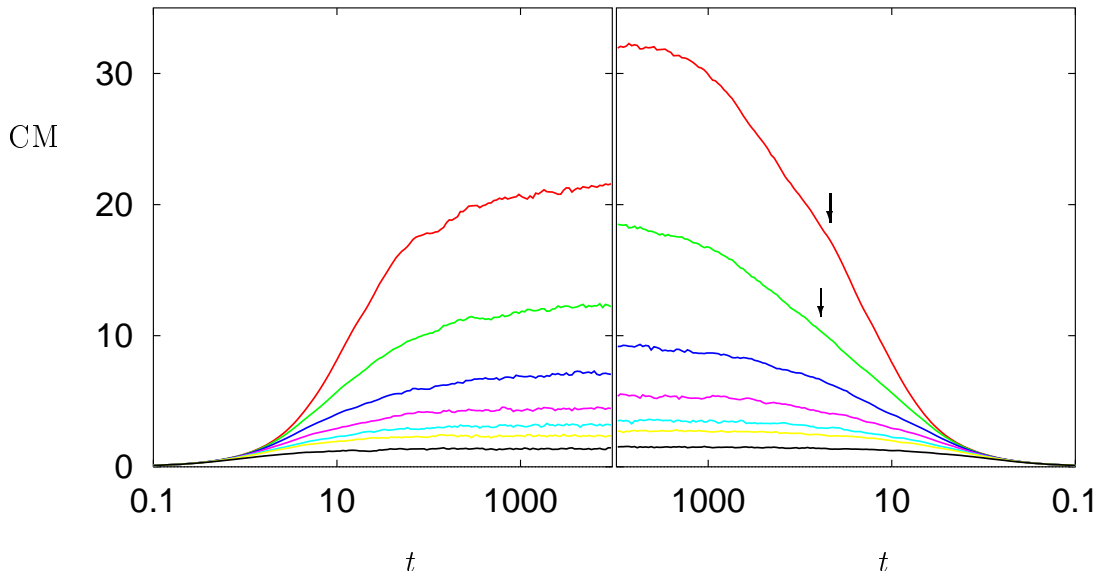


Figure 10: Time dependence of center of mass extension for  $U=0$  (left) and  $U=1$  (right) for disorder values,  $W=2, 3, 4, 5, 6, 7$  and  $10$  (top to bottom) and a system size  $L=139$ .

turns out to be most suitable for representing the data, see figure 11. The interaction-induced

delocalization is obvious, leading to larger saturation values of the center of mass extension in the presence of interaction. After the single particle localization time is reached (arrows in figure 10), the center of mass extension grows very slowly such that a logarithmic time-scale is appropriate. In contrast to the situation without interaction, where only a crossover from a ballistic to a localized regime takes place, figure 4, the interaction establishes an intermediate regime characterized by a logarithmically slow growth of the center of mass extension with time. These three regimes are visible in figure 11, showing the size dependence of the results for a single disorder value. The ballistic regime is most obvious in the right plot, where

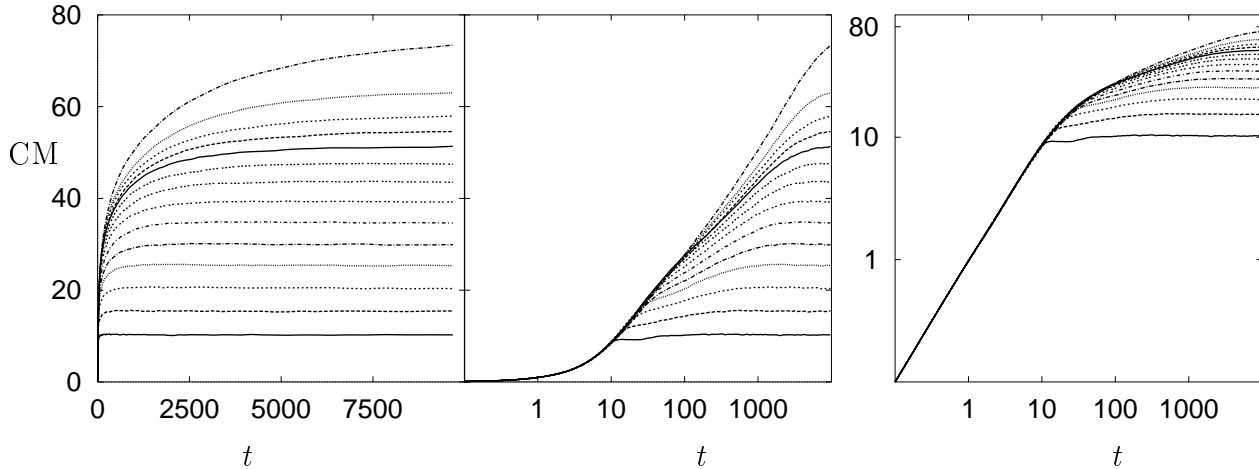


Figure 11: Time dependence of center of mass extension for  $U = 1$  and  $W = 1.75$  for system sizes  $L = 39, 59, 79, 99, 119, 139, 159, 179, 199, 219, 239, 259, 299,$  and  $399$  (bottom to top): normal scale (left), logarithmic time-scale (middle) and double logarithmic scale (right).

$CM(t) \propto t$  yields the straight line for  $t \leq 10$ . The intermediate regime is revealed on the logarithmic time-scale in the middle plot, indicating a growth  $CM(t) \approx a \log(t) + b$ . The scale is important since only the logarithmic time-scale really reveals the saturation of the growth, and hence the third regime.

To analyze better the influence of the interaction, the difference between the results with and without interaction is shown in figure 12 for a relatively large system size. For short times, the interaction suppresses the motion, most pronounced for the center of mass extension. After the single particle localization time is reached ( $F(U=0) = \text{const.}$ ), a slow logarithmic growth,

$$F(U=1) - F(U=0) = c_1 \log(t) + c_2, \quad (72)$$

is observed for all quantities for more than an order of magnitude in time. This can also be demonstrated by looking directly at the intermediate regime which exists with interaction, left part of figure 12. The presented data clearly indicates that the growth along the center of mass direction is *not* diffusive,  $F(U=1) = c_1 \sqrt{t} + c_2$ , in contrast to all theoretical predictions. This observation questions the validity of the underlying theory discussed in section 3.

For times longer than the two-particle localization time, the spreading of the wave packet stops and an asymptotic shape is reached. The profile of the wave packet in this asymptotic limit along the two important axis in configuration space is shown in figure 13. To obtain a

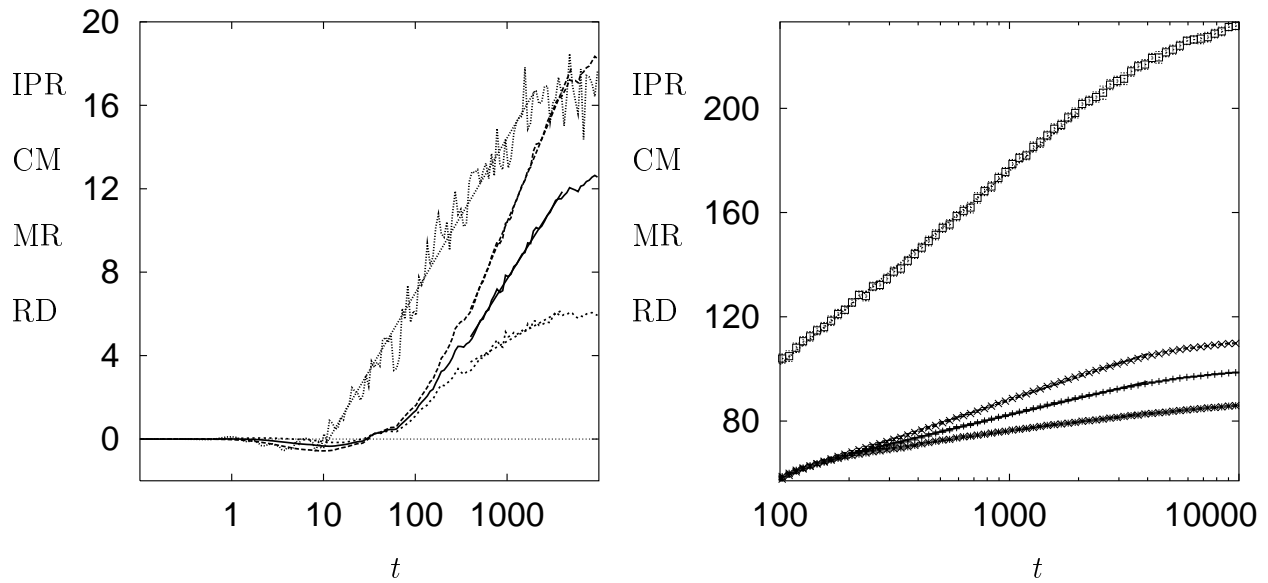


Figure 12: Left: time dependence of difference  $F(U=1) - F(U=0)$  for the mean radius (solid), the center of mass extension (dashed), the relative distance (short dashed), and the inverse participation ratio (dotted line). System size is  $L=279$ , disorder is  $W=2$ . Right:  $F(U=1)$  in the intermediate regime for IPR, CM, MR, RD (top to bottom),  $L=399$  and  $W=1$ . Straight lines are fits with  $c_1 \log(t) + c_2$  in both cases.

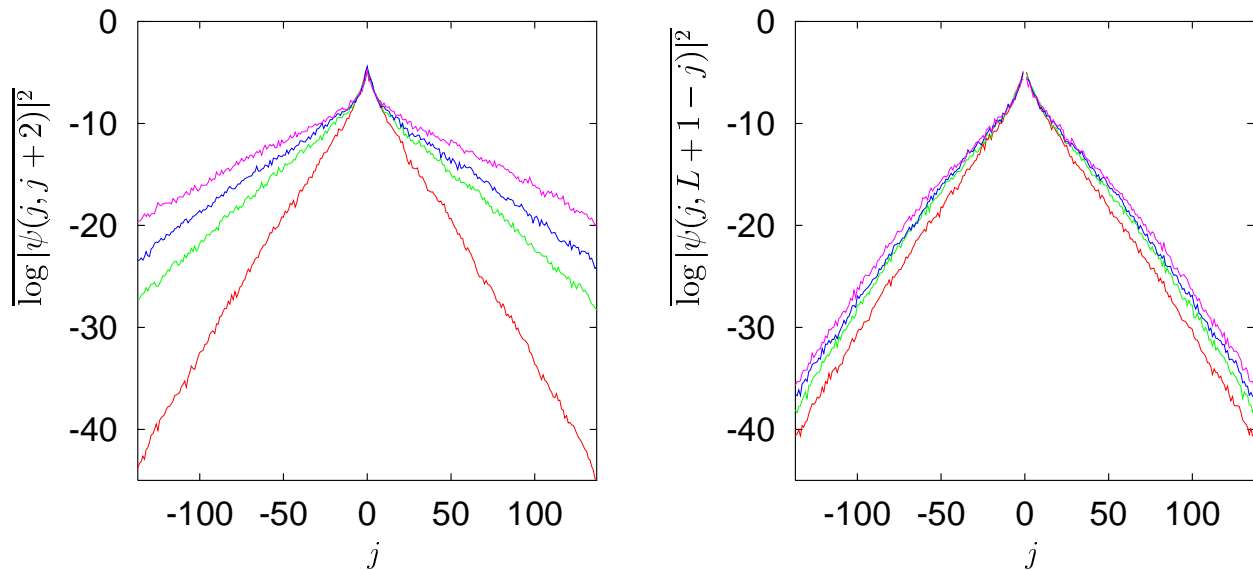


Figure 13: Typical wave packet profiles for long times along center of mass (left) and relative direction (right). Disorder strength:  $W=3$ , system size:  $L=279$  and interaction strengths:  $U=0.0$  (red),  $0.5$  (green),  $1.0$  (blue), and  $4.0$  (magenta), bottom to top.

typical shape, logarithmic averaging is performed over 50 disorder realizations. Along both the relative and the center of mass direction, the wave packet is exponentially localized. While the interaction hardly influences the localization length along the relative direction, it

increases strongly the localization length along the center of mass direction. In the vicinity of the starting point, the curves are similar, dominated by the single particle localization length. Only for distances larger than  $\lambda_1 (\approx 11)$ , the two-particle localization length is relevant. Note that the localization length increases further even for  $U=4$ . This indicates that the duality described on page 21 for an on-site interaction and a symmetric wave packet does not hold in the case of a nearest neighbor interaction. The interaction dependence will be analyzed in detail below.

A high resolution plot of the full wave packet at saturation is shown in figure 14. Six

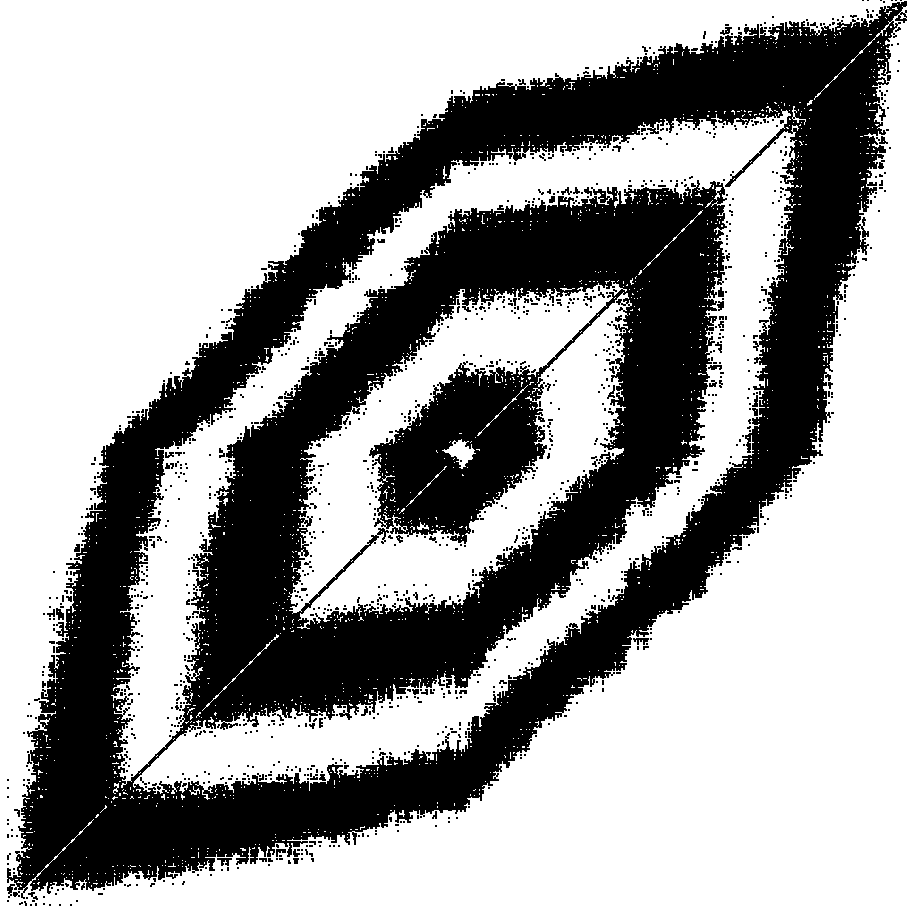


Figure 14: Two-particle wave packet after the localized regime is reached,  $L = 800$ ,  $U = 2$ , and  $W = 2$ . Amplitude coding is described in the text.

orders of magnitude are shown. The mean value of  $|\psi(i, j)|^2$  is defined to be one. From the center, white indicates first order of magnitude,  $100 < |\psi(i, j)|^2 \leq 1000$ , black indicates second order,  $10 < |\psi(i, j)|^2 \leq 100$ . In the following, white, black, white, and black indicate each the decrease of  $|\psi(i, j)|^2$  by another order of magnitude. The central region reveals still the quadratic structure of a non-interacting wave packet, only beyond the one-particle localization border, the interaction-induced delocalization leads to the asymmetric shape, as seen already in figure 13.

### 5.3 The two-particle localization length

As for the one-particle calculations, the long-time saturation values of the quantities defined in equations (65, 66, 67, 68) determine the different two-particle localization lengths. To obtain these values from the disorder averaged time evolution of figures 10 and 11, the complete long-time behavior is taken into account instead of only the value for the largest time. This procedure increases the quality of the results for two reasons. First, small oscillations around the saturation value are average out. Second, as can best be seen in the middle plot of figure 11, saturation might not be complete for the lowest disorder values. Fitting the complete long-time behavior then gives a reasonable extrapolation. That long enough times have been considered in the calculations presented here can be seen from the fact, that the extrapolated saturation values are within the statistical error bars of the disorder averaged value for the longest times considered. This statistical error is smaller than 1% for the most important low disorder values. As the same number of samples was used for the larger disorder values  $W \geq 6$  for which the wave packets explore a much smaller number of lattice sites, the relative accuracy is only around 3% in this case. This is the reason for the small scatter in the large disorder region of the scaling plots. For the results without interaction, an exponential ansatz of the form

$$f(t) = c_1 (1 - e^{-c_2 t^{c_3}}) \quad (73)$$

was used due to its flexibility. With interaction, based on the knowledge that the intermediate regime is best described by a logarithmic growth,

$$g(t) = [c_1 \log(t) + c_2] e^{-t/c_3} + c_4 (1 - e^{-t/c_3}) \quad (74)$$

is used. The use of  $g(t)$  instead of  $f(t)$  for the interacting case enhances the quality of the fits. The non-linear fitting was performed with the Levenberg-Marquardt method [253]. For most of the fits, the time range  $t \in [100, 10000]$  was considered, in some cases the lower bound had to be shifted slightly to ensure a good fit. For the large disorder results one is deep in the asymptotic regime for the times considered. Since the logarithmic growth is not very pronounced problems with  $g(t)$  can occur. In that case an average over the asymptotic regime provides the most accurate result for the saturation value. The quality of the fits is demonstrated in figure 23. The resulting localization lengths in dependence of system size and disorder strength have then been used for the finite size scaling analysis.

#### 5.3.1 Mean radius and inverse participation ratio

Figure 15 displays the results for the mean radius without interaction. Calculations were performed for disorder strengths  $W = 1.25, 1.5, 1.75, 2.0, 2.5, 3.0, 4.0, 5.0, 6.0, 7.0, 8.0, 9.0,$  and  $10.0$ , top to bottom in left plot in figure 15. System sizes were  $L = 39, 59, 79, 99, 119,$  and  $139$  (right to left), sufficient for an accurate calculation of localization lengths up to 70. The resulting localization lengths scale with disorder as the transfer matrix results of the one-particle localization length, only the absolute value is by a factor of 1.22 larger than expected naïvely, figure 17. This difference is related to the averaging over the single particle energies (20), conjectured in [8] and proven in [9]. This result demonstrates that the quantum diffusion method is well suited for studying interaction effects on the localization properties

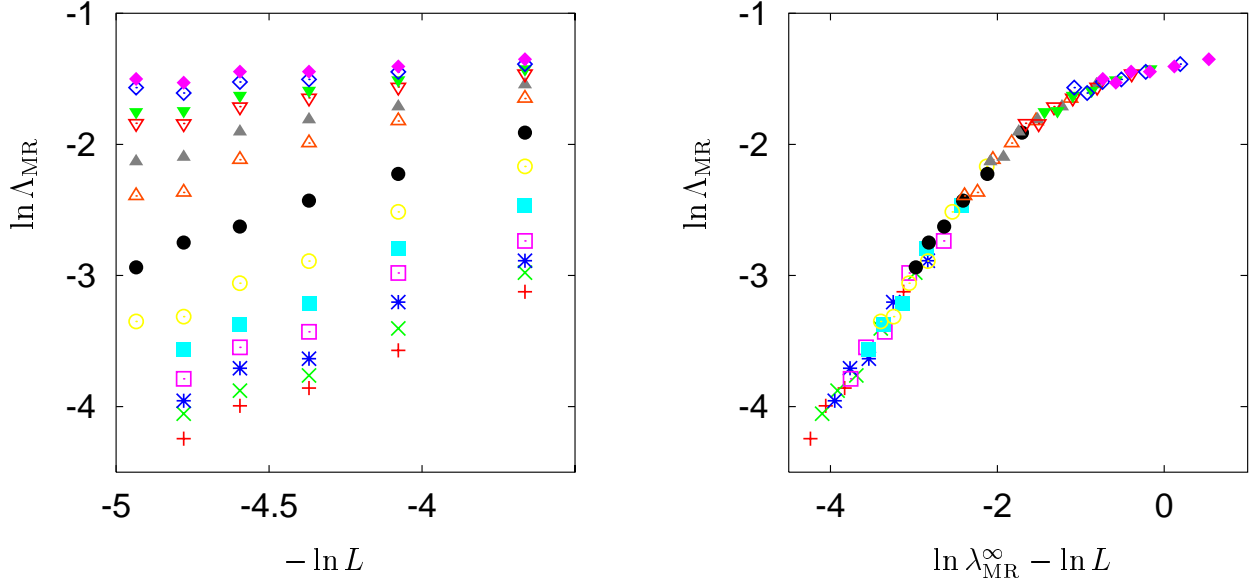


Figure 15: Finite size scaling for the mean radius for  $U = 0$ . Left: raw data; right: corresponding scaling curve.

of few-particle wave packets because it gives the correct results for the non-interacting case, in contrast to the transfer matrix method. The scaling for the saturation values of the mean radius with interaction is shown in figure 16. The disorder values are apart from an

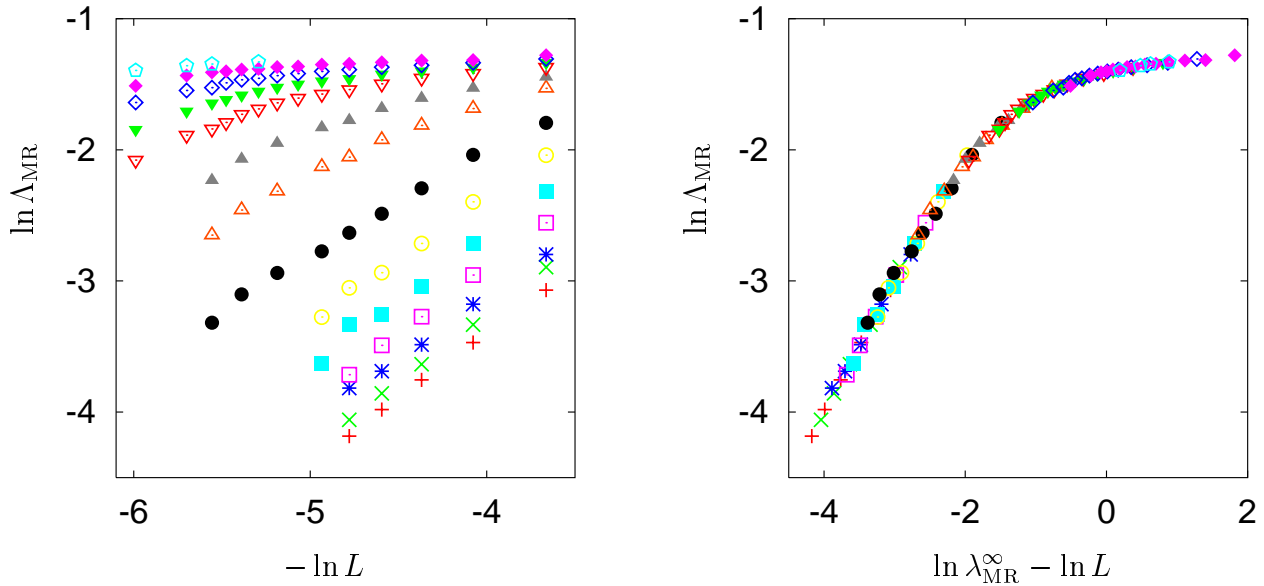


Figure 16: Same as figure 15 for  $U = 1$ .

extra point at  $W = 1$  the same as above. Due to the larger localization lengths, the range of system sizes is enlarged,  $L = 39, 59, 79, 99, 119, 139, 159, 179, 199, 219, 239, 259, 299, 399$ . Figure 17 demonstrates the increase of the localization length with the interaction. The

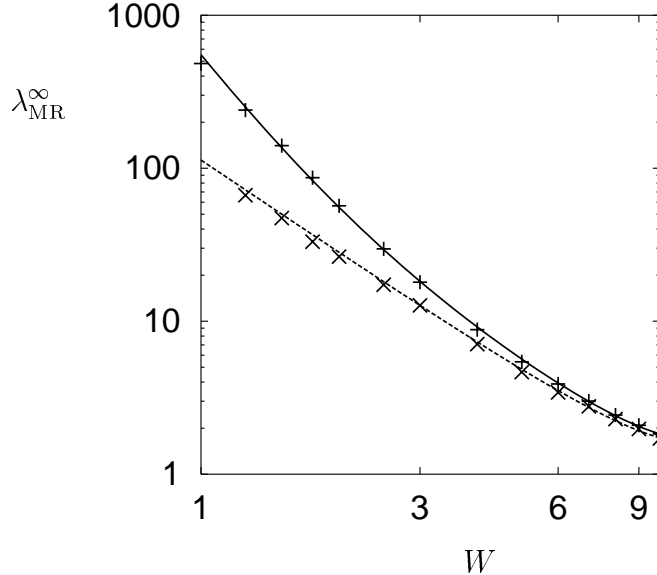


Figure 17: Mean radius localization length in the infinite system for  $U = 1$  (+) and  $U = 0$  (×). Solid line: equation (75), dashed:  $1.22\lambda_1$ .

data can be perfectly fitted with a crossover from the one-particle localization length  $\lambda_1$  to  $\lambda_1^2$  for decreasing disorder,

$$\lambda_{\text{MR}}^{\infty}(U = 1, W) = (1.225 \pm 0.008)\lambda_1(W) + (0.051 \pm 0.002)\lambda_1^2(W). \quad (75)$$

In order to obtain the errors of the fit parameters, error bars for the scaling parameter  $\lambda_{\text{MR}}^{\infty}$  are necessary. Estimated from the slope of the scaling curve, the error is small for large disorder values where the data points are in a region of the scaling curve with a slope close to one. It gets larger for smaller disorder values with data points in the flat region of the scaling curve. The goodness of the fit as estimated with a  $\chi^2$  analysis [253] is roughly  $Q = 0.3$ . For the  $U = 0$  data, a fit with equation (75) leads to a negative sign and a very large error for the  $\lambda_1^2$  term, indicating its irrelevance for describing the data.

In the literature, a power law fit for the low disorder behavior was widely used to quantify the enhancement effect. In the range  $W \in [1, 3]$ ,  $\lambda_{\text{MR}}^{\infty}(U = 1, W) \propto W^{-2.94 \pm 0.04}$  is found, similar to results obtained with the Green function method [8, 9], see section 3.1.3. The original prediction by Shepelyansky  $\lambda_2 \propto \lambda_1^2$  is dominant only for disorder values  $W \leq 1$  but the crossover to that regime is visible.

The results for the inverse participation ratio are displayed in figure 18. As for the mean radius, the finite size scaling ansatz works and the localization length is enhanced due to the interaction. Discrepancies exist between the  $U = 0$  data and the one-particle localization length, even though they are smaller than for a single particle without energy selection, figure 6. The logarithmic singularity in the density of states provides a kind of energy selection. The remaining difference is as for a single particle related to the averaging over eigenstates performed upon calculating the inverse participation ratio of the wave packets, page 40. However, even if the energy would have been restricted, an average over all single particle energies is performed, see equation (20). Nevertheless, the data can still be described using

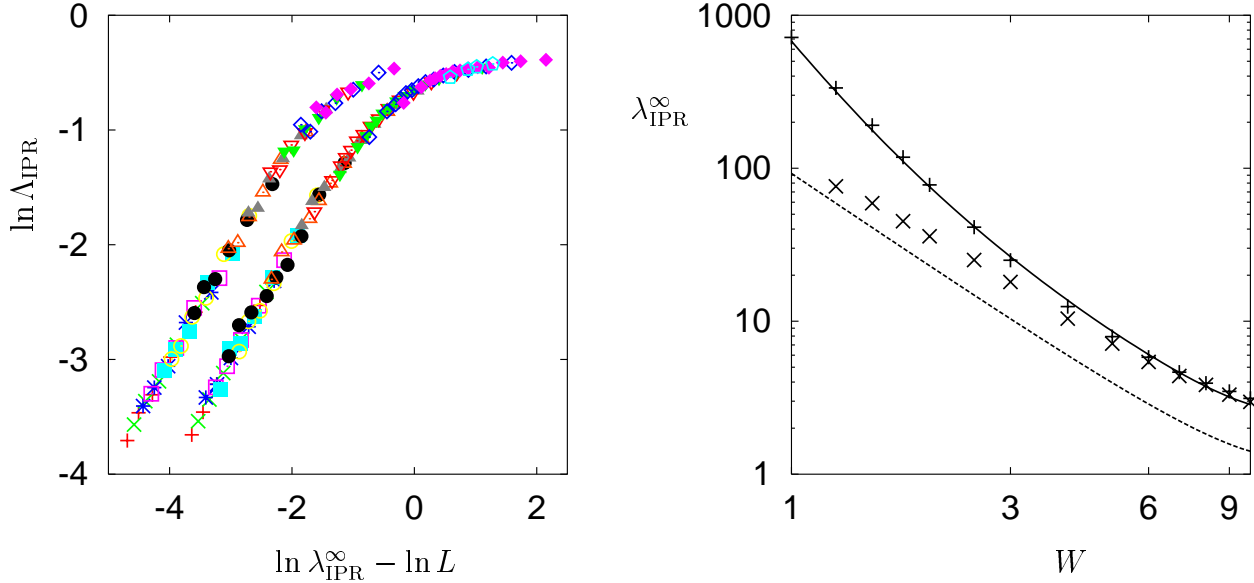


Figure 18: Finite size scaling for the inverse participation ratio. Left: scaling curves for  $U=0$  (left, data shifted by -1) and  $U=1$  (right). Right: localization length in the infinite system for  $U=1$  (+) and  $U=0$  (x) compared to the one-particle localization length  $\lambda_1$  (dashed line). Solid line is equation (77).

the logarithmic correction introduced on page 40.

Considering as for the mean radius only low disorder values and fitting the data for  $U=1$  with a power law yields,

$$\lambda_{\text{IPR}}^{\infty}(U=1, W) = (682 \pm 19)W^{-3.11 \pm 0.05}, \quad W \in [1, 2.5] \quad (76)$$

compared to the crossover fit

$$\lambda_{\text{IPR}}^{\infty}(U=1, W) = (1.94 \pm 0.04)\lambda_1(W) + (0.06 \pm 0.01)\lambda_1^2(W), \quad W \in [1, 10]. \quad (77)$$

Both the mean radius and the inverse participation ratio are insensitive to the spatial shape of the wave packet in configuration space. As can be seen already from the plots of the time evolution (figure 8), from the cross sections of the stationary wave packets (figure 13) and from the shape of the wave packet in the long time limit (figure 14), along different directions in configuration space the localization lengths differ. This anisotropy will be analyzed in the next section.

### 5.3.2 Anisotropic localization

The result for the saturation value of the center of mass extension is shown in figure 19. As expected, the delocalization is more pronounced than for the mean radius and the inverse participation ratio, compare with figures 17 and 18. For  $U=0$ , again a very good agreement with the one-particle localization length is observed, strengthening the applicability of the method. To perform the scaling in the presence of the interaction, the smallest sample

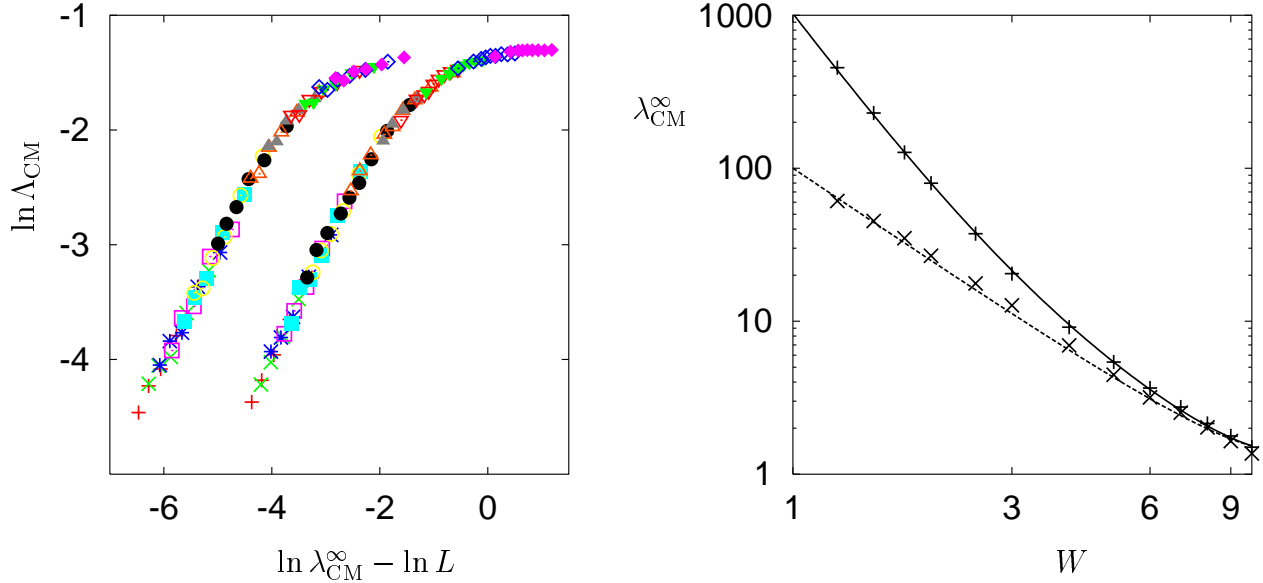


Figure 19: Finite size scaling for the saturation value of the center of mass extension. Left: scaling curves for  $U=0$  (left, shifted by -2) and  $U=1$  (right). Right: localization length in the infinite system for  $U=1$  (+), fitted with equation (79) (solid line), and  $U=0$  (x), fitted with  $1.08\lambda_1$  (dashed line).

sizes have been left out for the lowest disorder values since they showed dominant finite size errors. Along the center of mass direction, the largest localization lengths and consequently the largest finite size errors are observed. Leaving out the sample sizes with dominant finite size errors reduces the error bars for the localization length and yields a more reliable scaling curve. The resulting localization length can be fitted with,

$$\lambda_{\text{CM}}^\infty(U=1, W) = (987 \pm 40)W^{-3.60 \pm 0.06}, \quad W \in [1, 2.5], \quad (78)$$

$$\lambda_{\text{CM}}^\infty(U=1, W) = (0.93 \pm 0.01)\lambda_1(W) + (0.11 \pm 0.003)\lambda_1^2(W), \quad W \in [1, 10]. \quad (79)$$

The influence of the  $\lambda_1^2$  term is more pronounced than for all other quantities, indicating the proximity to the regime  $\lambda_2 \propto \lambda_1^2$  predicted by Shepelyansky. This proximity is also seen from the slope of  $-3.6 \pm 0.06$  for the low disorder power law fit, very close to the predicted value of  $-4$ .

For comparison, the results for the extension in relative direction are shown in figure 20. As expected from the cross sections of the wave packets at saturation, right plot in figure 13, the relative extension is hardly influenced by the interaction. Only a very small effect is visible, which is related to the logarithmically slow increase of the pair size predicted in [189, 200] and observed in [140] and figure 12. Fitting as above yields,

$$\lambda_{\text{RD}}^\infty(U=1, W) = (195 \pm 2)W^{-2.32 \pm 0.02}, \quad W \in [1, 2.5], \quad (80)$$

$$\lambda_{\text{RD}}^\infty(U=1, W) = (1.42 \pm 0.02)\lambda_1(W) + (0.0094 \pm 0.0008)\lambda_1^2(W), \quad W \in [1, 10]. \quad (81)$$

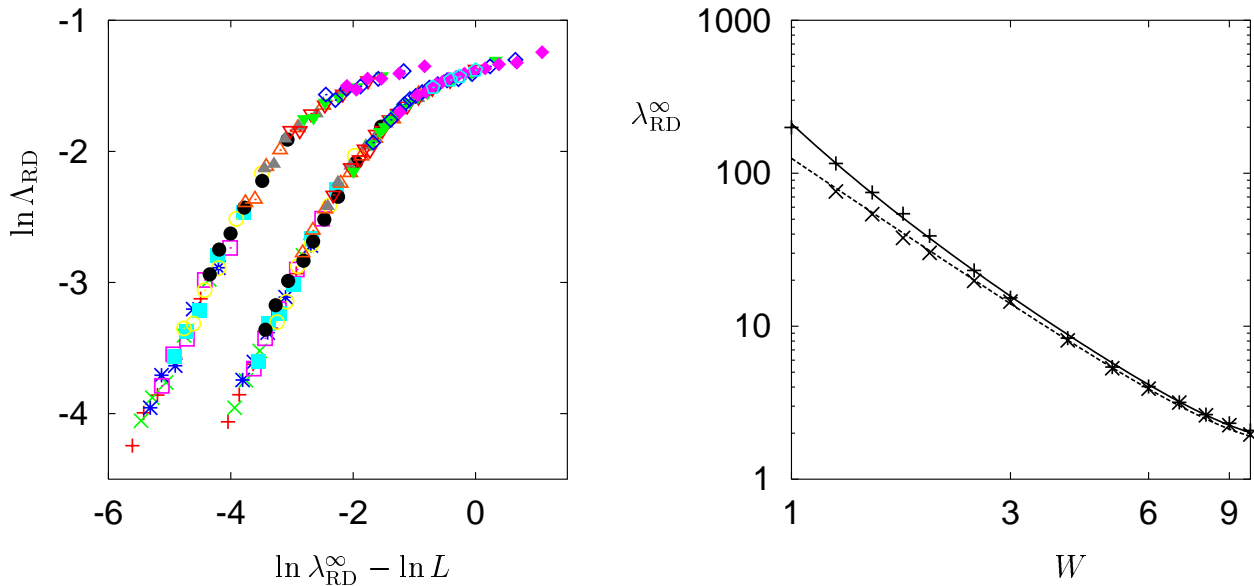


Figure 20: Finite size scaling for the extension in relative direction. Left: scaling curves for  $U=0$  (left, data shifted by -1.5) and  $U=1$  (right). Right: localization length in the infinite system for  $U=1$  (+), fitted with equation (81) (solid line), and  $U=0$  (x), fitted with  $1.35\lambda_1$  (dashed line).

The comparison with the extensions in center of mass directions indicates the importance of the interaction. A larger localization length is only observed along directions in configuration space where the interaction is relevant. Thus the short range interaction leads to a highly anisotropic configuration space. The influence of a long range interaction will be discussed in the next part.

### 5.3.3 Influence of the interaction

In figure 21, the influence of a Coulomb,  $U(i, j) = 1/|i - j|$ , and a random interaction,  $U(i, j) \in [-1, 1]$ , is shown. For the random interaction, no anisotropy in configuration space is found. Considered system sizes are  $L = 39, 59, 79, 119, 159, 199$  for the Coulomb interaction and  $L = 39, 59, 79, 119, 159, 199, 239, 299, 399$  for the random interaction. The long range Coulomb interaction shows a larger delocalization effect than a short range interaction both for the center of mass extension and the relative distance, but qualitatively the results are similar. A different result is obtained for a random interaction which does not provide a preferred direction of propagation in configuration space. The large enhancement of the localization length in comparison to the other interaction potentials can be understood because the spatial correlations in the random potential, see equation (53), lose importance if a random interaction is present everywhere in configuration space. In the zero disorder limit, the Hamiltonian is that of a single particle in two dimensions with the interaction strength replacing the disorder strength.

Having discussed the influence of the interaction range and form, what about its strength? For an on-site interaction and the necessarily spatially symmetric two-particle wave function,

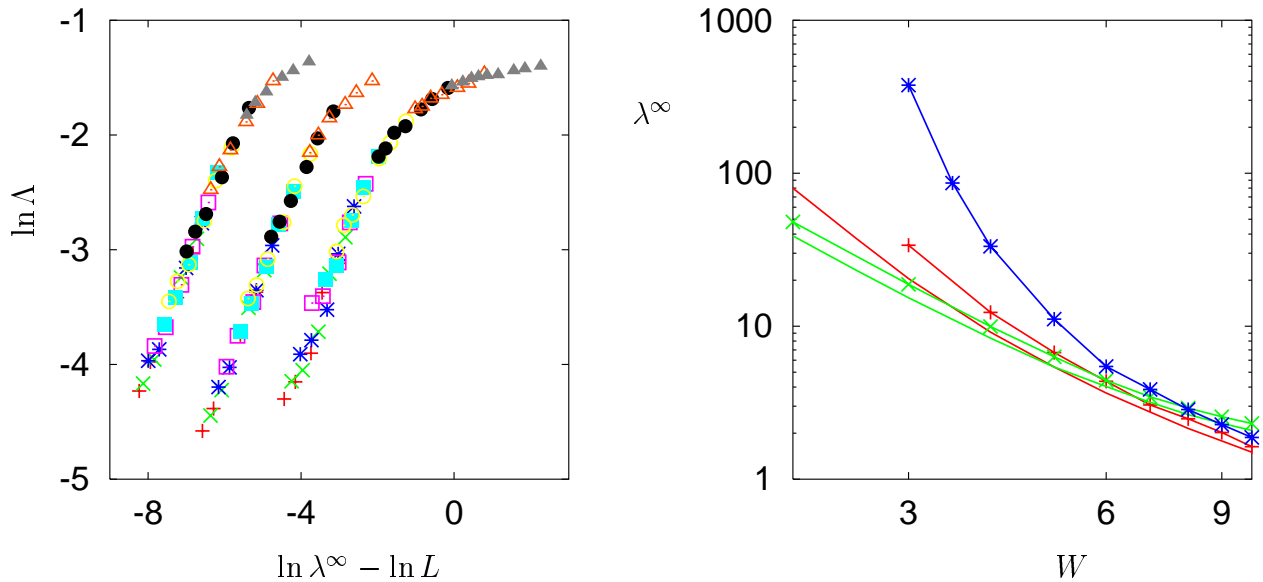


Figure 21: Finite size scaling for different kinds of interaction potentials. Left: from right to left: scaling curves for a random interaction (MR) and for a Coulomb interaction (CM and RD, shifted by -2 and -4). Right: localization length for the random,  $\lambda_{\text{MR}}^\infty$  (\*, blue line), and Coulomb interaction,  $\lambda_{\text{CM}}^\infty$  (+, red) and  $\lambda_{\text{RD}}^\infty$  ( $\times$ , green), compared to  $\lambda_{\text{CM}}^\infty$  and  $\lambda_{\text{RD}}^\infty$  for a nearest neighbor interaction, red and green line, respectively.

a duality between the small and large interaction limits was predicted and observed for the level statistics in [141]. For the localization length, qualitative but not quantitative agreement with the duality prediction was reported [9], the maximum of the localization length for example depended on the disorder strength in contrast to the prediction. The results of calculations with a nearest neighbor interaction and an antisymmetric spatial wave function are shown in figure 22. The finite size scaling analysis for the nearest neighbor interaction has been performed with system sizes  $L = 39, 79, 119, 159, 199, 239, 279$ . Even for the largest interaction strength considered, the localization length continued to increase, neglecting the little scatter for large disorders related to the disorder averaging. No sign of the duality is observed. Apparently, it is valid only for the special case of an on-site interaction, see the right plot in figure 22, comparing both interactions for a single disorder value and system size. This observation indicates that one has to be careful with simplified predictions about the dependence of the localization length on interaction strength because a very small difference in the interaction range can drastically alter the results. So far, there is no theoretical understanding of the interaction-induced delocalization that can explain these differences. In a mapping to a random matrix model, both interactions would give the same results! Maybe this difference can be resolved by investigating both interactions in perturbation theory. Such an approach revealed a different influence of a nearest neighbor and an on-site Hubbard interaction on the persistent current [254].

The interaction dependence in the right plot of figure 22 seems to be logarithmic, the curves resemble straight lines for  $U \leq 1$ . For the nearest neighbor interaction the increase with interaction strength seems to be even slower than logarithmic. These are only qualita-

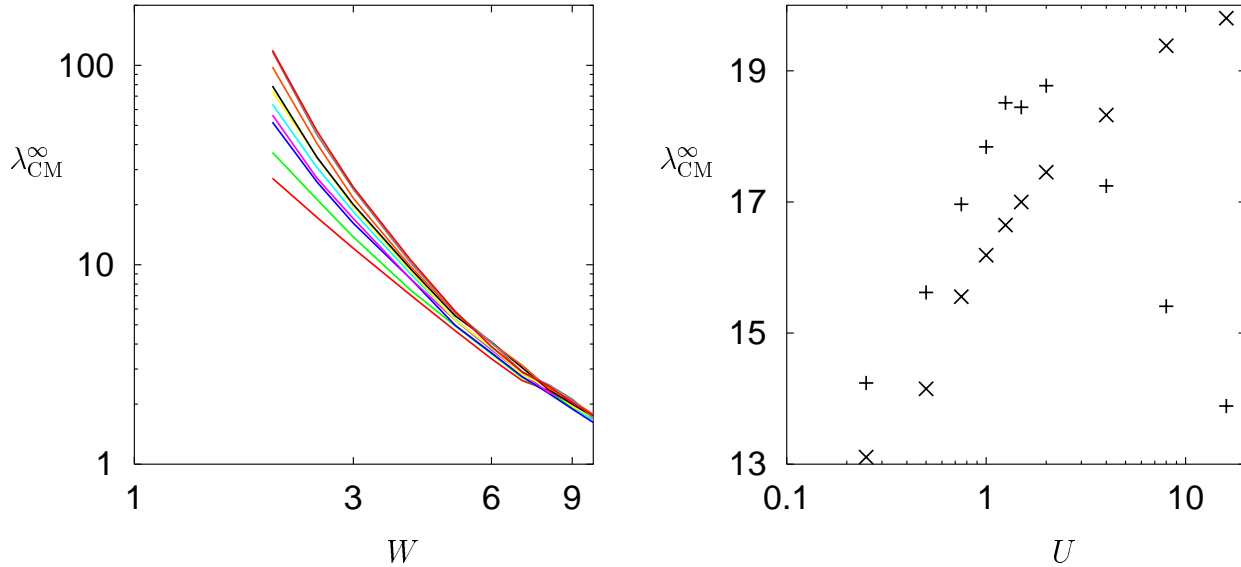


Figure 22: Finite size scaling for different strengths of the nearest neighbor interaction. Left: center of mass localization length in the infinite system for  $U=0.0, 0.25, 0.5, 0.75, 1.0, 1.25, 1.5, 2.0, 4.0, 8.0$  (bottom to top curves). Right:  $\lambda_{\text{CM}}^{\infty}(U)$  for an on-site interaction (symmetric wave function, +) and a nearest neighbor interaction (anti-symmetric wave function, x) for a finite sample of size  $L=119$  and disorder strength  $W=3$ .

tive statements due to the limited number of data points but a similar observation was made in [9]. The difficulty to explain the numerical data on the interaction dependence justifies to consider only a fixed interaction value for higher particle numbers. In addition, a huge amount of computing power would be needed to obtain the results of figure 22 for more than two particles.

In this chapter, the time evolution method in combination with finite size scaling has been used to study the localization properties of two-particle wave packets. These investigations allowed for an independent check of the results obtained with the different versions of the Green function method with a positive outcome. This agreement demonstrates that our method is well suited for studying localization properties of interacting particles. Having thus established the new method, it will now be applied to higher particle numbers, which cannot be treated easily with the Green function method. *For the first time, a direct and numerically exact investigation of the localization properties of few-particle wave packets is performed. In addition, the results presented in the following chapter provide an exact starting point for the approximations which are necessary in order to achieve a better understanding of the metal-insulator-transition in two dimension.*

## 6 More than two particles

What are the changes in the results when the particle number is increased? As already discussed, the time evolution method is well suited for calculating the localization length of

few-particle wave packets, employing the generalization discussed in section 4.

First, results for three particles are presented. Three particles are much stronger delocalized than two particles. The delocalization is even stronger than predicted previously by studying the Breit-Wigner width [174] and by generalizing Dorokhovs approach [190]. Based on the hierarchical structure of the configuration space, an upper bound for the  $n$ -particle localization length is derived. Predicting a superexponential increase of the localization length with increasing particle number, the upper bound is in agreement with the three-particle results. Increasing the already substantial numerical effort even further, localization lengths for four-particle wave packets are calculated and shown to be in accordance with the theory. Finally, the scaling with particle number is demonstrated and the numerical effort is discussed in detail.

## 6.1 Three-particle wave packets

Examples for the time evolution of three-particle wave packets are shown in figure 23, compared to the two-particle results. The three-particle wave packets have much larger satu-

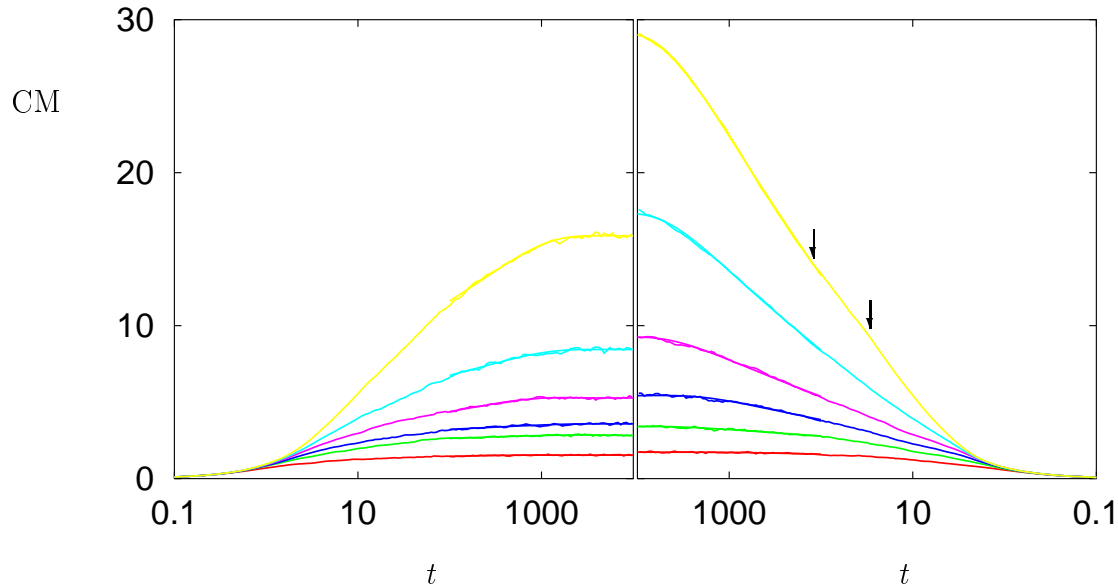


Figure 23: Time dependence of center of mass extension for two (left) and three particles (right) for disorder values  $W=3, 4, 5, 6, 7,$  and  $10$  (top to bottom). All curves are fitted for  $t \in [100, 10000]$  with equation (74), saturation values are within the error bars due to disorder averaging.

ration values than the two-particle ones, indicating a stronger influence of the interaction. The system sizes for the two-particle wave packets in the left plot of figure 23 were chosen in correspondence to those of the three-particle ones in the right plot, being  $L=103$  for  $W=3$ ,  $97$  for  $W=4$ ,  $71$  for  $W=5$  and  $W=6$ ,  $55$  for  $W=7$  and  $47$  for  $W=10$ .

In order to quantify the influence of the interaction, again a complete one parameter scaling analysis was performed. To prove the reliability of the method, figure 24 shows the results for non-interacting particles. Only relatively small system sizes  $L=23, 31, 39, 47$  have

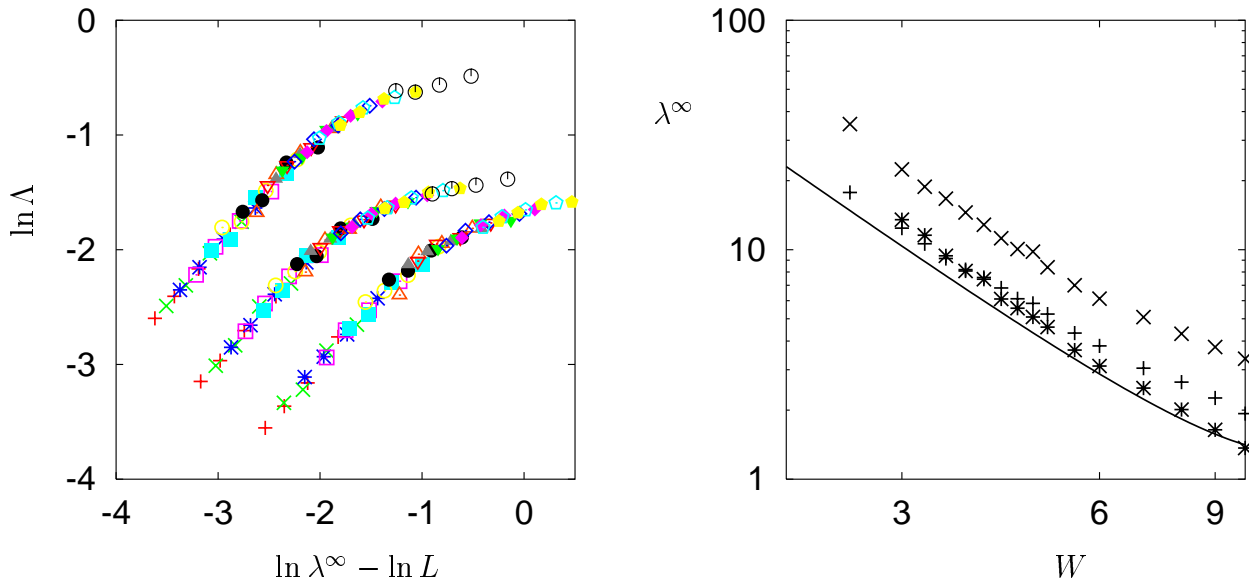


Figure 24: Finite size scaling and localization lengths for three-particle wave packets without interaction. Left: scaling curves for IPR (left, data shifted by -1), MR (middle), and CM (right, shifted by 1). Right: localization lengths in the infinite system, IPR ( $\times$ ), MR ( $+$ ), and CM ( $*$ ) compared to the one-particle localization length  $\lambda_1$  (solid line).

been used. With such small sizes, it is important to realize that due to the antisymmetry of the wave function, the real volume in configuration space is not  $L^3$ , but rather  $L(L-1)(L-2)$ . This has to be taken into account when calculating the reduced localization length. The agreement with the disorder dependence of the one-particle localization length proves as for two particles the reliability of the method. Small deviations are visible only for large disorder values. These deviations are related to the initial diameter of the wave packet which is comparable to the localization length in the large disorder regime. All three localization lengths scale with disorder like  $W^{-2}$ , as observed for two particles.

To investigate the influence of the interaction on the localization length, much larger system sizes had to be studied to perform an accurate finite size scaling analysis. Figure 25 displays raw data and scaling curve for the mean radius. System sizes  $L=23, 31, 39, 47, 55, 63, 71, 79, 87, 95, 103$  have been considered. The resulting localization length is shown in figure 26, compared to the result without interaction.

The influence of the interaction on the localization length is much more pronounced for three than for two particles. An enhancement factor  $\lambda_{\text{MR}}^\infty(U=1)/\lambda_{\text{MR}}^\infty(U=0) \approx 4.6$  is observed at  $W=3$  for the mean radius, compared to 1.42 for two particles. To observe such large enhancement factors for two particles, disorder values as low as  $W=1.25$  are necessary. Fitting the three-particle result with equation (75) fails for disorder values smaller than  $W=4$ . Instead, the third power has to be taken into account,

$$\lambda_{\text{MR}}^\infty = (1.47 \pm 0.03)\lambda_1 - (0.03 \pm 0.02)\lambda_1^2 + (0.03 \pm 0.003)\lambda_1^3, \quad (82)$$

see figure 25. The large uncertainty in the pre-factor of the second order term indicates its irrelevance. Indeed, the data can also be described without this term. The goodness of

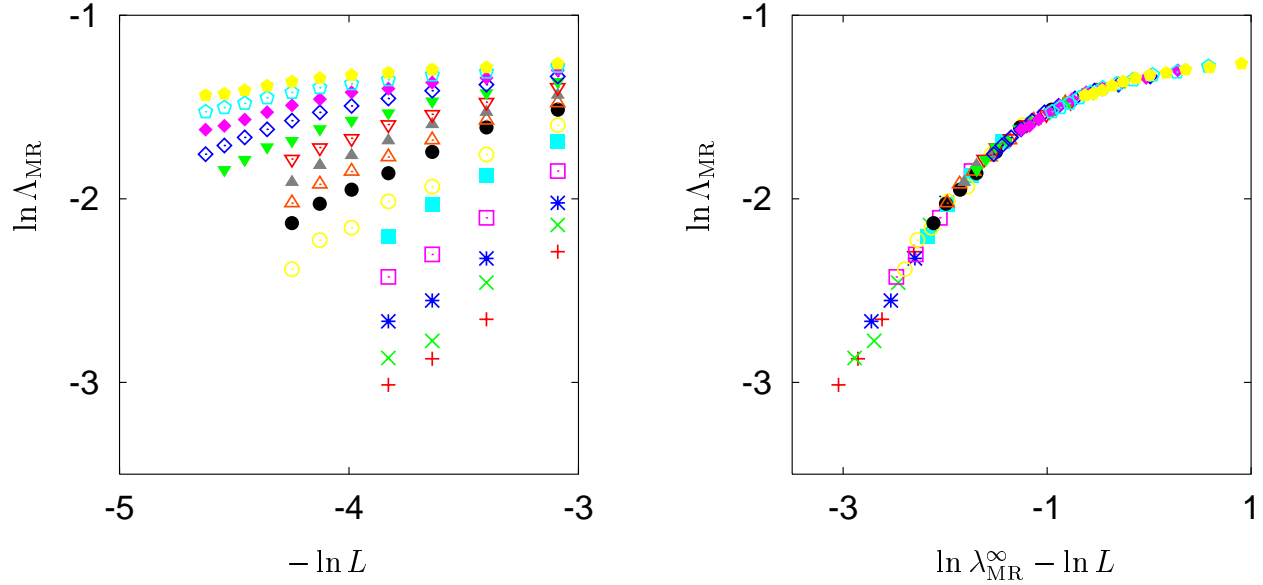


Figure 25: Finite size scaling for the mean radius of a three-particle wave packet for  $U=1$ . Left: raw data; right: corresponding scaling curve.

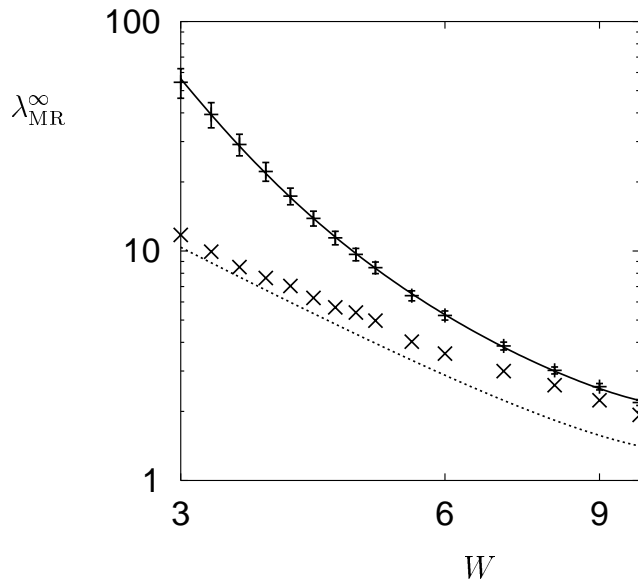


Figure 26: Mean radius localization length in the infinite system for  $U=1$  (+) and  $U=0$  (x). Solid line is a fit  $c_1 \lambda_1 + c_2 \lambda_1^2 + c_3 \lambda_1^3$ , equation (75), dotted line is again  $\lambda_1$ .

both fits is  $Q=0.44$ . A power law fit for the low disorder regime  $W \in [3,4]$  yields a slope of  $-3.96 \pm 0.03$ , much larger than observed for two particles at these disorder values. There, the slope was roughly  $-2.49$ .

The corresponding results for the inverse participation ratio are displayed in figure 27. The observation are very similar to those for the mean radius. The enhancement effect is

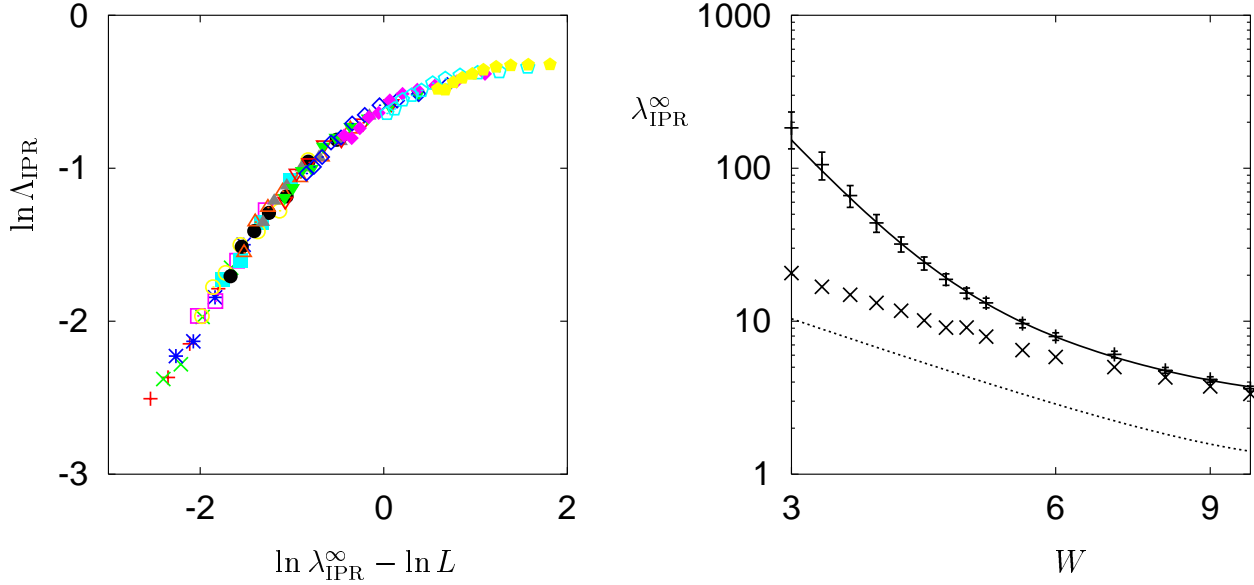


Figure 27: Finite size scaling for the inverse participation ratio,  $U = 1$ . Left: scaling curve; right: localization length in the infinite system (+) compared to the non-interacting results from figure 24 (x). Solid line is equation (83), dotted line is  $\lambda_1$ .

much stronger than for two particles,  $\lambda_{\text{IPR}}^{\infty}(U=1)/\lambda_{\text{IPR}}^{\infty}(U=0)=8.2$  at  $W=3$ , compared to 1.4. Fitting with a second order expansion in  $\lambda_1$  produces deviations for disorders  $W \leq 4.5$ . The third order fit

$$\lambda_{\text{IPR}}^{\infty} = (3.2 \pm 0.1)\lambda_1 - (0.65 \pm 0.08)\lambda_1^2 + (0.17 \pm 0.01)\lambda_1^3, \quad (83)$$

reproduces the data perfectly with a goodness  $Q = 0.41$ . A power law fit yields a slope of  $-5.9 \pm 0.2$  for  $W \in [3, 4]$ . A second order expansion in  $\lambda_1$  yielding a maximum slope of  $-4$  is insufficient to fit the data.

As for two particles, the mean radius and the inverse participation ratio average over all possible direction in configuration space. If the delocalization is related to a coherent motion of the three particles, the most pronounced effect is observable along the center of mass direction. The corresponding results are given in figure 28. The strongest delocalization occurs along this direction, with a ratio  $\lambda_{\text{CM}}^{\infty}(U=1)/\lambda_{\text{CM}}^{\infty}(U=0) = 19.9$  at  $W = 3.25$ , compared to 1.6 for two particles and to 4.6 and 8.2 for the mean radius and the inverse participation ratio for three particles, respectively. Since the center of mass extension is the most delocalized quantity, finite size effects are most pronounced for this quantity and the scaling could not be completed for the lowest disorder value considered. Extrapolating from the fit in figure 28, equation (85), a localization length around 400 is found at  $W = 3$ , too large to be reliably detectable with system sizes  $L \leq 103$ . In contrast to the mean radius and the inverse participation ratio, a third order fit (dashed line in figure 28) could not describe the data for the lowest disorder values. A fourth order fit (solid line) works much better, as indicated by the goodness of the fits, being  $Q = 0.32$  and  $Q = 0.38$ , respectively,

$$\lambda_{\text{CM}}^{\infty} = (1.2 \pm 0.2)\lambda_1 - (0.25 \pm 0.17)\lambda_1^2 + (0.16 \pm 0.03)\lambda_1^3, \quad (84)$$

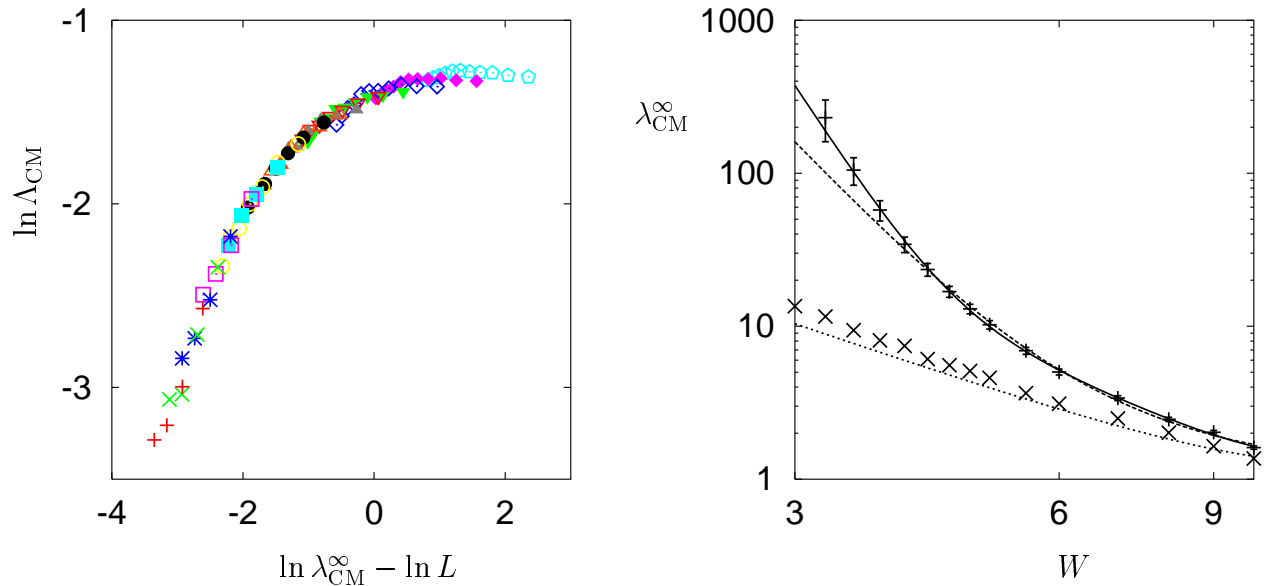


Figure 28: Finite size scaling for the center of mass extension,  $U = 1$ . Left: scaling curve; right: localization length in the infinite system (+) compared to the non-interacting results from figure 24 (×). Dashed and solid lines are equations (84) and (85), dotted line is  $\lambda_1$ .

$$\lambda_{\text{CM}}^{\infty} = (-0.04 \pm 0.2)\lambda_1 + (1.28 \pm 0.24)\lambda_1^2 - (0.39 \pm 0.09)\lambda_1^3 + (0.05 \pm 0.008)\lambda_1^4. \quad (85)$$

The occurrence of negative terms reveals that too many fit parameters are used. Important in this context is only that the highest order contribution is positive. A power law fit for the lowest disorder values yields a slope of  $-8.8 \pm 0.4$  in this case. While the error is rather large the slope itself is much larger than  $-6$ , the slope expected on the base of the analytical prediction,  $\lambda_3 \propto \lambda_1^3$  [174, 190].

As outlined in section 3, the assumptions leading to this analytical result are questionable. The numerical evidence of an even stronger delocalization puts forward the task to improve the theory and to derive the correct dependence of the localization length on the particle number.

## 6.2 Upper bound for the $n$ -particle localization length

In order to understand the above results, consider the  $n$ -electron problem in the  $n$ -dimensional configuration space. Without interaction, the random potential is correlated such that one obtains the one-particle localization length,  $\lambda_1(W)$ , apart from pre-factors. The correlations originate from fixing  $L^n$  site energies using only  $L$  random numbers, since the potential is still one-dimensional,  $\varepsilon_{j_1 \dots j_n}^{(n)} = \sum_{i=1}^n \varepsilon_{j_i}$ , equation (54). Each direction can be considered independently since all directions are equal and the one-particle localization length is obtained, as expected. This separability is destroyed by the interaction. For two particles, the interaction is relevant along lines in configuration space defined by  $x_1 = x_2 \pm 1$ . Along these lines, the site energies in configuration space are essentially uncorrelated. The interaction creates

a quasi one-dimensional subspace of the configuration space with uncorrelated disorder. The transverse size of this subspace can be estimated. Only when the relative distance between the two electrons is smaller than or comparable to  $\lambda_1$ , the electrons feel the interaction. Hence, the transverse extension of the quasi one-dimensional part of the configuration space is of the order  $\lambda_1$ . The localization length of a quasi one-dimensional system is given by the product of the one-dimensional localization length multiplied by the number of channels  $N_{\text{CH}} \approx \lambda_1$ , yielding  $\lambda_2 \propto \lambda_1^2$ . Along other directions in configuration space, the localization length will be different [136] but only the largest one is relevant for transport and this is the one of the two-particle mode along the CM direction.

For three particles, the interaction affects the diffusion within planes in the 3D configuration space, defined by  $x_i = x_j \pm 1$ . However, if two particles are far away from the third one, the situation is as above since the third particle is completely decoupled. But along the CM direction, if all three particles are within a mutual distance of  $\lambda_1$ , again a quasi one-dimensional subspace of the configuration space with an uncorrelated potential exists, now with transverse dimension two. The number of transverse channels,  $N_{\text{CH}}$ , is larger than for two particles. This leads to the enhancement of the localization length with increasing particle number,  $\lambda_3 \gg \lambda_2$ . To be precise, the increase of  $N_{\text{CH}}$  is not only due to the higher transverse dimension, but also due to the growing transverse size. The latter is not limited by  $\lambda_1$  since two particles close to each other can reach the third particle even if the latter is at a distance  $\lambda_2 \gg \lambda_1$ . Hence,  $N_{\text{CH}}$  is roughly  $\lambda_2 \lambda_1$ , the area covered by the two particle wave packet. Again, there are many other modes with localization lengths smaller than that of the CM mode.

While in [174] only coupling between two general three-particle states is taken into account, the above estimate considers the hierarchical structure of the configuration space induced by the interaction. Points in configuration space corresponding to two nearby particles being a distance  $\lambda_2$  away from the third one can contribute to transport along the center of mass direction since the two particles can reach the third one. In the estimate given in [174], page 20, this situation is not distinguished from the general one with all particles further away than  $\lambda_1$  from each other and hence does not give an additional contribution. In addition, the estimate by Shepelyansky is based on a diffusive growth of the wave packet in contrast to the observations on page 46 and figure 23.

The hierarchical structure of the wave packet in configuration space is sketched in figure 29, showing a cross section perpendicular to the center of mass direction. The cross section reveals as for two particles the number of contributing channels. Along the symmetry lines, the two body interaction leads to an enhanced propagation, limited by  $\lambda_2 \equiv \lambda_2^{(\text{CM})}$ . Perpendicular to that, only an extension of the order of  $\lambda_1 \equiv \lambda_2^{(\text{RD})}$  is reached. To observe this structure in a calculation, the ratio  $\lambda_2^{(\text{CM})}/\lambda_2^{(\text{RD})}$  has to be sufficiently large. More specifically, the angle  $\alpha$  in the left part of figure 29 has to be smaller than  $\pi/6 = 30^\circ$ . Otherwise, single particle diffusion perpendicular to the symmetry axis smears out the indicated structure. Relating the angle to the localization lengths yields the constraint

$$\frac{\lambda_2^{(\text{CM})}}{\lambda_2^{(\text{RD})}} > \frac{1}{\tan(\pi/6)} \approx 1.732, \quad (86)$$

which is fulfilled only for  $W \leq 2.0$  according to the two-particle data. Extrapolating from equation (85), for this disorder the three-particle localization length is larger than 1000 and

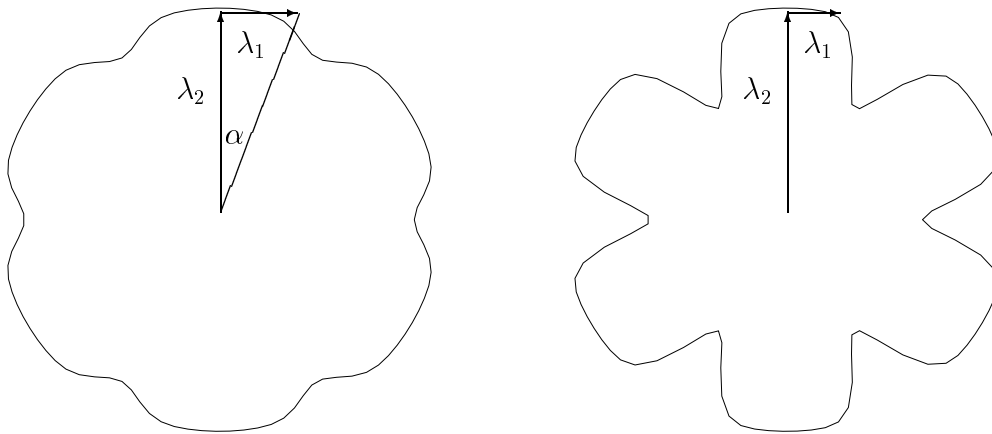


Figure 29: Sketch of the cross section perpendicular to the center of mass direction of the three-particle wave packet for  $\lambda_2/\lambda_1$  small (left) and large (right).

cannot be calculated reliably with the available system sizes. Nevertheless, the calculation reveals that the cross sections sketched in figure 29 are correct, as can be seen in figure 30. The cross section of the wave packet is not circular as it would be if all directions are.

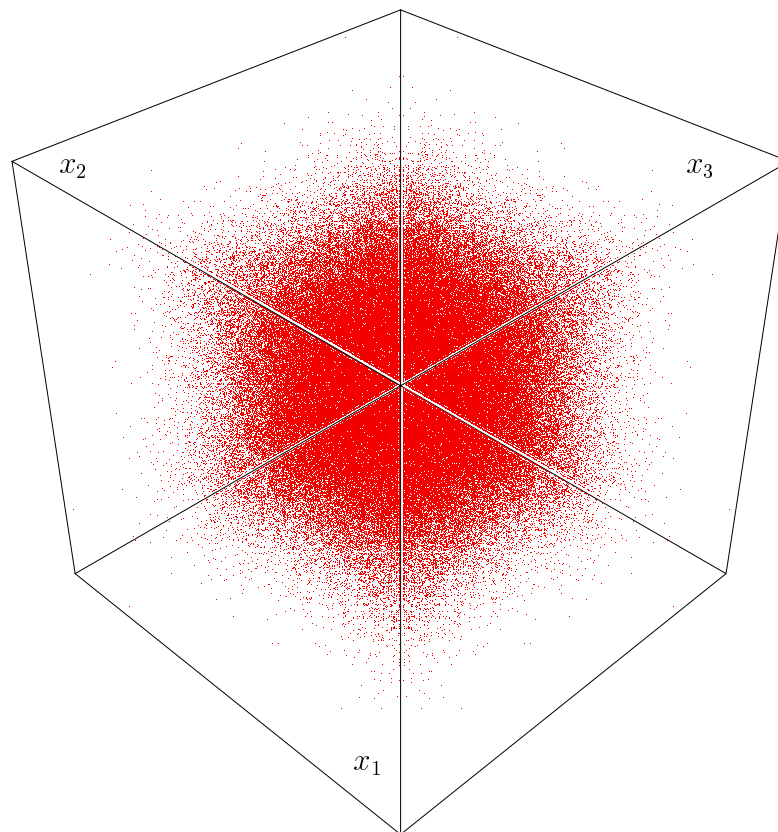


Figure 30: Cross section of a three-particle wave packet for  $W=2$  and  $L=159$  perpendicular to the center of mass direction. Points are drawn if value of wave function is larger than 1.7 times the mean value. Averaging is performed over 30 realizations of the random potential.

Even more, the bumps along the six symmetry axis indicate the preferred propagation along these directions. This can best be seen with some distance to the plot. The relationship to pointilism is obvious, the plot is based on roughly 200000 out of four million possible points. The cross section shown in figure 30 can be constructed from the two particle wave packet displayed in figure 14 by placing two copies rotated by  $60^\circ$  and  $120^\circ$  on top of it. The important point is that only the first two orders of magnitude shown in figure 14, white center and black surrounding, are within the available system size for three particles. This emphasizes the difficulties to observe the cross sections of figure 29. The system size  $L = 159$  for three particles has to be compared with the maximal system size of  $113 \times 113 \times 113$  for which exact diagonalizations of the three-dimensional Anderson Hamiltonian were performed [255, 256]. Keep in mind that the symmetry reduces the Hilbert space and that the time evolution contains information about the whole spectrum while only a the few eigenstates are calculated with the Lanczos algorithm.

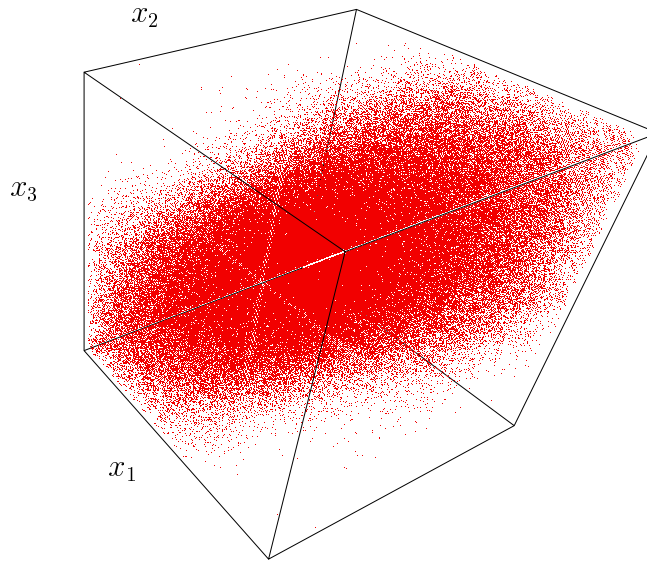


Figure 31: Center of mass direction of a three-particle wave packet for  $W = 2$  and  $L = 159$ . Points are the same as in figure 30.

The cigar like shape of the wave packet is shown in figures 31 and 32. In contrast to the two-particle situation [137], it is a real cigar, not a flat one. However, the plot of the cross section, figure 30, reveals that smoking would be difficult due to the hexagonal rather than circular cross section. Along the symmetry axis, the interaction exists and the wave packet reaches further than along the other directions, indicated by the little bumps at the corners. Unfortunately, as discussed above, the shape of the right plot of figure 29 is only observable for smaller disorder values. In any case, the number of channels will not be proportional to  $\lambda_1^2$ , but rather to  $\lambda_2 \lambda_1$ , even for the left plot in figure 29.

Extending these arguments to  $n > 3$  yields,

$$\lambda_n \leq c \lambda_1 N_{\text{CH}} \approx c_n \lambda_1 [\lambda_{n-1} \lambda_{n-2} \dots \lambda_1] \approx c_{n'} \lambda_1^{2^{n-1}}. \quad (87)$$

*The localization length increases superexponentially with increasing particle number. The modes with the largest localization lengths are associated with quantum diffusion in quasi*

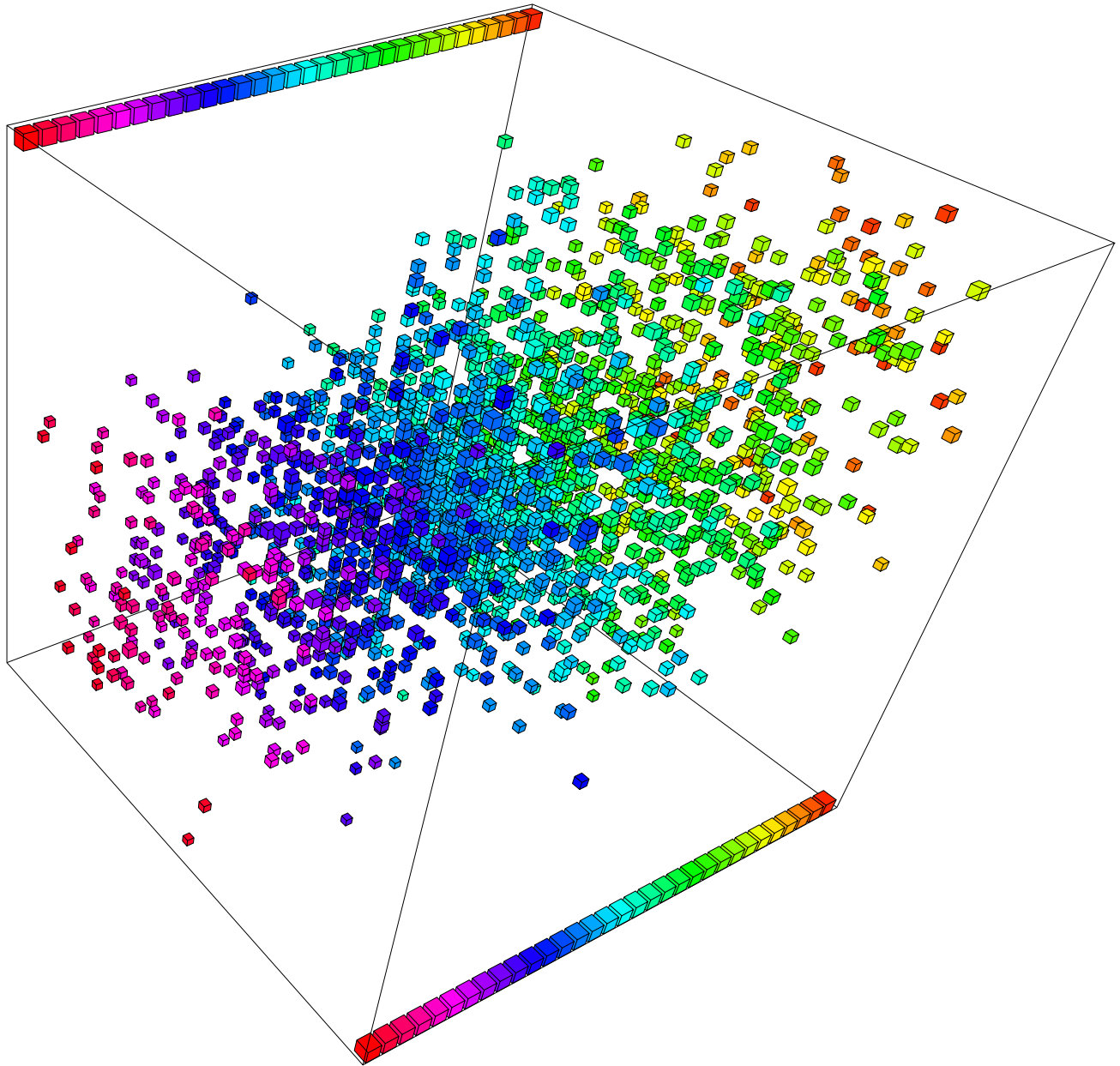


Figure 32: Three-particle wave packet for  $W = 2$  and  $L = 159$ . Every fifth points along  $x_1$  and  $x_2$  is drawn if the value of wave function is larger than twice the mean value.

*one-dimensional sub-spaces of finite cross-sectional areas in configuration space. However, equation (87) suggests that for interactions of finite range the  $n$ -particle states remain localized for any finite  $n$  and  $\lambda_1$  although the localization length can become arbitrarily large.*

Being derived for an energy in the middle of the band, the sign of the interaction is irrelevant. Closer to the ground state, only an attractive interaction leads to a significant delocalization [128, 202]. Nevertheless, the “delocalized” ground state found for an attractive interaction in [229] on the basis of a density matrix renormalization group study, contradicts the result above. The energy change upon changing the boundary conditions, page 15, times

the system size was shown to be insensitive to the system size. This insensitivity corresponds to a flat region in a finite size scaling curve. For a disorder  $W = 1$  and the large number of particles considered, the localization lengths can easily be larger than the system size by a factor of 1000, according to equation (87). Thus, the apparent divergence of the localization length upon approaching the phase boundary [257], could well be the signature of too small system sizes available. Small system sizes are also the limiting factor for the analysis of four-particle wave packets discussed in the next part.

### 6.3 Four-particle wave packets

In spite of the enormous, superexponential increase of the localization length with increasing particle number predicted by equation (87) and the limited system sizes available due to the exponentially growing configuration space with particle number, it will be shown in the following that the four particle localization length is in accordance with the predictions.

To prove equation (87) poses a twofold problem: first, an increasing localization length requires larger system sizes since only localization lengths of the order of the system size can be calculated reliably. Second, the numerical effort for the calculation scales with the volume of the configuration space, that is the system size to the power of the particle number,  $L^n$ . In addition, the number of elementary matrix operations needed for a single time step increases with the particle number according to equations (54), (55), and (56). This twofold problem can only be tackled by optimizing the numerical routines as good as possible and using up to date computing technology, discussed in more detail below.

As in the preceding sections, results in the absence of interaction are presented first, strengthening the reliability of the method. Then, three- and four-particle wave packets with interaction are compared for finite systems, before the results of the complete finite size scaling analysis are given. Keep in mind that equation (87) holds only for the extension in center of mass direction.

The main results without interaction are shown in figure 33. As for three particles, only relatively small system sizes  $L = 15, 23, 31, 39, 47$  have been used. Again, the real volume of the configuration space was taken into account,  $L(L-1)(L-2)(L-3)$  instead of  $L^4$ . Only for the center of mass extension an agreement with the one-particle localization length is observed. The mean radius and the inverse participation ratio increase slower with decreasing disorder strength. This discrepancy is related to the influence of the initial condition. Four particles outside the range of their mutual two-body nearest neighbor interaction can at most sit on next nearest places. Therefore, the initial value for both the mean radius and the inverse participation ratio is larger than two. This initial value is larger than the localization length for  $W = 9$  and 10 and comparable to the localization length in the whole disorder regime considered. Keep in mind that  $\lambda_1(W=4)=6.2$  and  $\lambda_1(W=3)=10.3$ , section 4.2, and that the results for the center of mass extension which is not affected by the initial condition are only slightly larger. This offset changes the slope of the scaling curve and leads to observed deviations for the localization length.

Correcting for this offset produces a much better agreement with the single particle localization length, see figures 35 and 37. It remains only a slight deviations for all three quantities

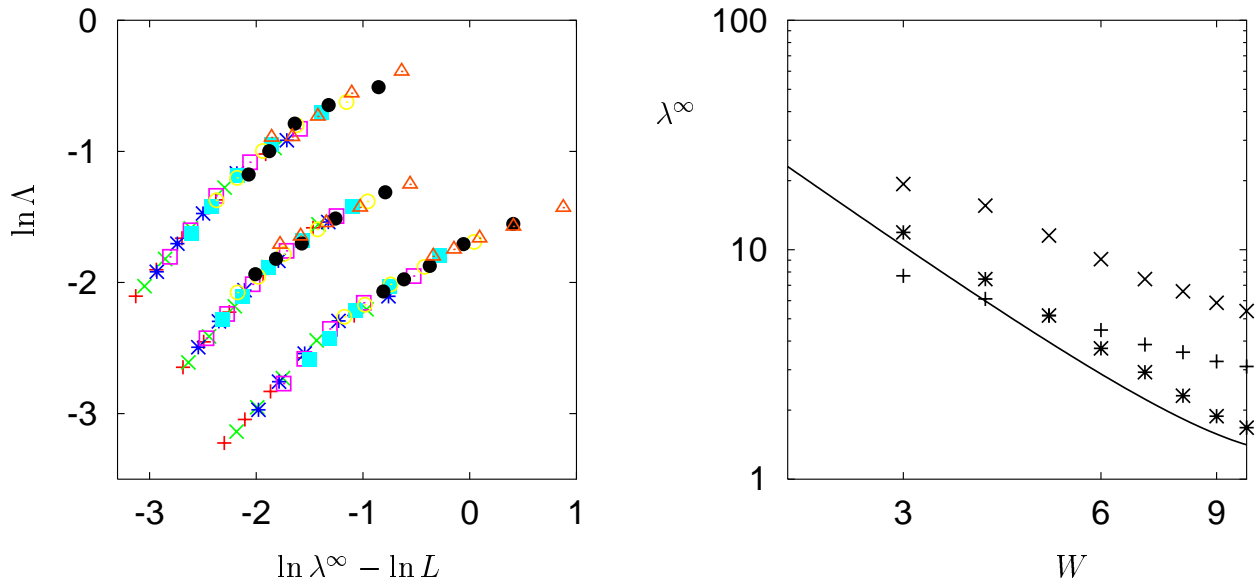


Figure 33: Finite size scaling and localization lengths for four-particle wave packets in the absence of interaction. Left: scaling curves for IPR (left, data shifted by -1), MR (middle), and CM (right, shifted by 1). Right: localization lengths in the infinite system, IPR ( $\times$ ), MR ( $+$ ), and CM ( $*$ ) compared to the single particle localization length  $\lambda_1$  (solid line).

for the smallest disorder value which is attributed to too small system sizes considered. But it does not influence the main observation that even for the four-particle wave packets, the time evolution method produces the expected results in the non-interacting limit.

In the presence of interaction, system sizes  $L = 15, 23, 31, 39, 47, 55, 63, 71$  have been used, allowing a reliable detection of localization lengths up to 100. A direct comparison between three- and four-particle wave packets is given in figure 34. Fitting with equation (74) works very well for the four-particle data, too. For the lowest disorder values, the saturation value exceeds in some cases the 1% statistical error bar related to disorder averaging by a factor of 1.5. Although one extrapolates a little bit further for four than for three particles the extrapolation is still reliable since the chosen fit function describes accurately more than 90% of the time evolution.

While the average behavior is again logarithmic in time, it seems that the slope changes during the time evolution. This can best be seen at the top curves in figure 34, arrows in the right plot, and occurs roughly at the saturation values obtained for smaller particle numbers. A similar observation can be made for three particles, see the top curve of figure 23. This indicates the existence of a hierarchy of time scales: for short time scales diffusion is dominated by single particle motion, then by two-particle coherent motion and only afterwards by three- and then four-particle coherent motion. Unfortunately this assumption can only be proven by considering much smaller disorder values for which the differences between these time scales is more pronounced. Only then it is meaningful to fit the slopes in the different regimes and perform an analysis like in the two-particle case, see figure 12. The data above is more a series of crossovers between the different regimes, which are each smaller than a decade in time.

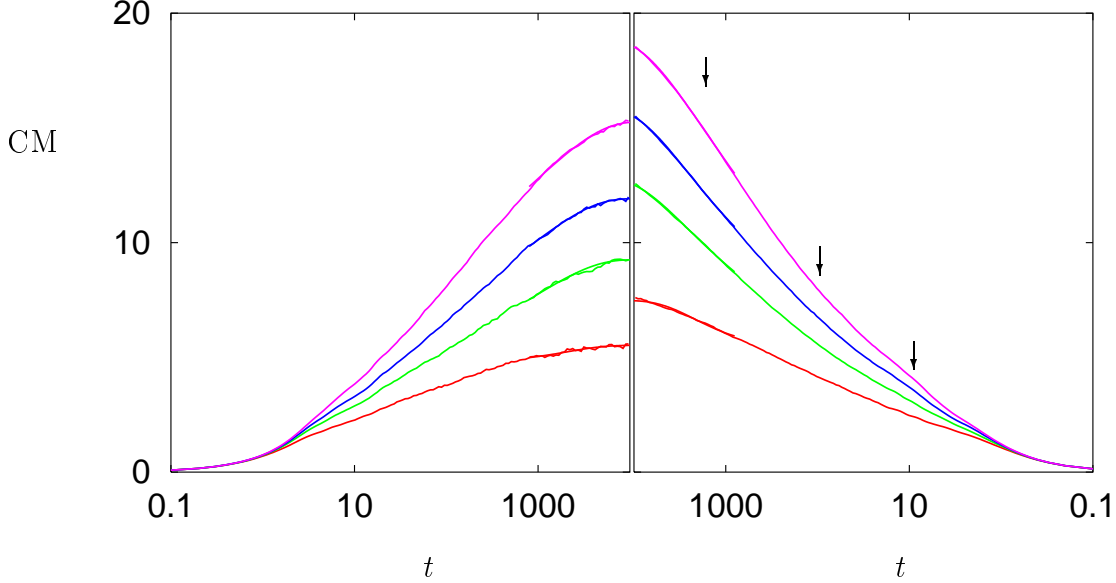


Figure 34: Time dependence of center of mass extension for three (left) and four particles (right) for disorder values,  $W = 4, 4.5, 5,$  and  $6$  (top to bottom) and system size  $L = 71$ . All curves are fitted for  $t \in [800, 10000]$  with equation (74).

Even though the complete analysis of the time evolution is impossible with nowadays computing technology, the localization properties can be analyzed accurately, at least for not too small disorder values. Raw data and scaling for the mean radius are presented in figure 35. The resulting localization length is compared to the result without interaction in figure 36.

The scaling with the complete data set, left scaling curve and open symbols in the right plot of figure 35, yields already an enhancement factor of  $\lambda_{\text{MR}}^{\infty}(U=1)/\lambda_{\text{MR}}^{\infty}(U=0) = 4.24$  at  $W=4$  in comparison to 2.46 for three particles.

Correcting for the initial offset discussed above, right scaling curve in figure 35 and filled symbols in figure 36, the enhancement factor is 5.43. For the lowest disorder values in this case, the reduced localization length increases initially with increasing system sizes before decreasing for larger system sizes (not shown). To avoid an influence of this obvious finite size effect, the corresponding data points have not been used for scaling. The scaling with the corrected data is more reliable since the  $U=0$  result is in much better agreement with the one-particle localization length.

While this result strongly indicates an even more pronounced delocalization than for two and three particles, a third order fit remains sufficient to describe the data. Higher order terms would be necessary only for smaller disorder values. For these values the localization lengths cannot be calculated reliably due to the limitations in the available system sizes. The data in figure 36 is fitted with

$$\lambda_{\text{MR}}^{\infty} = (0.93 \pm 0.03)\lambda_1 + (0.17 \pm 0.007)\lambda_1^3, \quad Q = 0.31. \quad (88)$$

A power law fit in the region  $W \in [4, 6]$  results in a slope of  $-3.9 \pm 0.1$  compared to an average slope of  $-2.9 \pm 0.1$  for three particles in the same regime.

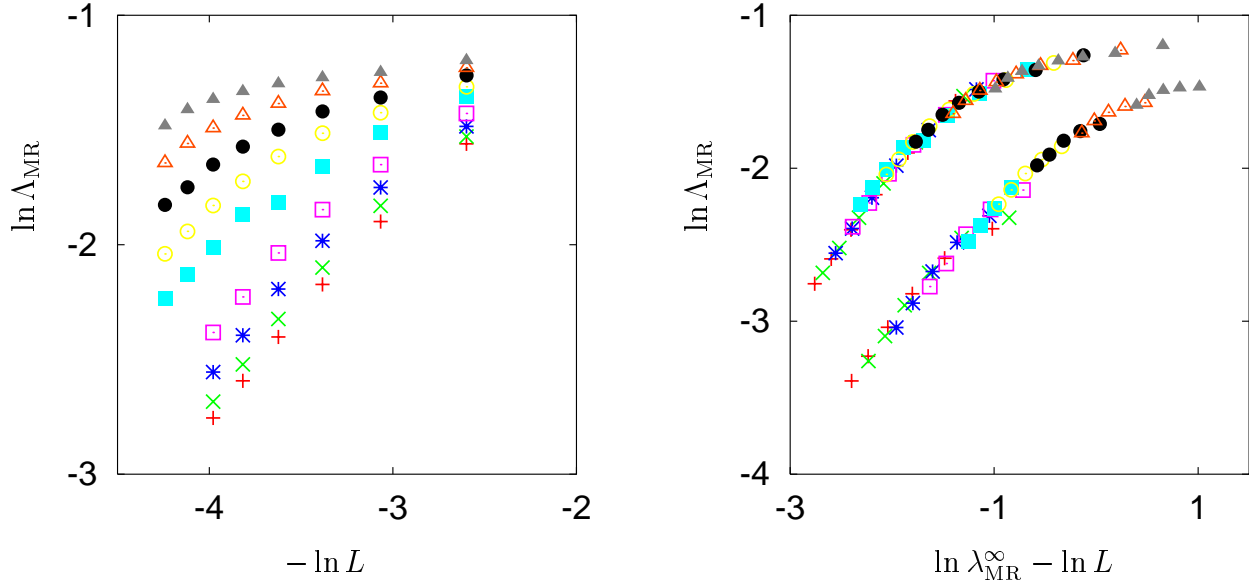


Figure 35: Finite size scaling for the mean radius of a four-particle wave packet for  $U = 1$ . Left: raw data; right: scaling curves for raw data (left) and after subtracting the offset and ignoring the smallest system sizes as discussed in the text (right, shifted by 1).

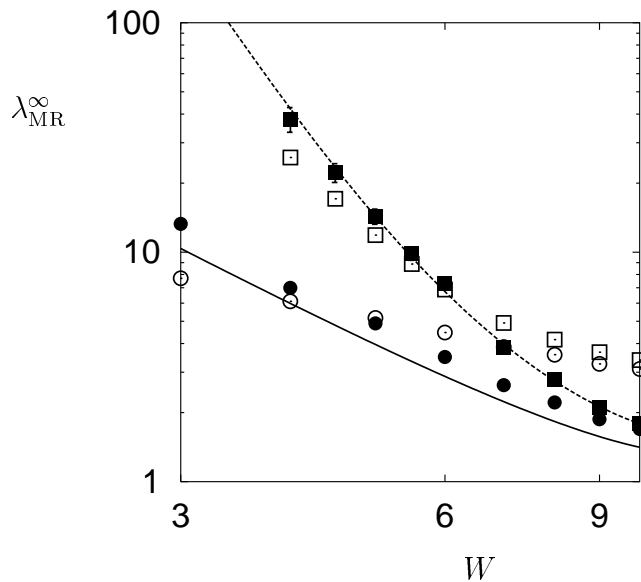


Figure 36: Mean radius localization length in the infinite system for  $U = 1$  (open squares) and  $U = 0$  (open circles). Filled symbols are the more reliable results obtained by subtracting the offset before the scaling. Solid line is  $\lambda_1$ , dotted line a third order fit, equation (88).

The results for the inverse participation ratio are very similar, figure 37. Again, the  $U = 0$  result is much better when the initial offset is subtracted before the scaling procedure. As above, data points for the smallest disorder and system sizes that show obvious finite size

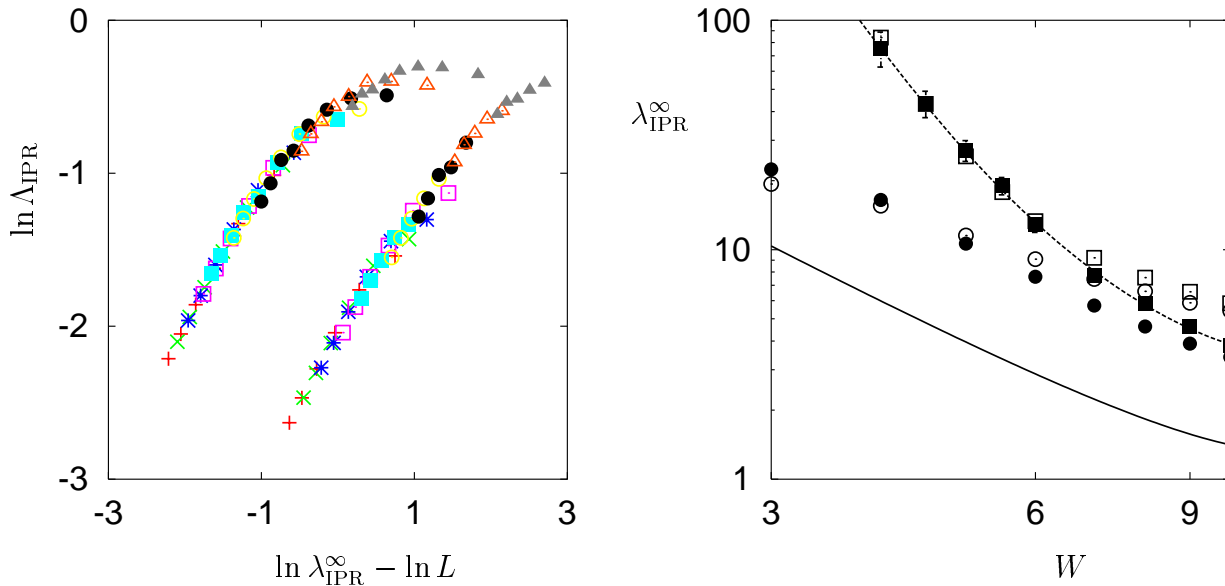


Figure 37: Finite size scaling for the inverse participation ratio,  $U=1$ . Left: scaling curve for the original data set (left) and after subtracting the offset and ignoring the smallest system sizes (right, shifted by 2). Right: localization lengths in the infinite system compared to the non-interacting result, symbols and lines as in figure 36, dashed line is equation (89).

effects were excluded from the scaling. Enhancement effects as large as  $\lambda_{\text{IPR}}^{\infty}(U=1)/\lambda_{\text{IPR}}^{\infty}(U=0)=4.59$  at  $W=4$  compared to 2.73 for three particles are observed. The localization length is fitted by,

$$\lambda_{\text{IPR}}^{\infty} = (2.16 \pm 0.05)\lambda_1 + (0.29 \pm 0.01)\lambda_1^3, \quad Q = 0.35. \quad (89)$$

The slope for  $W \in [4,6]$  is  $-4.3 \pm 0.1$  compared to  $-3.2 \pm 0.2$  for three particles. Although a third order fit is sufficient to describe the data, the slope indicates the dramatic increase of the localization length with increasing particle number. This increase becomes most pronounced for the center of mass extension.

As for two and three particles, the strongest delocalization is observed for the center of mass extension. Only for the localization length along this direction equation (87) is valid. In contrast to the mean radius and the inverse participation ratio, no initial offset has to be taken into account. Figure 38 displays the main results. In order to check the accuracy of the scaling, it was performed for the complete data set, right scaling curve, open symbols in right plot, as well as for a reduced data set ignoring as above some of the smallest disorder and system sizes for which dominant finite size effects were observed. As can be seen from the time evolution data, these values show hardly any error due to disorder averaging (not shown). Therefore, finite size effects scale differently than in the disorder dominated regime of interest. Indeed, the quality of the scaling curve is enhanced a bit in comparison to the scaling curve calculated from the complete data set. The localization length is slightly smaller, filled squares in figure 38. For both data sets, the scaling failed for the smallest disorder value  $W=4$ . As for three particles, this is related to the fact that for the most delocalized quantity, finite size effects are most pronounced and eventually too strong to perform a reliable scaling. At  $W=4.5$ , enhancement factors are 16.29 and 7.41, for the

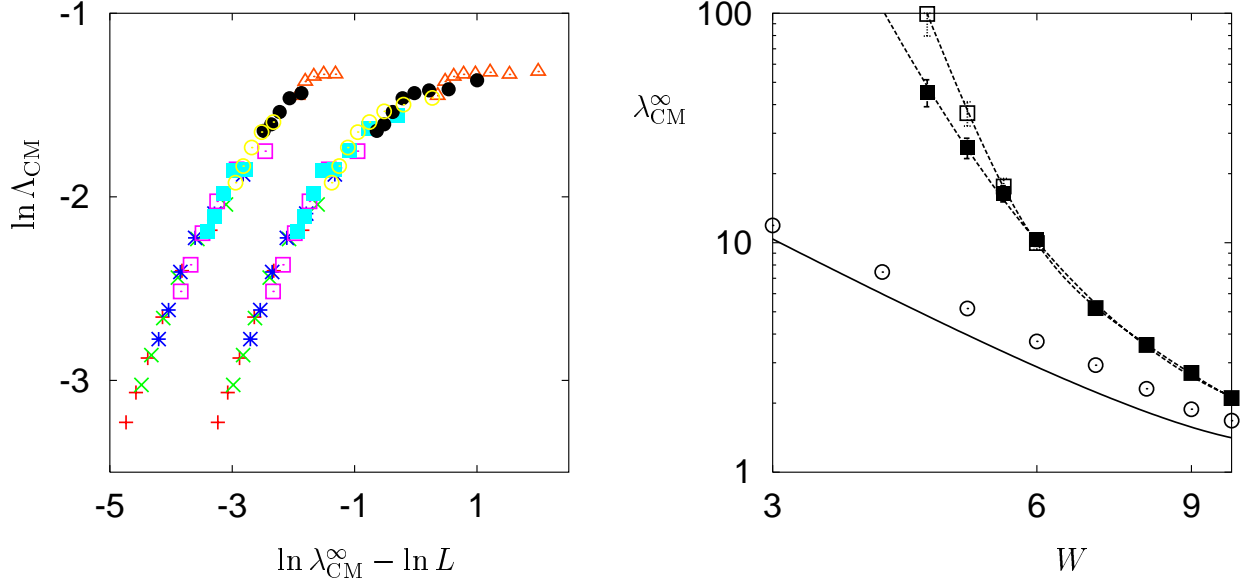


Figure 38: Finite size scaling for the center of mass extension,  $U = 1$ . Left: scaling curves for the complete data set (right) and a reduced data set (left, shifted by  $-1.5$ ), see text. Right: localization length in the infinite system for the complete (open squares) and reduced (closed squares) data set, compared to the non-interacting result (open circles). Solid line is  $\lambda_1$ , dotted lines are fourth order fits, equations (90) and (91) for open and closed symbols, respectively.

complete and reduced data set, in comparison to  $3.03$  for three particles. In contrast to the mean radius and the inverse participation ratio, a fourth order fit is necessary to describe the data,

$$\lambda_{\text{CM}}^{\infty} = (-4.7 \pm 0.4)\lambda_1 + (8.6 \pm 0.6)\lambda_1^2 - (4.0 \pm 0.3)\lambda_1^3 + (0.69 \pm 0.04)\lambda_1^4, \quad Q = 0.4, \quad (90)$$

$$\lambda_{\text{CM}}^{\infty} = (0.7 \pm 0.3)\lambda_1 + (0.5 \pm 0.2)\lambda_1^2 + (0.06 \pm 0.01)\lambda_1^4, \quad Q = 0.2, \quad (91)$$

for the complete and reduced data set, respectively. However, equations (90) and (91) are only one way to fit the data. For the limited disorder range available for four particles one can see a stronger delocalization than for two and three particles. Higher orders in  $\lambda_1$  as predicted by equation (87) yield similar results, figure 39 and equations (92) and (93). A clear distinction will only be possible smaller disorder values. Fitting the low disorder range,  $W \in [4.5, 6]$ , with a power law yields  $-7.4 \pm 0.5$  and  $-5.11 \pm 0.08$ , compared to  $-4.1 \pm 0.1$  for three particles. The comparison with the mean radius and the inverse participation ratio reveals again the anisotropy in configuration space, the largest localization length is found along the center of mass direction.

For a general comparison of the enhancement effect, figure 39 displays the results for the center of mass extension for two-, three-, and four-particle wave packets. The localization length increases dramatically with the number of particles. However, according to the estimate made above, equation (87), for any finite number of interacting particles and any finite

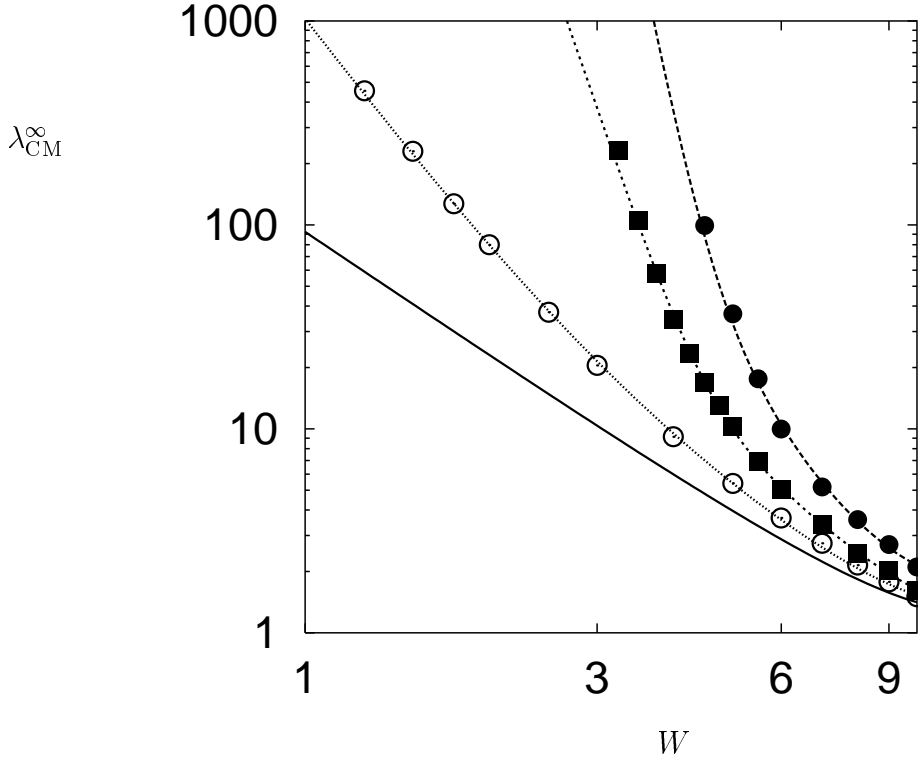


Figure 39: Center of mass extension for two-, three-, and four-particle wave packets, fitted with equations (79),(85),and (92), open circles, filled squares and filled circles, respectively, compared to  $\lambda_1$  (solid line).

*amount of disorder, the localization length will remain finite and no transition to a metallic state will occur in one dimension.*

To demonstrate this scaling with particle number, figure 40 shows the reduced localization lengths  $\lambda_n^\infty / c_n \lambda_1^{2^{n-1}}$ , with an adjustable constant  $c_n$ . According to the estimated upper bound of the  $n$ -particle localization length, equation (87), curves for different particle numbers should converge towards a finite value in the low disorder regime. This convergence works perfectly for two and three particle. For four particles, the regime dominated by the leading power of  $\lambda_1$  just begins at the smallest disorder value. In order to approach it as close as possible, two scaling curves including all disorder values are presented in figure 40. They are necessarily extrapolations since as discussed above, the scaling fails for the lowest disorder value  $W = 4$ . The scaling is done by hand such that a smooth scaling curve is obtained. This has been performed for the complete and a reduced data set ignoring system sizes that show obvious finite size effects as discussed above. The difference between the two localization lengths is relevant only for the three smallest disorder values. Both localization lengths were then fitted with a polynomial in  $\lambda_1$ . Due to the limited number of data points, only a few terms have been considered,

$$\lambda_{\text{CM}}^\infty = (0.93 \pm 0.07)\lambda_1 + (0.29 \pm 0.03)\lambda_1^3 + (0.00018 \pm 0.00003)\lambda_1^8, \quad Q = 0.40 \quad (92)$$

$$\lambda_{\text{CM}}^\infty = (0.84 \pm 0.06)\lambda_1 + (0.34 \pm 0.02)\lambda_1^3 + (2.1 \pm 0.8)10^{-5}\lambda_1^8, \quad Q = 0.37, \quad (93)$$

for the complete and the reduced data set, respectively. This demonstrates that the four-particle localization length is in accordance with the prediction of equation (87). These fits and the estimated error bars are given in figure 40. For two and three particles, the crossover

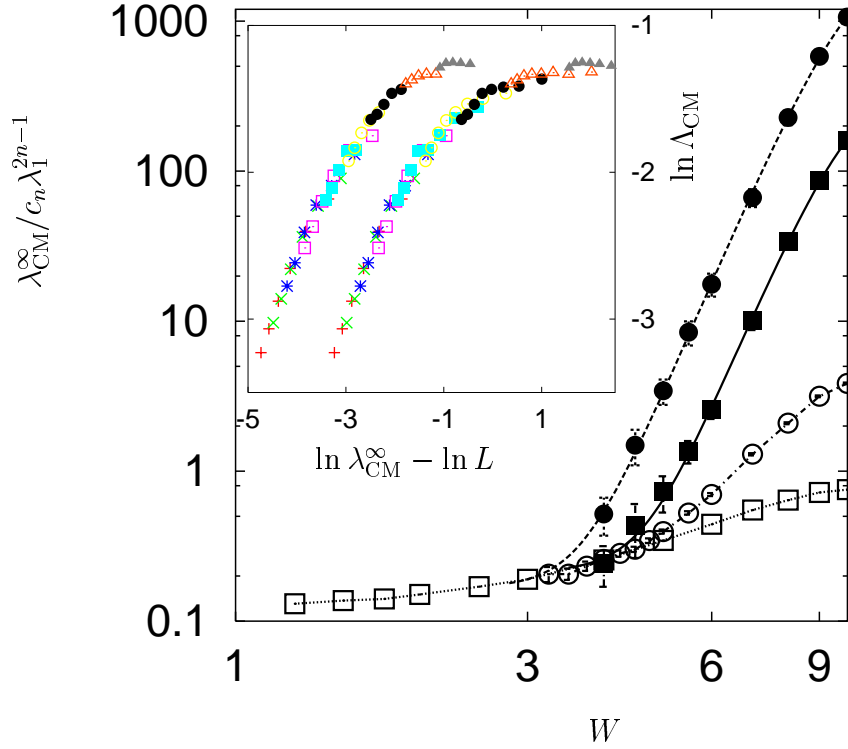


Figure 40: Scaling with particle number for the center of mass extension,  $U = 1$ . Localization lengths divided by the predicted low disorder behavior, equation (87); two particles (open squares), three particles (open circles), and four particles, closed squares and circles for complete and reduced data set, fitted according to equations (92) and (93) respectively. Inset: four-particle scaling curves for the complete data set (right) and a reduced data set (left, shifted by -1.5), including the lowest disorder value.

to a constant value of  $\lambda_{\text{CM}}^\infty / c_n \lambda_1^{2n-1}$  for low disorders is obvious, indicating the validity of equation (87). For four particles, only the crossover is visible, more data points would be needed to enter the limiting regime. Unfortunately, extending the four-particle calculations to lower disorder values is not that easy. In order to understand the problems, the numerical effort needed to obtain these results, will be briefly discussed in the following.

## 6.4 Numerical effort

As discussed in section 4.1, The CPU-time requirement increases with the system size to the power of the localization length. In addition, there is an  $n$  dependent pre-factor which is simply the number of matrix multiplication necessary for performing a single time step,

which is  $2n + 1$ , equations (54), (55), and (56). Making use of the symmetry of the wave function gives a reduction of  $n!$ ,

$$\text{CPU-time} \propto \frac{(2n + 1)L^n}{n!} \quad \text{or} \quad \text{CPU-time} \propto \frac{(2n + 1)}{n!} \prod_{i=0}^{n-1} (L - i) \quad , \quad (94)$$

where the second term takes the the anti-symmetry of the wave function properly into account. Given maximum system sizes of  $L = 1400, 399, 103$ , and  $71$  for one, two, three, and four particles, equation (94) yields factors of  $4.2 \times 10^3$ ,  $2.38 \times 10^5$ ,  $8.84 \times 10^5$ , and  $6.80 \times 10^6$ . This indicates that the effort spent for the calculations has increased with the number of particles. The simple underlying reason is the strong enhancement effect, leading to a localization length which increases more than exponentially with the particle number,  $\lambda_n \propto \lambda_1^{2^n - 1}$ . *The larger the particle number, the more important it is to reach the maximal possible system sizes.* In addition, more powerful computers became available when the larger particle numbers were reached.

The initial calculations have been performed on the VMS-cluster of DEC-alpha workstations at the PHYSnet of the university of Hamburg. In the beginning, one DEC 3000/400 AXP, one DEC 3000/600 AXP, three AlphaStation 255/233, and two AlphaStation 255/300 were available. While the first five showed an approximately equal performance, the last two are faster by a factor of 1.17 for a large system size and a three-particle wave packet. This has to be compared to the SPEC benchmarks [258] of 5.09 and 5.81 for optimized floating point operations, yielding an enhancement of 1.14. Soon afterwards two AlphaStation 500/333 (SPEC benchmark: 12.5) were included into the network, one of them was purchased directly for the project described here. They are a factor of 2.45 faster than an AlphaStation 255/233, exactly as predicted by the benchmarks. The main calculations for two and three particles have been performed on this cluster.

For the set-up of a new Unix-cluster, up to date workstations were purchased in the last 18 months. This enabled calculations on seven Personal Workstations 433AU (SPEC benchmark: 18.1) and one Professional Workstation XP1000 (SPEC benchmark: 65.5). Without these, a reasonable scaling for the four particles would have been impossible. Even though being a factor of 1.40 and 5.04 faster than an AlphaStation 500/333, the calculation of a single sample for four particles and  $L = 71$  takes roughly five days on a Personal Workstations 433AU. The good agreement with the benchmarks indicates that memory requirements are not the important. On all workstations, the calculations can be performed without swapping. For the heaviest four-particle calculations, only up to 67MB of memory are needed. Crucial for the calculations is the speed of the memory system, the use of cache, and the operating frequency, i. e. exactly the quantities relevant for the SPEC benchmarks.

Taking into account that not all workstations have been available from the beginning, the largest sample size alone required almost a year of calculations due to the disorder averaging needed. An extrapolation of equation (93) yields at  $W = 3.5$  localization lengths  $\lambda_{\text{CM}}^\infty \approx 2300$  and  $\lambda_{\text{CM}}^\infty \approx 400$  for the complete and reduced scaling curve. Going down to  $W = 3$  gives localization lengths 24000 and 3000, respectively. Keeping in mind that for a reliable calculation of the localization length, the system size has to be of the same order,  $L = 400$  is the *minimal* requirement that has to be fulfilled,  $L = 2000$  is much more appropriate. According to equation (94), such a system size yields an additional factor of 1000 (or more appropriately  $6.84 \times 10^5$ ) in CPU-time. In addition, for these system sizes the code has to be

parallelized because memory requirements can only be fulfilled on parallel computers. This has already been done, but not used so far since the speedup is *not* superlinear. Hence, due to the disorder averaging required, it is more effective to distribute the samples on different processors and calculate them at the same time than to use the parallel version and calculate the samples one after the other. But not only the parallelization will reduce the efficiency, apparently also larger times would be required to perform a reliable extrapolation to the saturation value. *Even if one could gain a factor of 100 by performing calculations on a supercomputer, the calculations would still take too long. The results displayed in figures 39 and 40 are based on state of the art computing. Doing better is impossible in the moment due to the tremendous, superexponential increase of the localization length with particle number,  $\lambda_n \propto \lambda_1^{2^n - 1}$ .*

## 7 Finite densities: time-dependent Hartree-Fock

In the preceding chapter, the time evolution method in its exact form was used to calculate the localization properties of up to four interacting particles. Reliable results for larger particle numbers are out of reach due to the limitations in the system size posed by nowadays computing technology and the superexponential increase of the localization length with particle number. Therefore, one has to rely on some approximation in order to arrive at finite densities. A possible approach is outlined in the last part of this thesis. It is based on the time-dependent Hartree-Fock equations, which can be solved with methods similar to those used for the exact few-particle calculations in the previous sections [250, 259].

The time evolution method will be generalized to time dependent Hamiltonians. This generalization enables us to treat the interaction during the time evolution on a Hartree-Fock level. On this level of approximation, the dimension of the Hilbert space is significantly reduced, allowing the treatment of finite densities up to half filling for system sizes of up to  $L = 640$ .

After a short introduction of the time-dependent Hartree-Fock equations, the generalization of the time evolution method to time dependent Hamiltonians will be presented. In the second part, results for two particles will be compared to the exact two-particle results discussed in section 5 and results for finite densities are shown. The analysis of the deviations between the approximate and the exact results gives further insight into the physical mechanism underlying the interaction-induced delocalization.

### 7.1 Method

In the time-dependent Hartree-Fock approximation, the many-body wave function is a Slater determinant constructed from single particle wave functions. These wave functions are chosen such that at every time step the deviation between the real and the approximate wave function is minimized. For fermions with spin subject to an on-site interaction, the time-dependent Hartree-Fock equations are

$$i\hbar \frac{\partial \psi_{s,\nu}(i,t)}{\partial t} = -\psi_{s,\nu}(i+1,t) - \psi_{s,\nu}(i-1,t) + \varepsilon_i \psi_{s,\nu}(i,t) + U \rho_{-s}(i,t) \psi_{s,\nu}(i,t), \quad (95)$$

with the spin index  $s$ , the lattice sites labeled by  $i$  and the different wave functions denoted by  $\nu$ . The on-site interaction with the other electrons is described by the charge density  $\rho_s(i, t) = \sum_{\nu} \psi_{s,\nu}^*(i, t) \psi_{s,\nu}(i, t)$ .

On first glance, the solution of the problem is straightforward: start with a given set of orthonormal one-particle wave functions and calculate the Hartree-Fock potential  $U\rho_s$ . Then, calculate a single time step is for all particles, evaluate the new Hartree-Fock potential is and so on. Unfortunately, it is not that simple since in this case the energy is not conserved. Instead, the problem has to be solved in several steps.

The underlying theory was derived by Suzuki [250]. He generalized the approximations valid for time independent Hamiltonians to time-dependent problems. Any formula valid for time independent Hamiltonians can be directly transferred to time dependent ones if all time-dependent matrices are evaluated at the *mid-point* of the time interval. In the first guess above, the value of the Hamiltonian at the initial point is used which yields only a first order accurate result, independent of the approximation scheme used. The problem for the time dependent Hartree-Fock equations (95) is the a priori unknown mid-point value. This mid-point value has to be approximated first.

The solution proceeds as follows. First, the time evolution is calculated with the initial Hamiltonian. Since this calculation yields only a first order accurate result in the small time step  $\Delta t$  anyway, a first order approximation is sufficient,

$$T \exp \left[ -\frac{i}{\hbar} \int_{t_i}^{t_{i+1}} dt' H_1(t) + H_2(t) \right] = \exp \left[ -\frac{i}{\hbar} H_1(t_i) \Delta t \right] \exp \left[ -\frac{i}{\hbar} H_2(t_i) \Delta t \right] + O((\Delta t)^2), \quad (96)$$

where  $T$  is the time ordering operator. Instead of dividing the one dimensional Hamiltonian into three parts as discussed in section 4, equation (44), the diagonal part is included into one of the off-diagonal parts.

$$H_1 = - \sum_{j \in \mathbb{N}_{\text{odd}}} c_{j+1}^\dagger c_j + c_j^\dagger c_{j+1} + \sum_j \varepsilon_j c_j^\dagger c_j, \quad (97)$$

$$H_2 = - \sum_{j \in \mathbb{N}_{\text{even}}} c_{j+1}^\dagger c_j + c_j^\dagger c_{j+1}. \quad (98)$$

As before, the exponentiation of  $H_1$  and  $H_2$  reduces to the calculation of the exponential of  $2 \times 2$  matrices, in the case of  $H_1$  with disorder dependent eigenvalues. Since the diagonalization of a  $2 \times 2$  matrix amounts to solving a quadratic equation the exponentials of  $H_1$  and  $H_2$  can be written down explicitly. However, in the case of  $H_1$ , the formula is much more complicated than for  $H_2$ , which is given by the example in equation (45). The reduction of the number of matrices needed for the calculation of a single time step is thus compensated by the increased effort to calculate the exponential of  $H_1$ .

Equation (96) determines the wave functions and consequently the Hamiltonian at the end point of the time step accurate to first order in  $\Delta t$  [259]. In a second step, the Hamiltonian at the mid-point of the interval is estimated by interpolating linearly between the Hamiltonian at the initial and final points giving a first order accurate result. This interpolation yields the required approximation of the Hamiltonian at the mid-point of the time interval. In a third step an expansion accurate up to second order in the time interval  $\Delta t$  is performed with the first order accurate mid point value of the Hamiltonian. This expansion yields a

second order accurate time evolution [259],

$$T \exp \left[ -\frac{i}{\hbar} \int_{t_l}^{t_{l+1}} dt' H_1(t') + H_2(t) \right] = \exp \left[ -\frac{i}{\hbar} \frac{H_1(t_l) + H_1(t_{l+1})}{2} \frac{\Delta t}{2} \right] \\ \exp \left[ -\frac{i}{\hbar} \frac{H_2(t_l) + H_2(t_{l+1})}{2} \frac{\Delta t}{1} \right] \exp \left[ -\frac{i}{\hbar} \frac{H_1(t_l) + H_1(t_{l+1})}{2} \frac{\Delta t}{2} \right] + O((\Delta t)^3), \quad (99)$$

which is used in the following. Higher order approximation can be derived iteratively using equation (99) to calculate second order approximations of the Hamiltonian at intermediate points as input for a third order decomposition scheme [259] and so on. The advantage of this scheme is that as for the time independent Hamiltonian the time evolution operator is approximated by a unitary operator. Thus, the one-particle wave functions remain orthonormal once they are chosen orthonormal initially and the energy is conserved much better than in the simplified approach discussed in the beginning.

## 7.2 Results

In order to compare with the exact results discussed in section 5, first results for just two particles are presented. However, among the quantities defined in section 4, only the mean radius remains useful. For a many-body wave function being a single Slater determinant, no preferred direction in configuration space exists. The wave packet is a product of single particle wave functions and cannot contain correlation effects. Extensions along the center of mass direction and relative direction are equal as can be seen upon inserting a Slater determinant into the definitions, equations (67) and (68). This observation already reveals that the time dependent Hartree-Fock calculation cannot reproduce the results of the exact two-particle calculation.

The time dependence of the mean radius is shown in figure 41 for different disorder values and interaction strengths. In the absence of interaction, a crossover from a ballistic to a localized regime is observed as for the exact calculations. In this case, there is no approximation and the time-dependent Hartree-Fock equations are correct. Localization lengths can be defined via the saturation values for long times. With interaction present, a crossover from a ballistic to a sub-diffusive regime takes place. The spreading of the wave packets with time in the sub-diffusive regime can be described by a power law,  $\text{MR}(t) \propto t^c$  with  $c < 0.5$ , in contrast to the logarithmically slow increase of the mean radius with time observed in section 5. Up to the longest times considered, the time-dependent Hartree-Fock calculation yields no saturation of the mean radius. This observation is in even sharper contrast to the findings from the exact calculations, where the mean radius saturated for long times indicating the complete localization of all states in the spectrum.

The power-law exponents in the sub-diffusive regime are given in table 1. The values are quite small in comparison to 0.5, the value for a diffusive spreading. The results for finite particle densities are very similar. The left plot of figure 42 displays the results for a density of 0.25 for 6 different system sizes. As for the few-particle calculations, the mean radius increases ballistically for short times  $t < 10$ . For long times, it saturates for smaller systems, while it continues to grow for the largest system sizes. The saturation values do not depend on the disorder strength and increase linearly with system size. Hence this

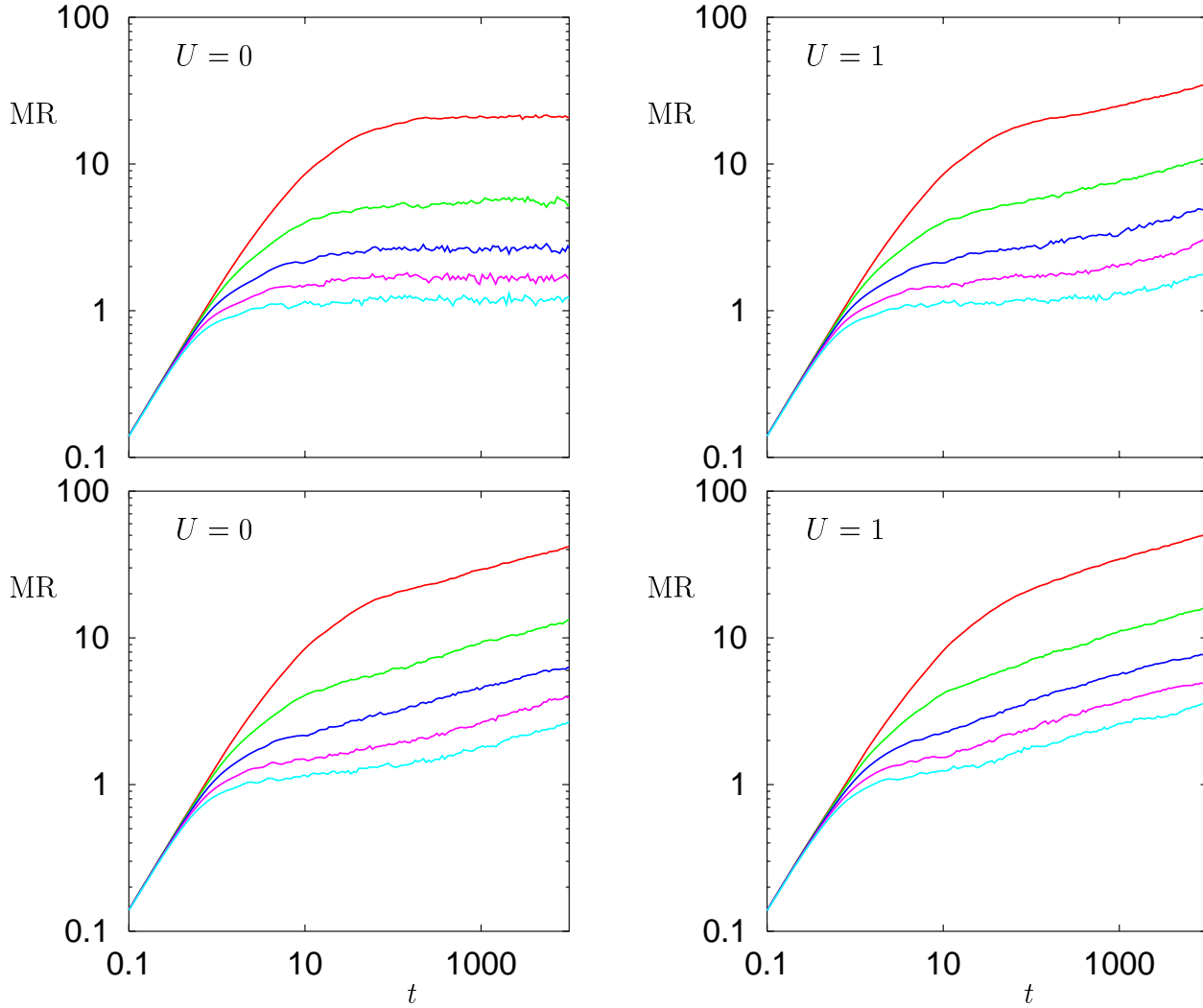


Figure 41: time-dependent Hartree-Fock results for two particles in a system of size  $L=600$  and different interaction strengths. Disorder values are  $W=2, 4, 6, 8$  and  $10$ , top to bottom curves.

	$W=2$	$W=4$	$W=6$	$W=8$	$W=10$
$U=1$	$0.150 \pm 0.002$	$0.167 \pm 0.004$	$0.174 \pm 0.008$	$0.213 \pm 0.011$	$0.186 \pm 0.007$
$U=2$	$0.155 \pm 0.003$	$0.159 \pm 0.005$	$0.140 \pm 0.006$	$0.181 \pm 0.009$	$0.160 \pm 0.005$
$U=4$	$0.170 \pm 0.001$	$0.169 \pm 0.002$	$0.161 \pm 0.002$	$0.160 \pm 0.002$	$0.149 \pm 0.002$

Table 1: Anomalous diffusion exponent  $c$  as a function of disorder (left to right) and interaction strength (top to bottom)

saturation is purely a finite size effect. The growth of the mean radius for larger system sizes is sub-diffusive as for just two particles,  $MR(t) \propto t^c$  with  $c < 0.5$  in contrast to the logarithmically slow growth observed for the exact few-particle calculations. Even for much larger disorder values, the treatment of the interaction on the level of the time dependent

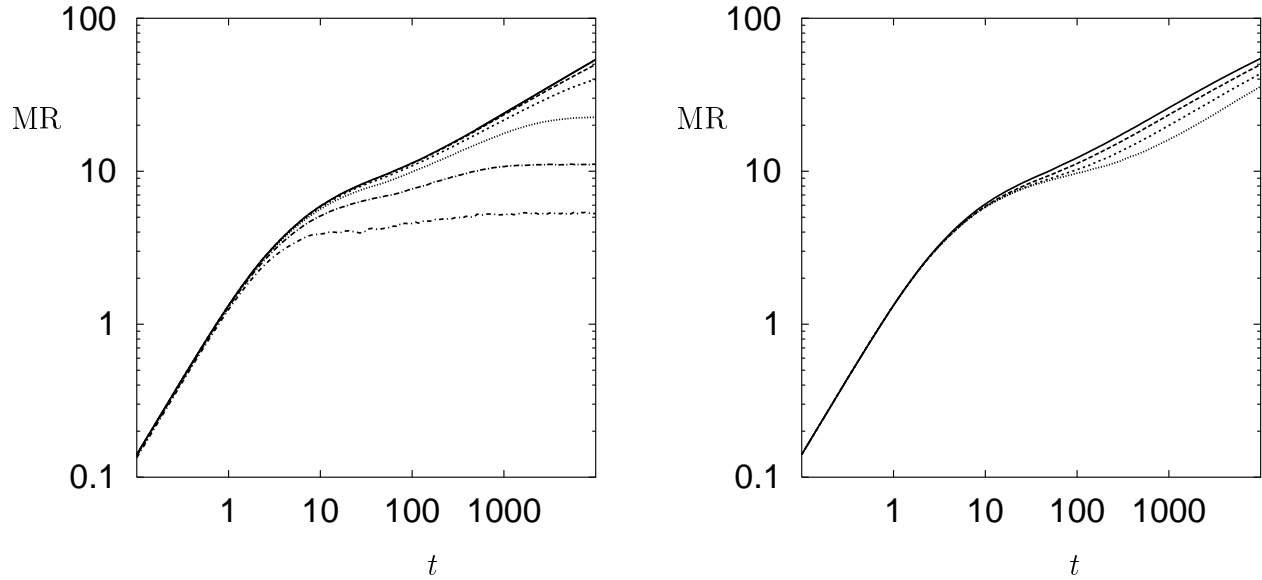


Figure 42: time-dependent Hartree-Fock results for  $W=3$  and  $U=1$ . Left: time dependence of the mean radius for a fixed density,  $n=0.25$ , and system sizes  $L=20, 40, 80, 160, 320, 640$  (bottom to top on the right). Right: time dependence for a fixed system size  $L=320$  and densities  $n=0.0625, 0.125, 0.25, 0.5$  (bottom to top on the right).

Hartree-Fock equations leads to a sub-diffusive growth of the mean radius. The right plot in figure 42 reveals the influence of the density on the time evolution. For a lower density, the sub-diffusive growth is reached later in time than for the higher densities. This retardation is related to the initial condition. At  $t=0$ , all particles are placed on equidistant lattice positions. For a smaller particle number it takes some time until the interaction comes into play. Once the sub-diffusive regime is reached, the growth is very similar for all densities. Table 2 gives the exponents of power law fits in the sub-diffusive regime. The exponents are

	40	80	160	320	640
0.0625	$0.1292 \pm 0.0024$	$0.2601 \pm 0.0025$	$0.3277 \pm 0.0007$	$0.3519 \pm 0.0012$	$0.3607 \pm 0.0011$
0.125	$0.1706 \pm 0.0083$	$0.2702 \pm 0.0011$	$0.3148 \pm 0.0008$	$0.3417 \pm 0.0005$	$0.3578 \pm 0.0002$
0.25	$0.1769 \pm 0.0030$	$0.2582 \pm 0.0007$	$0.3093 \pm 0.0003$	$0.3340 \pm 0.0005$	$0.3522 \pm 0.0001$
0.5	$0.1775 \pm 0.0010$	$0.2615 \pm 0.0009$	$0.3136 \pm 0.0003$	$0.3371 \pm 0.0004$	

Table 2: Anomalous diffusion exponent  $c$  as a function of system size (left to right) and particle density (top to bottom)

larger than those observed for just two particles. Nevertheless, the influence of the density is rather weak. There is some influence of the system size but this has to be considered with care. For the smaller sizes the power law fit could only be performed in the crossover region before the saturation. This regime is relatively small for  $L=40$  and  $L=80$  leading to strong dependencies of the exponents on the fit range.

There are two main differences between the exact and the approximated results. First, the spreading is sub-diffusive rather than logarithmically in time. Second, there is no saturation observed once the system sizes are large enough. For two particles, these differences are obvious. For a larger particle number, the estimate of the error is much less clear. It could well be that for a finite density of particles the localization length is so large, that no saturation can be observed, at least for the system sizes considered. Keep in mind the superexponential increase of the localization length with particle number found from the exact calculations, equation (87), and that up to 320 particles are considered. Hence, the error made by using the time-dependent Hartree-Fock equation might not be that large for larger particle numbers.

Trying to understand the differences between the two approaches helps a bit to estimate the error made at finite particle density and yields useful information about the mechanism underlying the interaction-induced delocalization. Let us start with the sub-diffusive spreading. This spreading is related to the phase memory of the electrons. Without interaction, the phase is conserved and interference effects lead to localization. In the presence of interaction, the potential depends on time due to the motion of the other electrons and the one-particle wave functions have no well defined phase throughout the iteration. Interference effects for the single particle wave functions are suppressed and consequently a diffusive motion sets in. This motion is similar to the motion of a single particle in a random potential under iterative measurement [260]. In a way, the other electrons measure the position of the electron under consideration due to the interaction. However, an iterative measurement of the position of a single electron leads exactly to a diffusive motion,  $MR(t) \propto t^{0.5}$ . This iterative measurement can be simulated numerical. Before the measurement the wave function can be written in the complete eigenbasis of the measuring operator,

$$|\psi\rangle = \sum_l |l\rangle \langle l|\psi\rangle = \sum_l c_l |l\rangle. \quad (100)$$

After the measurement the coefficients  $c_l$  are simply multiplied by random phase factors [261]

$$|\psi\rangle = \sum_l c_l e^{i\alpha_l} |l\rangle. \quad (101)$$

Implementing this multiplication into the time evolution for a single particle, Anderson localization is completely destroyed. Instead, a diffusive spreading of the wave packet takes place, see figure 43. For times larger than the measurement period  $T$ , the spreading is diffusive. The difference to the Hartree-Fock results is that no constant period  $T$  can be addressed for the Hartree-Fock calculation. Instead, the period seems to be an increasing function of time leading to a sub-diffusive growth. The increasing period is related to an effective interaction,

$$U_{\text{eff}}(t) = U \sum_i |\psi_{s,\nu}(i,t)|^2 \rho_{-s}(i,t) = \sum_i \sum_\nu |\psi_{s,\nu}(i,t)|^2 |\psi_{-s,\nu}(i,t)|^2, \quad (102)$$

measuring the influence of the other particles. Being a sum over cross participation ratios of different wave functions that spread with time,  $U_{\text{eff}}(t)$  is a decreasing function with time. The more delocalized the particles are, the smaller is the overlap and hence the influence of the interaction. Thus the reduction of the exponent  $c$  in comparison to the iterative measurement and consequently the sub-diffusive behavior.

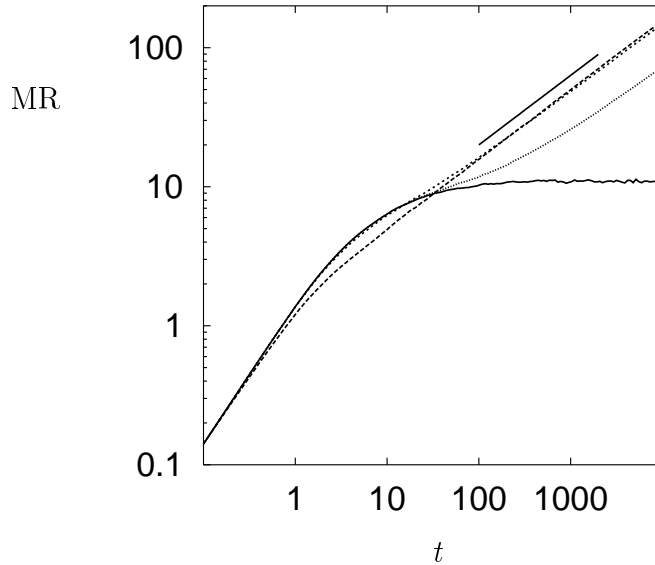


Figure 43: Single particle in a one-dimensional random potential under iterative measurement: period  $T = \infty$  (solid line), 10 (dotted line), 1 (short dashed line), and 0.1 (long dashed line). Short solid line indicates slope  $\text{MR}(t) \propto t^{0.5}$

The further reduction to a logarithmically slow growth for the exact few-particle calculations is unexplained so far, see the discussion in section 5. All theories predict a diffusive behavior, maybe with a logarithmic correction to it. A logarithmic growth was observed in percolating system subject to an external field [262] and was recently related to broad waiting-time distributions [263], but the relation to the present problem has not been clarified so far.

Simpler is the explanation of the final saturation in the exact calculation. This saturation is related to the fact that the phase of the complete  $n$ -particle wave function remains well defined throughout the entire calculation in contrast to the time-dependent Hartree-Fock approximation. Thus, the saturation is simply related to the localization of all exact  $n$ -particle eigenstates. Nevertheless, the interaction can still be viewed as a kind of measurement process randomizing single electron phases, thus delocalizing the wave packet. Since the diffusion describes a non-equilibrium process, there is no direct relation to the debate on zero temperature dephasing due to electron-electron interaction [264, 265, 266, 267].

## 8 Summary

The experimental discovery of a metal-insulator transition in two dimensions has renewed the theoretical interest on the influence of interaction on disorder-induced localization. Two main approaches have been used to tackle this problem numerically. Interaction effects have been studied for just two particles and relatively large system sizes as well as for small samples with larger particle number. Only in the first case, low disorder values could be reached and a coherent motion of the two electrons resulting in a much larger localization length than for a single electron was observed. In the second case, only strong disorder could

be studied since the single particle localization length had to be smaller than the system size in order to reduce finite size effects.

From the experimental point of view, the transition is only observed in very clean systems with small electron densities. This situation is better recovered by the first approach even though it is not directly related to ground state properties. Our aim was to generalize the two-particle approach to higher particle numbers, maintaining the low disorder regime which we think is more relevant with respect to the experimental situation.

In the first part of this thesis a short introduction to the topic of localization and interaction was presented. An overview on theoretical approaches to the combined problem of electron-electron interaction and disorder-induced localization was given, focusing mainly on recent numerical work for small particle numbers  $n \geq 2$ . The failure of the transfer matrix method was discussed as well as the success of methods calculating matrix elements of the two-particle Green function. A variety of other approaches to the two-particle problem was presented which however did not allow for a direct calculation of localization properties. Finally, results for finite densities were discussed, obtained for very small system sizes and particle numbers or relying on more or less appropriate approximations. The tendency to delocalization due to the interaction, found for  $n=2$ , seems to persist for finite densities.

On the one hand, the analytical estimates of the few-particle localization lengths all had their shortcomings and the numerical calculation did not go beyond the two-particle problem. On the other hand, the results at finite densities were obtained for very small system sizes and their relation to the experimentally observed metal-insulator transition in two dimension is therefore questionable.

In the second part of the thesis, a new numerical tool to calculate the localization length of few-particle wave packets was introduced: the calculation of the time evolution of wave packets in combination with a finite size scaling analysis of the saturation values in the localized regime. The methods were presented using the example of a particle in a one-dimensional random potential. This example revealed the possibility to use the time evolution method for studying disorder-induced localization.

In the next step, the method was generalized in order to calculate the localization properties of two interacting particles. The zero interaction limit,  $\lambda_2(U=0) \propto \lambda_1$ , was correctly reproduced and the results in the presence of interaction were in qualitative agreement with the findings obtained by calculating matrix elements of the two-particle Green function,  $\lambda_2 = a\lambda_1 + b\lambda_1^2$ . These results established the combination of a quantum diffusion calculation and a finite size scaling analysis of the saturation values of the mean radius and related quantities as a second, independent method for analyzing the localization properties of few interacting particles.

Main advantages of the new method were a simple generalization to more than two particles and the additional information that was gained about the time evolution. This information helped to understand the physical mechanism underlying the interaction-induced delocalization. The delocalization of a two-electron wave function was shown to proceed very slowly, i. e. logarithmically in time, in contrast to analytical predictions of a diffusive spreading. This observation indicated once more that one has to be very careful with simplified analytical estimates.

After the new method was established, extensive numerical calculations were performed to determine the localization lengths for three and four particles. This regime with relatively weak disorder and more than two particles was not reached before.

The localization length of few-particle wave packets was shown to increase strongly with increasing particle number. The originally proposed scaling  $\lambda_n \propto \lambda_1^n$ , section 3, could not describe the three-particle data. The observed localization length was larger than predicted. Taking into account the hierarchical structure of the configuration space, an upper bound for the  $n$ -particle localization length was derived,  $\lambda_n \propto \lambda_1^{2^{n-1}}$ . Although increasing superexponentially with increasing particle number, the localization length remained finite for any non-zero disorder and any finite particle number. The predicted upper bound was shown to be in agreement with the three-particle localization length. Furthermore, the shape of the wave function in configuration space revealed the hierarchical structure of the configuration space and supported the argument leading to the upper bound.

In spite of the exponential increase of the configuration space with particle number and the superexponential increase of the localization length with particle number, the four-particle localization length was calculated in order to collect further evidence for the proposed scaling of the localization length with particle number. This result could only be obtained due to a huge numerical effort. Although being restricted to relatively large disorder values for computational reasons, the four-particle localization length was shown to be in accordance with the proposed scaling,  $\lambda_n \propto \lambda_1^{2^{n-1}}$ . In spite of the numerical limitations, the regime dominated by the leading power of  $\lambda_1$  could be reached. To collect stronger evidence by performing calculations at lower disorder values is unfortunately out of reach with nowadays computing technology.

Applying the same arguments that led to the upper bound for the localization length in one dimension to the two-dimensional case, the propagation in CM direction is equivalent to a one-particle system with a *finite* number of coupled planes. Since the number of planes is finite for any *non-zero* disorder and any *finite* particle number, no “real” transition can be expected, although the localization length can be arbitrarily large. This finding provides some evidence that spin degrees of freedom which have not been considered for the exact calculations are relevant for the theoretical explanation of the metal insulator transition in two dimensions, in agreement with recent experiments.

In the last part of the thesis, a possible approximation for higher particle numbers up to finite particle densities was proposed. As discussed above, the exact method reached its computational limits with the four particle calculation due to the tremendous increase of the localization length and the configuration space.

After having generalized the quantum diffusion method to time dependent Hamiltonians, it could be applied to the time-dependent Hartree-Fock equations. A comparison for just two particles revealed two differences. First, the propagation was sub-diffusive rather than logarithmic. Second, no saturation could be observed up to the longest times considered. Similar results were obtained for finite densities. The differences for two particles could be understood by looking at the phase of the electron wave function. This analysis helped to understand the underlying mechanism of the delocalization on a qualitative level. In some sense, one electron “measures” the position of the other due to the interaction and as a

consequence, the single electron phase is not well defined throughout the time evolution in contrast to the phase of the  $n$ -electron wave packet in the exact calculation. For the finite density calculations, it might well be that the large number of particles considered yields localization lengths far beyond the numerically reachable system sizes. But extrapolating from the data, a saturation of the mean radius is expected for the exact calculation since the phase of the  $n$ -electron wave packet is well defined. Since this phase is undefined within the time-dependent Hartree-Fock approximation no saturation is expected. But the real error made due to the approximation is difficult to estimate.

## References

- [1] S. V. Kravchenko, W. E. Mason, G. E. Bowker, J. E. Furneaux, V. M. Pudalov, and M. D'Iorio, *Phys. Rev. B* **51**, 7038 (1995).
- [2] S. V. Kravchenko, D. Simonian, M. P. Sarachik, W. Mason, and J. E. Furneaux, *Phys. Rev. Lett.* **77**, 4938 (1996).
- [3] D. Popović, A. B. Fowler, and S. Washburn, *Phys. Rev. Lett.* **79**, 1543 (1997).
- [4] M. Y. Simmons, A. R. Hamilton, M. Pepper, E. H. Linfield, P. D. Rose, D. A. Ritchie, A. K. Savchenko, and T. G. Griffiths, *Phys. Rev. Lett.* **80**, 1292 (1998).
- [5] B. Kramer and A. MacKinnon, *Rep. Prog. Phys.* **56**, 1469 (1993).
- [6] D. L. Shepelyansky, *Phys. Rev. Lett.* **73**, 2607 (1994).
- [7] K. M. Frahm, *Eur. Phys. Jour. B* **10**, 371 (1999).
- [8] P. H. Song and D. Kim, *Phys. Rev. B* **56**, 12217 (1997).
- [9] M. Leadbeater, R. A. Römer, and M. Schreiber, *Eur. Phys. Jour. B* **8**, 643 (1999).
- [10] G. Baym, *Lectures on Quantum Mechanics* (Benjamin/Cummings Publishing Company, Inc., New York, 1973).
- [11] C. Kittel, *Introduction to Solid State Physics* (John Wiley & Sons, Inc., New York, 1976).
- [12] P. W. Anderson, *Phys. Rep.* **109**, 1492 (1958).
- [13] N. F. Mott, *Philosophical Magazin* **17**, 1259 (1968).
- [14] N. F. Mott and W. D. Twose, *Adv. Phys.* **10**, 107 (1961).
- [15] K. Ishii, *Supplement of the Progress of Theoretical Physics* **53**, 77 (1973).
- [16] D. J. Thouless, *Phys. Rev. Lett.* **39**, 1167 (1977).

- [17] M. E. Gershenson, Y. B. Khavin, A. G. Mikhalechuk, H. M. Bozler, and A. L. Bogdanov, *Phys. Rev. Lett.* **79**, 725 (1997).
- [18] Y. B. Khavin, M. E. Gershenson, and A. L. Bogdanov, *Phys. Rev. B* **58**, 8009 (1998).
- [19] K. B. Efetov and A. I. Larkin, *Sov. Phys. JETP* **58**, 444 (1983).
- [20] O. N. Dorokhov, *Sov. Phys. JETP* **58**, 606 (1983).
- [21] M. Pepper, S. Pollitt, C. J. Adkins, and R. E. Oakley, *Phys. Lett. A* **47**, 71 (1974).
- [22] M. Pepper, S. Pollitt, and C. J. Adkins, *Phys. Lett. A* **48**, 113 (1974).
- [23] D. C. Tsui and J. S. J. Allen, *Phys. Rev. Lett.* **32**, 1200 (1974).
- [24] N. Mott, M. Pepper, S. Pollitt, R. H. Williams, and C. J. Adkins, *Proc. Roy. Soc. Lond. A* **345**, 169 (1975).
- [25] E. Abrahams, P. W. Anderson, D. C. Licciardello, and T. V. Ramakrishnan, *Phys. Rev. Lett.* **42**, 673 (1979).
- [26] K. Efetov, *Adv. Phys.* **32**, 53 (1983).
- [27] J. Verbaarschot, H. Weidenmüller, and M. Zirnbauer, *Phys. Rep.* **129**, 367 (1985).
- [28] A. MacKinnon and B. Kramer, *Phys. Rev. Lett.* **47**, 1546 (1981).
- [29] A. MacKinnon and B. Kramer, *Z. Phys. B* **53**, 1 (1983).
- [30] J. Pichard and G. Sarma, *J. Phys. C* **14**, L127 (1981).
- [31] J. Pichard and G. Sarma, *J. Phys. C* **14**, L617 (1981).
- [32] B. Altshuler and A. G. Aronov, in *Electron-Electron Interaction in Disordered Systems*, edited by A. L. Efros and M. Pollak (North Holland Physics Publishing, Amsterdam, 1985), Chap. 1, pp. 1–154.
- [33] D. J. Bishop, D. C. Tsui, and R. C. Dynes, *Phys. Rev. Lett.* **44**, 1153 (1980).
- [34] M. J. Uren, R. A. Davies, M. Kaveh, and M. Pepper, *J. Phys. C* **14**, 5737 (1981).
- [35] G. Bergmann, *Phys. Rep.* **107**, 1 (1984).
- [36] F. Keuls, H. Mathur, H. W. Jiang, and A. J. Dahm, *Phys. Rev. B* **56**, 13263 (1997).
- [37] S. V. Kravchenko, G. V. Kravchenko, J. E. Furneaux, V. M. Pudalov, and M. D’Iorio, *Phys. Rev. B* **50**, 8039 (1994).
- [38] K. Ismail, J. O. Chu, D. Popović, A. B. Fowler, and S. Washburn, preprint, cond-mat/9707061, (1997).
- [39] P. T. Coleridge, R. L. Williams, Y. Feng, and P. Zwadzki, *Phys. Rev. B* **56**, R12765 (1997).

- [40] J. Lam, M. D'Iorio, D. Brown, and H. Lafontaine, *Phys. Rev. B* **56**, R12741 (1997).
- [41] A. R. Hamilton, M. Y. Simmons, M. Pepper, E. H. Linfield, P. D. Rose, and D. A. Ritchie, *Phys. Rev. Lett.* **82**, 1542 (1999).
- [42] Y. Hanein, U. Meirav, D. Shahar, C. C. Li, D. C. Tsui, and H. Shtrikman, *Phys. Rev. Lett.* **80**, 1288 (1998).
- [43] Y. Hanein, D. Shahar, J. Yoon, C. C. Li, D. C. Tsui, and H. Shtrikman, *Phys. Rev. B* **58**, R7520 (1999).
- [44] Y. Hanein, D. Shahar, J. Yoon, C. C. Li, D. C. Tsui, and H. Shtrikman, *Phys. Rev. B* **58**, R13338 (1999).
- [45] D. Popović and S. Washburn, *Phys. Rev. B* **56**, R10048 (1997).
- [46] D. Simonian, S. V. Kravchenko, and M. P. Sarachik, *Phys. Rev. Lett.* **79**, 2304 (1997).
- [47] V. M. Pudalov, G. Brunthaler, and G. B. A. Prinz, *Sov. Phys. JETP* **65**, 932 (1997).
- [48] T. Okamoto, K. Hosoya, S. Kawaji, and A. Yagi, *Phys. Rev. Lett.* **82**, 3875 (1999).
- [49] X. G. Feng, D. Popović, and S. Washburn, *Phys. Rev. Lett.* **83**, 368 (1999).
- [50] X. G. Feng, D. Popović, and S. Washburn, *Physica E* **6**, 280 (2000).
- [51] S. V. Kravchenko, D. Simonian, M. P. Sarachik, A. D. Kent, and V. M. Pudalov, *Phys. Rev. B* **58**, 3553 (1998).
- [52] D. Simonian, S. V. Kravchenko, M. P. Sarachik, and V. M. Pudalov, *Phys. Rev. B* **57**, R9420 (1998).
- [53] S. V. Kravchenko, D. Simonian, K. Mertes, M. P. Sarachik, and T. M. Klapwijk, *Phys. Rev. B* **59**, R12740 (1999).
- [54] D. Simonian, S. V. Kravchenko, and M. P. Sarachik, *Phys. Rev. B* **55**, R13421 (1997).
- [55] Y. Hanein, N. Nenadovic, D. Shahar, H. Shtrikman, J. Yoon, C. C. Li, and D. C. Tsui, *Nature* **400**, 735 (1999).
- [56] V. M. Pudalov, Intern. Conf. on Localization and Quantum Transport in Solids, Jaszowiec, Poland; T. Dietl ed., Inst. of Physics PAN, Warsaw 34 (1996).
- [57] V. M. Pudalov, *Sov. Phys. JETP* **66**, 175 (1997).
- [58] S. J. Papadakis, E. P. de Poortere, H. C. Manoharan, M. Shayegan, and R. Winkler, *Science* **283**, 2056 (1999).
- [59] M. Y. Simmons, A. R. Hamilton, M. Pepper, E. H. Linfield, P. D. Rose, D. A. Ritchie, A. K. Savchenko, and T. G. Griffiths, *Phys. Rev. Lett.* **84**, 2489 (2000).
- [60] V. M. Pudalov, G. Brunthaler, A. Prinz, and G. Bauer, *JETP Lett.* **68**, 534 (1998).

- [61] S. Washburn, D. Popović, K. P. Li, and A. B. Fowler, *Superlattices and Microstructures* **23**, 581 (1997).
- [62] V. M. Pudalov, G. Brunthaler, A. Prinz, and G. Bauer, *JETP Lett.* **68**, (1998).
- [63] V. M. Pudalov, G. Brunthaler, A. Prinz, and G. Bauer, *JETP Lett.* **70**, 48 (1999).
- [64] V. M. Pudalov, G. Brunthaler, A. Prinz, G. Bauer, and B. I. Fouks, preprint, cond-mat/9907401, (1999).
- [65] E. Ribeiro and R. D. Jäggi and T. Heinzel and K. Ensslin and G. Medeiros-Ribeiro and P. M. Petroff, *Phys. Rev. Lett.* **82**, 996 (1999).
- [66] S. A. Vitkalov, H. Zheng, K. M. Mertes, M. P. Sarachik, and T. M. Klapwijk, preprint, cond-mat/9907395, (1999).
- [67] S. Washburn, N. J. Kim, X. G. Feng, and D. Popović, *Ann. Phys. (Leipzig)* **8**, 569 (1999).
- [68] D. Popović, A. B. Fowler, and S. Washburn, *Physica B* **249-251**, 701 (1998).
- [69] P. Phillips, Y. Wan, I. Martin, S. Knysh, and D. Dalidovich, *Nature* **395**, 253 (1998).
- [70] D. Belitz and T. R. Kirkpatrick, *Phys. Rev. B* **58**, 8214 (1998).
- [71] J. S. Thakur and D. Neilson, *Phys. Rev. B* **58**, 13717 (1998).
- [72] J. S. Thakur and D. Neilson, *Phys. Rev. B* **59**, R5280 (1999).
- [73] B. L. Altshuler and D. L. Maslov, *Phys. Rev. Lett.* **82**, 145 (1999).
- [74] V. Dobrosavljevic, E. Abrahams, E. Miranda, and S. Chakravarty, *Phys. Rev. Lett.* **79**, 455 (1997).
- [75] S. He and X. C. Xie, *Phys. Rev. Lett.* **80**, 3324 (1998).
- [76] Y. Meir, *Phys. Rev. Lett.* **83**, 3506 (1999).
- [77] J. Shi, S. He, and X. C. Xie, *Phys. Rev. B* **60**, R13950 (1999).
- [78] W. Zheng and Y. Yu, preprint, cond-mat/9710105, (1997).
- [79] E. A. Sudip Chakravarty, Lan Yin, *Phys. Rev. B* **58**, R559 (1998).
- [80] P. A. L. C. Castellani, C. Di Castro, *Phys. Rev. B* **57**, R9381 .
- [81] Q. Si and C. M. Varma, *Phys. Rev. Lett.* **81**, 4951 (1998).
- [82] A. M. Finkelstein, *Z. Pyhs B* **56**, 189 (1984).
- [83] G.-H. Chen and M. E. Raikh, *Phys. Rev. B* **60**, 4826 (1999).

- [84] G.-H. Chen, M. E. Raikh, and Y.-S. Wu, *Phys. Rev. B* **61**, R10539 (2000).
- [85] Y. Lyanda-Geller, *Phys. Rev. Lett.* **80**, 4273 (1998).
- [86] X. Waintal, G. Benenti, and J.-L. Pichard, *Ann. Phys. (Leipzig)* **8**, 691 (1999).
- [87] D. L. Shepelyansky and P. H. Song, *Ann. Phys. (Leipzig)* **8**, 665 (1999).
- [88] X. Waintal, G. Benenti, and J.-L. Pichard, *Europhys. Lett.* **49**, 466 (2000).
- [89] T. Vojta, F. Epperlein, and M. Schreiber, *Phys. Rev. Lett.* **81**, 4212 (1998).
- [90] M. Ortuño and E. Cuevas, *Europhys. Lett.* **46**, 224 (1999).
- [91] E. Cuevas, *Phys. Rev. Lett.* **83**, 140 (1999).
- [92] D. L. Shepelyansky, *Phys. Rev. B* **61**, 4588 (2000).
- [93] G. Benenti, X. Waintal, and J.-L. Pichard, preprint, cond-mat/9812339, (1998).
- [94] G. Benenti, X. Waintal, and J.-L. Pichard, *Phys. Rev. Lett.* **83**, 1826 (1999).
- [95] G. Benenti, X. Waintal, J.-L. Pichard, and D. L. Shepelyansky, preprint, cond-mat/9903339, (1999).
- [96] J. Talamantes, M. Pollak, and I. Varga, *phys. stat. sol.* **218**, 119 (2000).
- [97] E. Cuevas and M. Ortuño, *Ann. Phys. (Leipzig)* **8**, SI 37 (1999).
- [98] P. J. H. Denteneer, R. T. Scalettar, and N. Trivedi, *Phys. Rev. Lett.* **83**, 4610 (1999).
- [99] R. A. Römer and M. Leadbeater and M. Schreiber, *Ann. Phys. (Leipzig)* **8**, 675 (1999).
- [100] J. S. Thakur, L. Liu, and D. Neilson, *Phys. Rev. B* **59**, 7255 (1999).
- [101] K. M. Itoh, E. E. Haller, J. W. Beeman, W. L. Hansen, J. Emes, L. A. Reichertz, E. Kreysa, T. Shutt, A. Cummings, W. Stockwell, B. Sadoulet, J. Muto, J. W. Farmer, and V. I. Ozhigin, *Phys. Rev. Lett.* **77**, 4058 (1996).
- [102] G. Thomas, Y. Ootuka, S. Katsumoto, S. Kobayashi, and W. Sasaki, *Phys. Rev. B* **25**, 4288 (1982).
- [103] M. Hirsch, U. Thomanschefskey, and D. F. Holcomb, *Phys. Rev. B* **37**, 8257 (1988).
- [104] A. G. Zabrodskii and K. Zinov'eva, *Sov. Phys. JETP* **59**, 425 (1984).
- [105] T. Rosenbaum, K. Andres, G. Thomas, and R. N. Bhatt, *Phys. Rev. Lett.* **45**, 1723 (1980).
- [106] P. Newman and D. F. Holcomb, *Phys. Rev. Lett.* **51**, 2144 (1983).
- [107] A. Ionov, M. Lea, and R. Rentzsch, *JETP Lett.* **54**, 473 (1991).

- [108] P. Dai, Y. Zhang, and M. P. Sarachik, *Phys. Rev. Lett.* **66**, 1914 (1991).
- [109] K. Slevin and T. Ohtsuki, *Phys. Rev. Lett.* **82**, 382 (1999).
- [110] J. Chayes, L. Chayes, D. S. Fisher, and T. Spencer, *Phys. Rev. Lett.* **54**, 2375 (1986).
- [111] S. Waffenschmidt and C. Pfeiderer and H. v. Löhneysen, *Phys. Rev. Lett.* **83**, 3005 (1999).
- [112] S. Bogdanovich, M. Sarachik, and R. N. Bhatt, *Phys. Rev. Lett.* **82**, 137 (1999).
- [113] S. Bogdanovich, M. Sarachik, and R. N. Bhatt, *Phys. Rev. B* **60**, 2292 (1999).
- [114] K. M. Itoh, M. Watanabe, Y. Ootuka, and E. E. Haller, *Ann. Phys. (Leipzig)* **8**, 631 (1999).
- [115] A. L. Efros and B. I. Shklovskii, *J. Phys. C: Solid State Physics* **8**, L49 (1975).
- [116] R. B. Laughlin, *Phys. Rev. Lett.* **50**, 1395 (1983).
- [117] L. P. Lévy, G. Dolan, J. Dunsmuir, and H. Bouchiat, *Phys. Rev. Lett.* **64**, 2074 (1990).
- [118] V. Chandrasekhar, R. A. Webb, M. J. Brady, M. B. Ketchen, W. J. Gallagher, and A. Kleinsasser, *Phys. Rev. Lett.* **67**, 3578 (1991).
- [119] P. Mohanty, E. M. Q. Jariwala, and R. A. Webb, *Phys. Rev. Lett.* **78**, 3366 (1997).
- [120] O. N. Dorokhov, *Sov. Phys. JETP* **71**, 360 (1990).
- [121] Y. Imry, *Europhys. Lett.* **30**, 405 (1995).
- [122] Y. Imry, *phys. stat. sol. (b)* **205**, 249 (1998).
- [123] K. Frahm, A. Müller-Groeling, J.-L. Pichard, and D. Weinmann, *Europhys. Lett.* **31**, 169 (1995).
- [124] R. A. Römer and M. Schreiber, *Phys. Rev. Lett.* **78**, 515 (1997).
- [125] K. Frahm, A. Müller-Groeling, J.-L. Pichard, and D. Weinmann, *Phys. Rev. Lett.* **78**, 4889 (1997).
- [126] R. A. Römer and M. Schreiber, *Phys. Rev. Lett.* **78**, 4888 (1997).
- [127] O. Halfpap, *Diplomarbeit, Universität Hamburg*, 1996.
- [128] O. Halfpap, A. MacKinnon, and B. Kramer, *Solid State Comm.* **107**, 379 (1998).
- [129] R. A. Römer and M. Schreiber, *phys. stat. sol. (b)* **205**, 275 (1998).
- [130] O. Halfpap, I. K. Zharekeshev, A. MacKinnon, and B. Kramer, *Ann. Phys. (Leipzig)* **7**, 503 (1998).

- [131] G. Benettin, L. Galgani, A. Giorgilli, and J.-M. Strelcyn, *Meccanica* **15**, 9 (1980).
- [132] K. Frahm, unpublished (1998).
- [133] F. von Oppen, T. Wettig, and J. Müller, *Phys. Rev. Lett.* **76**, 491 (1996).
- [134] B. Huckestein, *Rev. Mod. Phys.* **67**, 357 (1995).
- [135] F. von Oppen and T. Wettig, *Europhys. Lett.* **32**, 741 (1995).
- [136] P. H. Song and F. von Oppen, *Phys. Rev. B* **59**, 46 (1999).
- [137] D. Weinmann, A. Müller-Groeling, J.-L. Pichard, and K. Frahm, *Phys. Rev. Lett.* **75**, 1598 (1995).
- [138] O. Halfpap, T. Kawarabayashi, and B. Kramer, *Ann. Phys. (Leipzig)* **7**, 483 (1998).
- [139] O. Halfpap and B. Kramer, *Ann. Phys. (Leipzig)* **8**, SI 85 (1999).
- [140] S. D. T. Arias, X. Waintal, and J.-L. Pichard, *Eur. Phys. Jour. B* **10**, 149 (1999).
- [141] X. Waintal, D. Weinmann, and J.-L. Pichard, *Eur. Phys. Jour. B* **7**, 451 (1999).
- [142] I. V. Ponomarev and P. G. Silvestrov, *Phys. Rev. B* **56**, 3742 (1997).
- [143] D. Weinmann and J.-L. Pichard, *Phys. Rev. Lett.* **77**, 1556 (1996).
- [144] M. Leadbeater, R. A. Römer, and M. Schreiber, *Excitonic Processes in Condensed Matter* **98-25**, 349 (1998), the Electrochemical Society Proceedings Series, Pennington, NJ (1998), ed. R. T. Williams and W. M. Yen.
- [145] D. Brinkmann, Ph.D. thesis, Universität Marburg, 1998.
- [146] A. MacKinnon, *Z. Phys. B* **59**, 385 (1985).
- [147] F. Borgonovi and D. L. Shepelyansky, *Physica D* **109**, 24 (1997).
- [148] P. Jacquod, D. L. Shepelyansky, and O. Sushkov, *Phys. Rev. Lett.* **78**, 923 (1997).
- [149] M. A. N. Araújo, M. Dzierzawa, C. Aebischer, and D. Baeriswyl, *Physica B* **244**, 9 (1998).
- [150] S. N. Evangelou, S.-J. Xiong, and E. N. Economou, *Phys. Rev. B* **54**, 8469 (1996).
- [151] J. T. Edwards and D. J. Thouless, *J. Phys. C* **5**, 807 (1972).
- [152] D. J. Thouless, *Phys. Rep.* **13**, 93 (1974).
- [153] D. Braun, E. Hofstetter, A. MacKinnon, and G. Montambaux, *Phys. Rev. B* **55**, 7557 (1997).
- [154] E. Akkermans and J.-L. Pichard, *Eur. Phys. Jour. B* **1**, 223 (1998).

- [155] A. Wobst and D. Weinmann, Eur. Phys. Jour. B **10**, 159 (1999).
- [156] T. Guhr, A. M. Groeling, and H. A. Weidenmüller, Phys. Rep. **299**, 189 (1998).
- [157] K. Frahm and A. Müller-Groeling, Europhys. Lett. **32**, 385 (1995).
- [158] Y. V. Fyodorov and A. D. Mirlin, Phys. Rev. B **52**, R11580 (1995).
- [159] Y. V. Fyodorov and A. D. Mirlin, Phys. Rev. Lett. **67**, 2405 (1991).
- [160] Y. V. Fyodorov and A. D. Mirlin, Phys. Rev. Lett. **69**, 1093 (1992).
- [161] Y. V. Fyodorov and A. D. Mirlin, Phys. Rev. Lett. **71**, 412 (1993).
- [162] P. Jacquod and D. L. Shepelyansky, Phys. Rev. Lett. **75**, 3501 (1995).
- [163] P. Jacquod and D. L. Shepelyansky, Phys. Rev. Lett. **78**, 4986 (1997).
- [164] P. Jacquod, phys. stat. sol. (b) **205**, 263 (1998).
- [165] J.-L. Pichard and B. Shapiro, J. Phys. I, France **4**, 623 (1994).
- [166] D. Weinmann, J.-L. Pichard, and Y. Imry, J. Phys. I France **7**, 1559 (1997).
- [167] B. Georgeot and D. L. Shepelyansky, Phys. Rev. Lett. **79**, 4365 (1997).
- [168] P. Jacquod and D. L. Shepelyansky, Phys. Rev. Lett. **79**, 1837 (1997).
- [169] B. L. Altshuler, Y. Gefen, A. Kamenev, and L. S. Levitov, Phys. Rev. Lett. **78**, 2803 (1997).
- [170] A. D. Mirlin and Y. V. Fyodorov, Phys. Rev. B **56**, 13393 (1997).
- [171] P. G. Silvestrov, Phys. Rev. Lett. **79**, 3994 (1997).
- [172] U. Sivan, F. P. Milliken, K. Milkove, S. Rishton, Y. Lee, J. M. Hong, V. Broegli, D. Kern, and M. deFranca, Europhys. Lett. **25**, 605 (1994).
- [173] U. Sivan, Y. Imry, and A. G. Aronov, Europhys. Lett. **28**, 115 (1994).
- [174] D. L. Shepelyansky and O. P. Sushkov, Europhys. Lett. **37**, 121 (1997).
- [175] B. I. Shklovskii, B. Shapiro, B. R. Sears, P. Lambrianides, and H. B. Shore, Phys. Rev. B **47**, 11487 (1993).
- [176] O. Halfpap, I. K. Zharekeshev, and B. Kramer, in *Proceedings of the 24th ICPS*, ICPS (World Scientific, Singapore, 1998), pp. Section II, D9.
- [177] D. L. Shepelyansky, Proceedings of the Rencontres de Moriond (1999).
- [178] P. Jacquod, Phys. Rev. Lett. **81**, 1913 (1998).
- [179] R. Berkovits, Europhys. Lett. **25**, 681 (1994).

- [180] R. Berkovits and Y. Avishai, Phys. Rev. Lett. **76**, 291 (1996).
- [181] R. Berkovits and Y. Avishai, Phys. Rev. Lett. **80**, 568 (1998).
- [182] R. Berkovits and B. I. Shklovskii, J. Phys. Condens. Matter **11**, 779 (1999).
- [183] R. Berkovits, Ann.Phys. (Leipzig) **8**, SI 25 (1999).
- [184] R. Berkovits, Phys. Rev. B **60**, 26 (1999).
- [185] R. Berkovits and B. I. Shklovskii, Phys. Rev. B **57**, 15076 (1998).
- [186] G. Benenti, X. Waintal, and J.-L. Pichard, Proceedings of the Rencontres de Moriond (1999).
- [187] G. Benenti, X. Waintal, and J.-L. Pichard, preprint, cond-mat/9910271, (1999).
- [188] R. Berkovits, J. W. Kantelhardt, Y. Avishai, S. Havlin, and A. Bunde, private communication (2000).
- [189] K. Frahm, A. Müller-Groeling, and J.-L. Pichard, Phys. Rev. Lett. **76**, 1509 (1996).
- [190] K. Frahm, A. Müller-Groeling, and J.-L. Pichard, Z. Phys. B **102**, 261 (1997).
- [191] S.-J. Xiong and S. N. Evangelou, Phys. Rev. B **56**, 13623 (1997).
- [192] R. A. Römer, M. Schreiber, and T. Vojta, phys. stat. sol. (b) **211**, 681 (1999).
- [193] X. Waintal and J.-L. Pichard, Eur. Phys. Jour. B **6**, 117 (1998).
- [194] R. A. Römer, M. Schreiber, and T. Vojta, submitted to Physica E (2000).
- [195] S. Fishman, D. R. Grempel, and R. E. Prange, Phys. Rev. Lett. **49**, 509 (1982).
- [196] S. Fishman, D. R. Grempel, and R. E. Prange, Phys. Rev. A **29**, 1639 (1984).
- [197] E. Doron and S. Fishman, Phys. Rev. Lett. **60**, 867 (1988).
- [198] D. L. Shepelyansky, Physica **D 8**, 208 (1983).
- [199] G. Casati, I. Guarneri, and D. L. Shepelyansky, Phys. Rev. Lett. **62**, 345 (1989).
- [200] F. Borgonovi and D. L. Shepelyansky, Nonlinearity **8**, 877 (1995).
- [201] F. Borgonovi and D. L. Shepelyansky, J. Phys. I France **6**, 287 (1996).
- [202] D. Brinkmann, J. Golub, S. Koch, P. Thomas, K. Maschke, and I. Varga, Eur. Phys. Jour. B **10**, 145 (1999).
- [203] D. L. Shepelyansky, Phys. Rev. B **54**, 14896 (1996).
- [204] A. Barelli, J. Belissard, P. Jacquod, and D. L. Shepelyansky, Phys. Rev. Lett. **77**, 4752 (1996).

- [205] A. Borelli, J. Belissard, P. Jacquod, and D. L. Shepelyansky, *Phys. Rev. B* **55**, 9524 (1997).
- [206] S. N. Evangelou and D. E. Katsanos, *Phys. Rev. B* **56**, 12797 (1997).
- [207] A. Eilmes, U. Grimm, R. A. Römer, and M. Schreiber, *Eur. Phys. Jour. B* **8**, 547 (1999).
- [208] A. Aharony, O. Entin-Wohlmann, and Y. Imry, *Phys. Rev. B* **61**, 5452 (2000).
- [209] A. Aharony, O. Entin-Wohlmann, Y. Levinson, and Y. Imry, *Ann. Phys. (Leipzig)* **8**, 685 (1999).
- [210] M. A. Tusch and D. E. Logan, *Phys. Rev. B* **48**, 14843 (1993).
- [211] M. Milovanović, S. Sachdev, and R. N. Bhatt, *Phys. Rev. Lett.* **63**, 82 (1989).
- [212] F. Epperlein, M. Schreiber, and T. Vojta, *Phys. Rev. B* **56**, 5890 (1997).
- [213] F. Epperlein, M. Schreiber, and T. Vojta, *phys. stat. sol. (b)* **205**, 233 (1998).
- [214] J. Talamantes, M. Pollak, and L. Elam, *Europhys. Lett.* **35**, 511 (1996).
- [215] J. Talamantes and A. Möbius, *phys. stat. sol. (b)* **205**, 45 (1998).
- [216] T. Vojta, F. Epperlein, and M. Schreiber, *Comp. Phys. Comm.* **121-122**, 489 (1999).
- [217] M. Schreiber, F. Epperlein, and T. Vojta, *Physica A* **266**, 443 (1999).
- [218] T. Vojta and F. Epperlein, *Ann. Phys. (Leipzig)* **7**, 493 (1998).
- [219] F. Epperlein, T. Vojta, and M. Schreiber, *Ann. Phys. (Leipzig)* **8**, SI 61 (1999).
- [220] T. Vojta, F. Epperlein, and M. Schreiber, *phys. stat. sol (b)* **205**, 53 (1998).
- [221] P. H. Song and D. L. Shepelyansky, *Phys. Rev. B* **61**, 15546 (2000).
- [222] G. Benenti, X. Waintal, J.-L. Pichard, and D. L. Shepelyansky, preprint, cond-mat/0003208, (2000).
- [223] J. Voit, *Rep. Prog. Phys.* **58**, 977 (1995).
- [224] W. Apel and T. M. Rice, *Phys. Rev. B* **26**, 7063 (1982).
- [225] W. Apel, *J. Phys. C* **15**, 1973 (1982).
- [226] T. Giamarchi and H. J. Schulz, *Phys. Rev. B* **37**, 325 (1988).
- [227] A. Furusaki and N. Nagaosa, *Phys. Rev. B* **47**, 4631 (1993).
- [228] S. White, *Phys. Rev. Lett.* **68**, 3487 (1992).

- [229] P. Schmitteckert, T. Schulze, C. Schuster, P. Schwab, and U. Eckern, *Phys. Rev. Lett.* **80**, 560 (1998).
- [230] P. Schmitteckert, Ph.D. thesis, Universität Augsburg, 1996.
- [231] P. Schmitteckert and U. Eckern, *Phys. Rev. B* **53**, 15397 (1996).
- [232] P. Schmitteckert, R. A. Jalabert, D. Weinmann, and J.-L. Pichard, *Phys. Rev. Lett.* **81**, 2308 (1998).
- [233] D. Weinmann, J.-L. Pichard, P. Schmitteckert, and R. A. Jalabert, *Proceedings of the Rencontres de Moriond* (1999).
- [234] A. Kambili and C. J. Lambert, *Phys. Rev. B* **60**, 7684 (1999).
- [235] D. Weinmann, private communication (2000).
- [236] J. Yi, L. Zhang, and G. S. Canright, *Phys. Rev. B* **49**, 15920 (1994).
- [237] D. Weaire and A. R. Williams, *J. Phys. C* **10**, 1239 (1977).
- [238] B. Kramer and D. Weaire, *J. Phys. C* **11**, L5 (1978).
- [239] B. Kramer, A. MacKinnon, and D. Weaire, *Phys. Rev. B* **23**, 6357 (1981).
- [240] H. de Raedt, *Europhys. Lett.* **3**, 139 (1987).
- [241] T. Ohtsuki and T. Kawarabayashi, *J. Phys. Soc. Jap.* **66**, 314 (1997).
- [242] B. Huckstein and R. Klesse, *Phys. Rev. B* **59**, 9714 (1999).
- [243] T. Nakanishi, T. Ohtsuki, and T. Kawarabayashi, *J. Phys. Soc. Jap.* **66**, 949 (1997).
- [244] F. M. Izrailev, T. Kottos, A. Politi, and G. P. Tsironis, *Phys. Rev. E* **55**, 4951 (1997).
- [245] A. Politi, S. Ruffo, and L. Tessieri, *Eur. Phys. Jour. B* **14**, 673 (2000).
- [246] J. Dräger and O. Halfpap, *Ann. Phys. (Leipzig)* **7**, 593 (1998).
- [247] M. Suzuki, *Comm. Math. Phys.* **51**, 183 (1977).
- [248] M. Suzuki, *Phys. Lett. A* **146**, 319 (1990).
- [249] M. Suzuki, *Phys. Lett. A* **165**, 387 (1992).
- [250] M. Suzuki, *Proc. Japan Acad. Ser. B* **69**, 43 (1993).
- [251] B. Derrida and E. J. Gardner, *Jour. Phys. France* **45**, 1283 (1984).
- [252] S. D. T. Arias and J. M. Luck, *J. Phys. A: Math. Gen.* **31**, 7699 (1998).
- [253] W. H. Press, B. P. Flannery, S. A. Teukolsky, and W. T. Vetterling, *Numerical Recipes* (Cambridge University Press, Cambridge, 1986).

- [254] M. Ramin, B. Reulet, and H. Bouchiat, Phys. Rev. B **51**, 5582 (1994).
- [255] F. Milde, Ph.D. thesis, Technische Universität Chemnitz, 2000.
- [256] R. Römer, Habilitationsschrift (1999).
- [257] T. Schulze, Diplomarbeit, Universität Augsburg, 1997.
- [258] SPEC-benchmarks, <http://www.specbench.org> .
- [259] A. Terai and Y. Ono, Prog. Th. Phys. Suppl. **113**, 177 (1993).
- [260] J. C. Flores, Phys. Rev. B **60**, 30 (1999).
- [261] D. Bohm, *Quantum Theory* (Prentice-Hall, inc., Englewood Cliffs, N.J., 1951).
- [262] J. Dräger and A. Bunde, Physica A **266**, 62 (1999).
- [263] J. Dräger and J. Klafter, Phys. Rev. Lett. **84**, 5998 (2000).
- [264] D. S. Golubev and A. D. Zaikin, Phys. Rev. Lett. **81**, 1074 (1998).
- [265] I. L. Aleiner, B. L. Altshuler, and M. E. Gershenson, Phys. Rev. Lett. **82**, 3190 (1999).
- [266] D. S. Golubev and A. D. Zaikin, Phys. Rev. Lett. **82**, 3191 (1999).
- [267] D. S. Golubev and A. D. Zaikin, Phys. Rev. B **59**, 9195 (1999).

## Acknowledgments

The extensive numerical calculation were performed mostly on the cluster of DEC-alpha workstation at the PHYSnet. While switching the operating system caused a lot of problems, the scaling for the four particles would not have been so accurate without the up to date computing power purchased for this purpose. Thanks to A. Puskeppel and his team for their continued support in spite of all the problems I wanted them to solve. The calculations to analyze the dependence of the localization length on the interaction form and strength were performed on the SC900 parallel computer of the computing center of the university of Hamburg.

Financial support is acknowledged from the DFG via project Kr 627/6 and SFB 508 of the University of Hamburg, from the EU via TMR contracts FMRX CT98-0180 and FMRX CT96-0042, and from the WE Heraeus foundation.

This work would not have been possible without the many stimulating discussion I had during the last three years. Especially, I have to thank three persons who contributed a lot to this thesis. Andrea Fechner always found time to listen and to discuss problems in detail. The open discussions I had with Rudolf A. Römer stimulated new ideas and spared me some of the programming work to create the plots of the three-particle wave packets. And Bernhard Kramer gave me the freedom to choose my own way and supported me a lot to present this work to the scientific community.

## Erklärung gemäß Promotionsordnung §6 (4)

Hiermit erkläre ich, daß ich die Arbeit selbständig angefertigt und nur die angegebenen Quellen (siehe Sektion “References” und Hilfsmittel (siehe Sektion 6.4) benutzt habe. Die Stellen, die im Wortlaut anderen Werken entnommen sind, habe ich als solche gekennzeichnet.

### A Data tables

$W$	MR	MR( $E=0$ )	IPR	IPR( $E=0$ )
9.0	1.80	2.20	3.38	3.07
8.0	2.14	2.52	3.85	3.49
7.0	2.58	3.28	4.45	4.25
6.0	3.22	3.91	5.31	5.17
5.0	4.35	5.54	6.66	7.06
4.0	6.22	8.14	8.60	10.20
3.0	10.29	14.08	12.30	17.71
2.0	21.96	30.40	21.13	38.31
1.5	38.21	54.56	31.90	70.12
1.0	83.61	132.99	58.27	173.32

Table 3: One-particle localization lengths.

$W$	MR	IPR	RD	CM	CM ( $U=0$ )
10.0	1.83	3.13	2.08	1.50	1.36
9.00	2.09	3.47	2.32	1.78	1.64
8.00	2.44	3.94	2.64	2.14	2.02
7.00	3.01	4.64	3.18	2.75	2.53
6.00	3.89	5.82	4.03	3.66	3.18
5.00	5.42	7.93	5.41	5.41	4.47
4.00	8.80	12.47	8.36	9.15	6.95
3.00	18.00	25.03	15.35	20.46	12.70
2.50	29.70	41.16	23.14	37.30	17.65
2.00	56.83	77.82	38.97	79.89	26.80
1.75	86.81	118.06	54.33	127.06	34.89
1.50	140.58	190.79	74.80	229.63	45.19
1.25	239.85	335.06	115.79	454.56	61.14
1.00	483.41	716.75	199.33		

Table 4: Two-particle localization lengths.

$W$	MR	IPR	CM	CM ( $U=0$ )
10.00	2.19	3.62	1.61	1.36631
9.000	2.56	4.17	2.03	1.64172
8.000	3.02	4.77	2.46	2.01213
7.000	3.86	6.07	3.39	2.49595
6.000	5.24	7.94	5.02	3.11337
5.500	6.39	9.64	6.91	3.65236
5.000	8.46	13.18	10.23	4.59848
4.750	9.67	15.28	12.97	5.09416
4.500	11.42	18.78	16.83	5.56029
4.250	13.88	23.94	23.46	6.10027
4.000	17.34	31.93	34.28	7.43717
3.750	22.22	43.92	57.44	8.08082
3.500	29.13	66.27	104.84	9.40344
3.250	39.36	105.59	230.92	11.5654
3.000	54.36	183.58		13.5174

Table 5: Three-particle localization lengths.

$W$	MR	IPR	CM	CM (red.)	CM ( $U=0$ )
10.0	1.79	3.84	2.10	2.10	1.68
9.00	2.11	4.62	2.71	2.71	1.88
8.00	2.77	5.82	3.58	3.59	2.31
7.00	3.85	7.73	5.19	5.14	2.93
6.00	7.29	12.82	9.97	10.30	3.72
5.50	9.84	18.99	17.58	16.40	
5.00	14.32	27.07	36.69	25.91	5.17
4.50	22.22	43.33	101.98	52.59	
4.00	38.01	75.69	331.03	105.85	7.45
3.00					11.89

Table 6: Four-particle localization lengths for the more reliable scaling curves, filled symbols in figures 36 and 37. For the center of mass, results including the extrapolation (figure 40) are given, using the full data set and a reduced one.